Multi-scale 4D imaging of fault zone environments

Yehuda Ben-Zion, University of Southern California
with A. Allam, D. Zigone, G. Hillers, M. Campillo, P. Roux, C. Tape, Z. Peng, M. Lewis and others

Complex hierarchical structures with:

- **Strong geometrical and material heterogeneities**
- **Strong attenuation**
- **Nonlinear propagation effects**
- **Many scales and secondary structures: interfaces (bimaterial), damage zones, basins, branching faults, bounding blocks**

Very challenging targets for detailed imaging

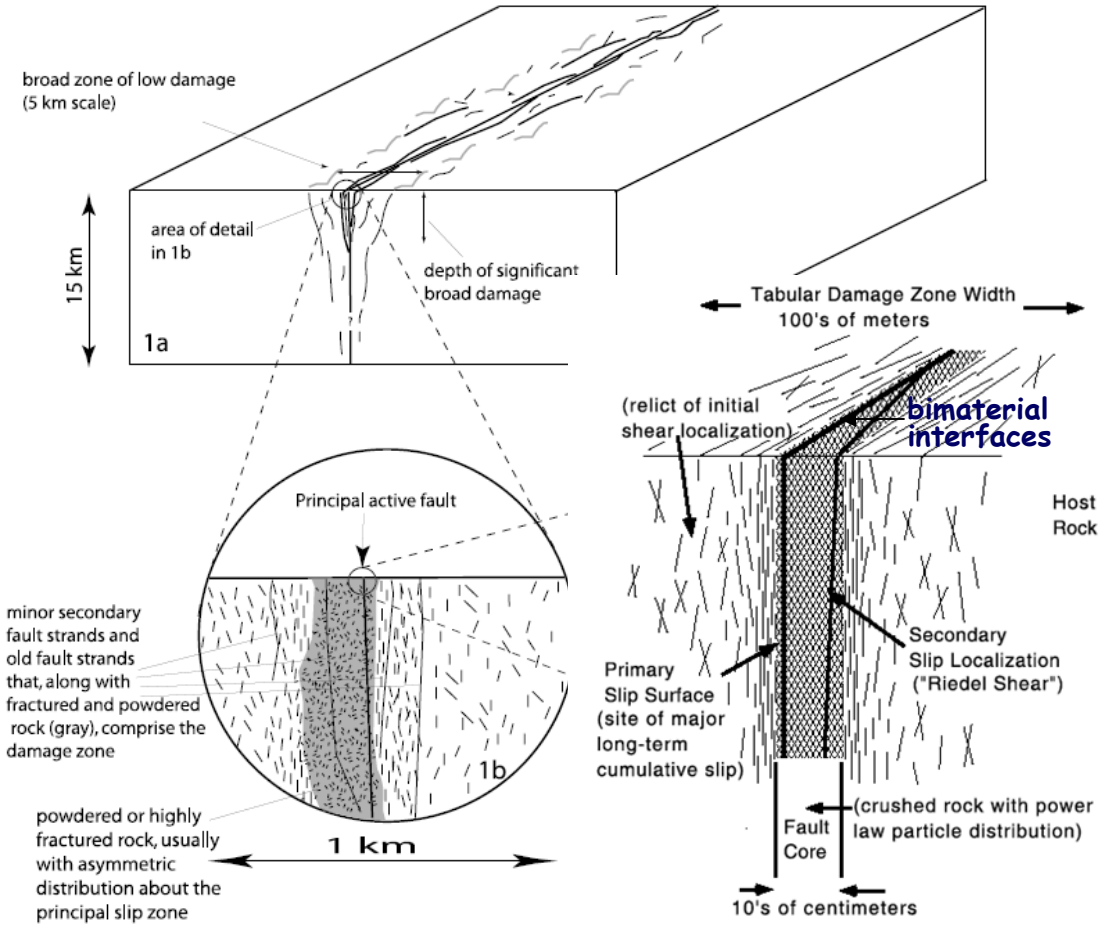

Ben-Zion and Sammis (2003)
Rockwell and Ben-Zion (2007)

Multi-scale 4D imaging of fault zone environments

Yehuda Ben-Zion, University of Southern California
with A. Allam, D. Zigone, G. Hillers, M. Campillo, P. Roux, C. Tape, Z. Peng, M. Lewis and others

Why image fault zones?

- Derivation of earthquake source properties.
- Evolutionary processes on long (tectonic) and short (e.g., precursory) timescales.
- Static/dynamic stress fields (e.g. from internal structure).
- Brittle rock rheology (e.g. from observing & monitoring rock damage).
- FZs control crustal fluid flow: hydrology, oil, sub-surface storage, etc.
- Elements of FZ structure (bimaterial interfaces and damage zones) can control future (and reflect past) earthquake rupture properties.

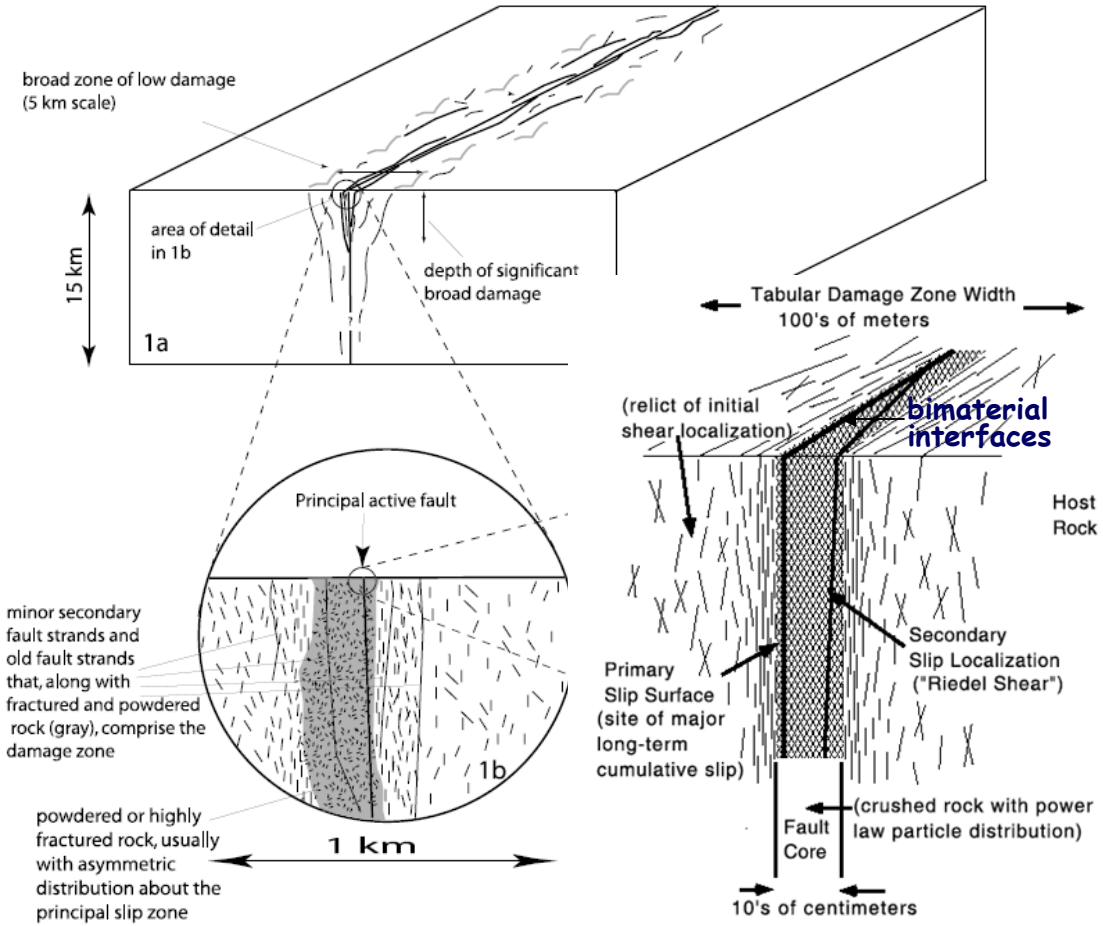

Ben-Zion and Sammis (2003)
Rockwell and Ben-Zion (2007)

Aside: Dynamic rupture on a bimaterial interface

1957 rupture, Gobi-Altai fault, Mongolia

S. Marco (pers. comm.)

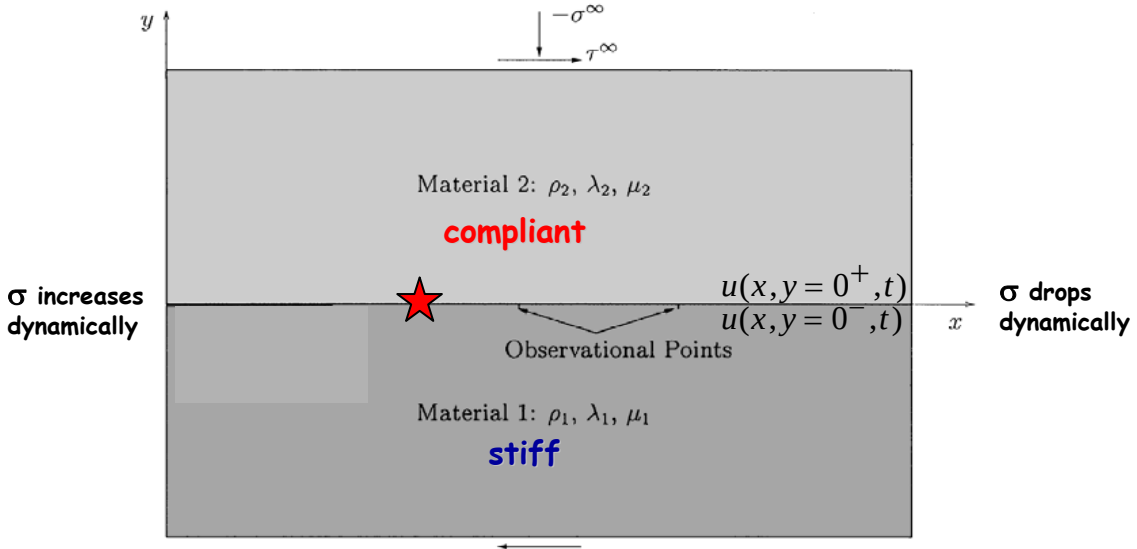

Andrews & Ben-Zion (1997)

Weertman (1980): 2D analytical solution for steady state mode II slip pulse on a frictional bimaterial interface

In-plane slip: δ = u+ − u-

Moving coordinate system: $\xi = x - ct$

Dislocation density: $B(\xi) = -d\delta/d\xi$

Dynamic shear stress: $\tau(\xi) = \tau^\infty + \frac{\bar{\mu}(c,\Delta\beta)}{\pi}\int_{-\infty}^{\infty}\frac{B(\xi')}{\xi-\xi'}d\xi'$

Dynamic normal stress: $\sigma(\xi) = \sigma^\infty - \mu^*(c,\Delta\beta)B(\xi)$

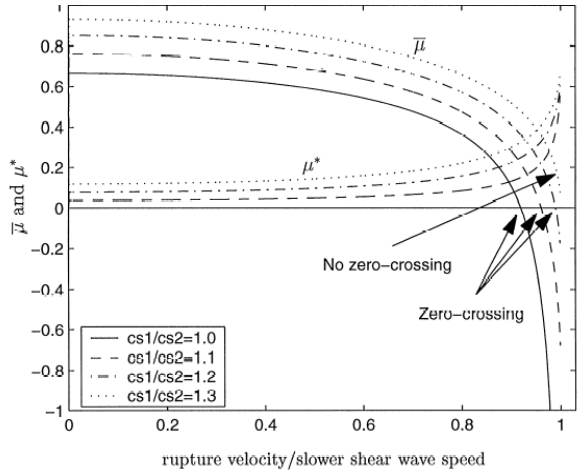

- In a homogeneous solid $\mu^* = 0$; there is no coupling between slip and σ.
- For subsonic rupture on a bimaterial interface in the direction of motion of the compliant solid, $\mu^* > 0$ and σ drops dynamically (producing local dilation).
- In the opposite direction, $\mu^* < 0$ and σ increases dynamically (local compression).

Wrinkle-like rupture on a bimaterial interface (Andrews and Ben-Zion, 1997)

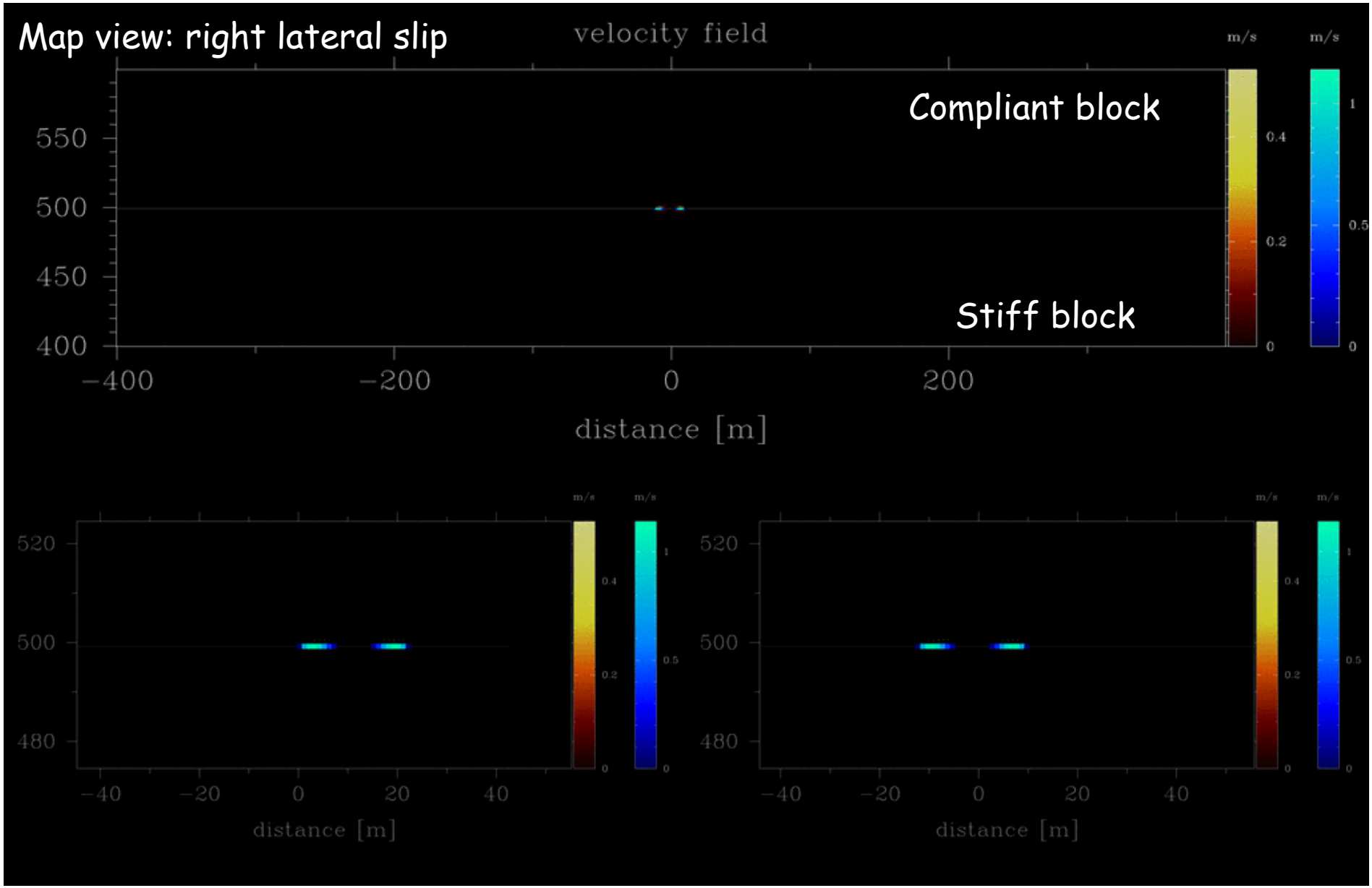

Wrinkle-like rupture pulse

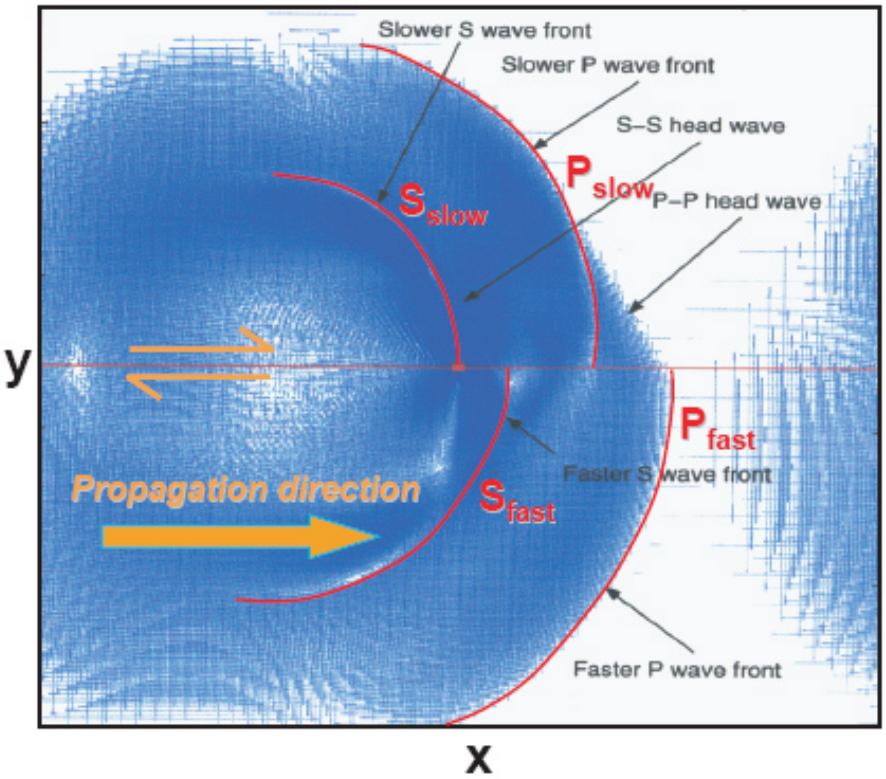

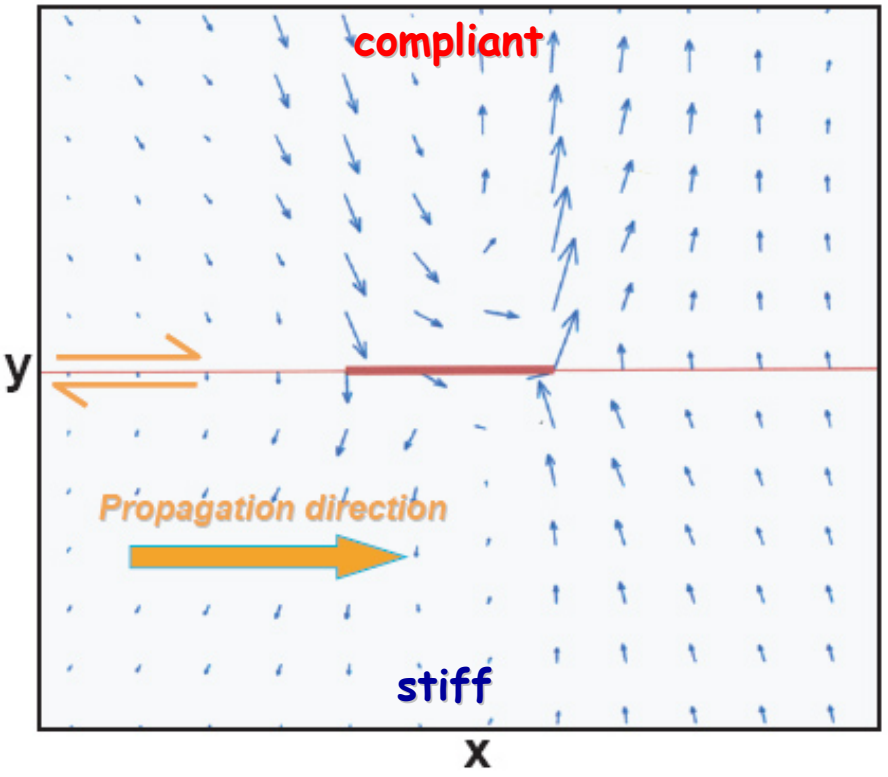

Andrews and Ben-Zion, 1997; Ben-Zion and Andrews, 1998; Cochard and Rice, 2000; Ben-Zion, 2001; Ben-Zion and Huang, 2002, Shi and Ben-Zion, 2006, Ampuero and Ben-Zion, 2008; Brietzke et al., 2009

Rupture Directivity and Ground Motion

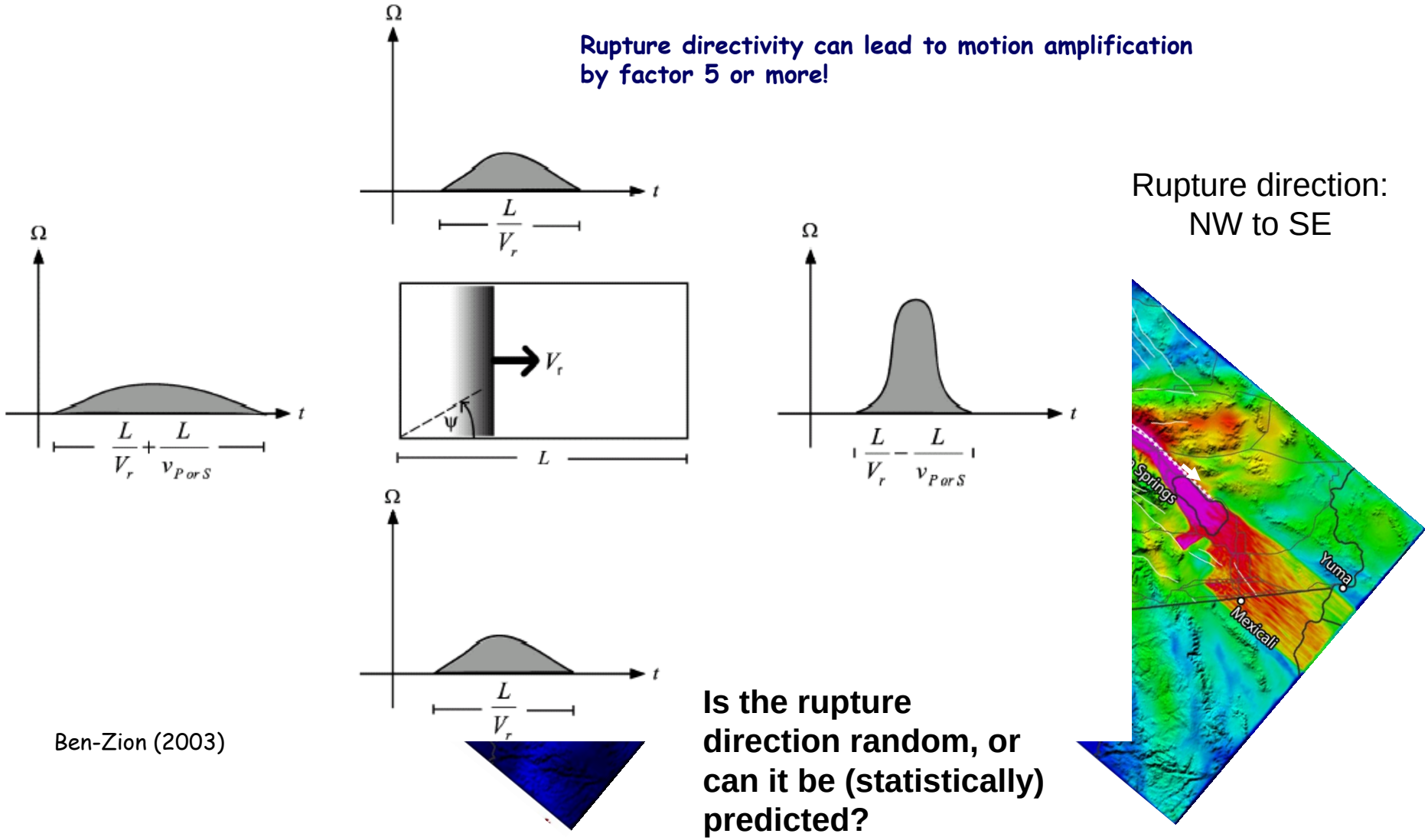

Rupture directivity can lead to motion amplification by factor 5 or more!

Rupture direction:
NW to SE

Ben-Zion (2003)

Is the rupture direction random, or can it be (statistically) predicted?

TeraShake simulations of M7.7 earthquake on Southernmost San Andreas (Olsen et al. 2006)

Following Slides: Multi-Scale Imaging results from the San Jacinto, San Andreas, Hayward and North Anatolian faults

Data

•**Earthquake waveforms** (high resolution in seismogenic zone; very good temporal coverage during aftershock sequences and other periods with high event rates like accelerating foreshock sequences)

•**Ambient seismic noise** (high resolution in shallow crust; great temporal coverage during intervals with little seismicity)

Techniques

•**Travel time tomography**
•**Cross/auto correlations**
•**Waveform/adjoint modeling**
•**Spectral ratios**

Signals

•**Body waves**
•**Surface waves**
•**Fault zone head and trapped waves**
•**Anisotropy**
•**Non linear propagation effects**

Seismic Velocity Structures in the Southern California Plate Boundary Environment from Double-difference Tomography (Allam and Ben-Zion, GJI, 2012)

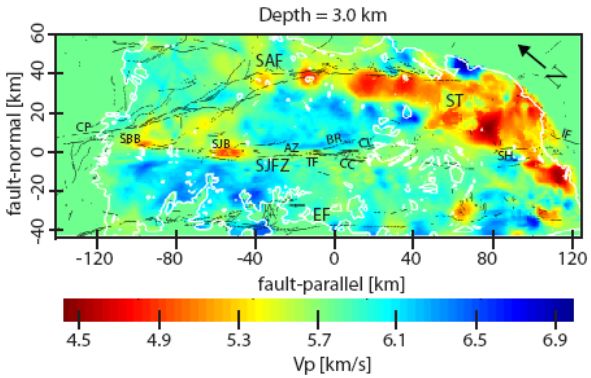

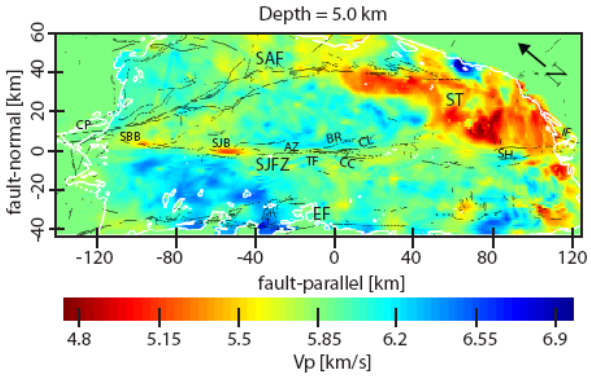

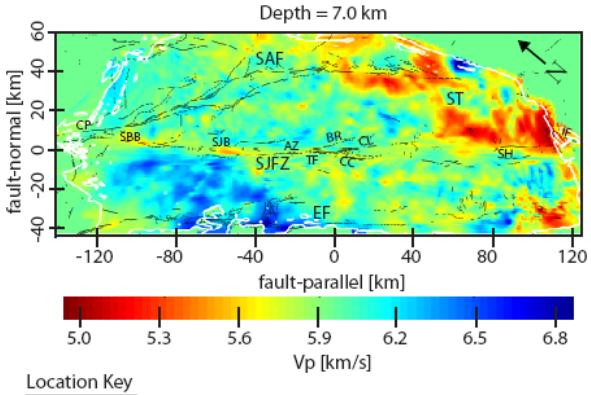

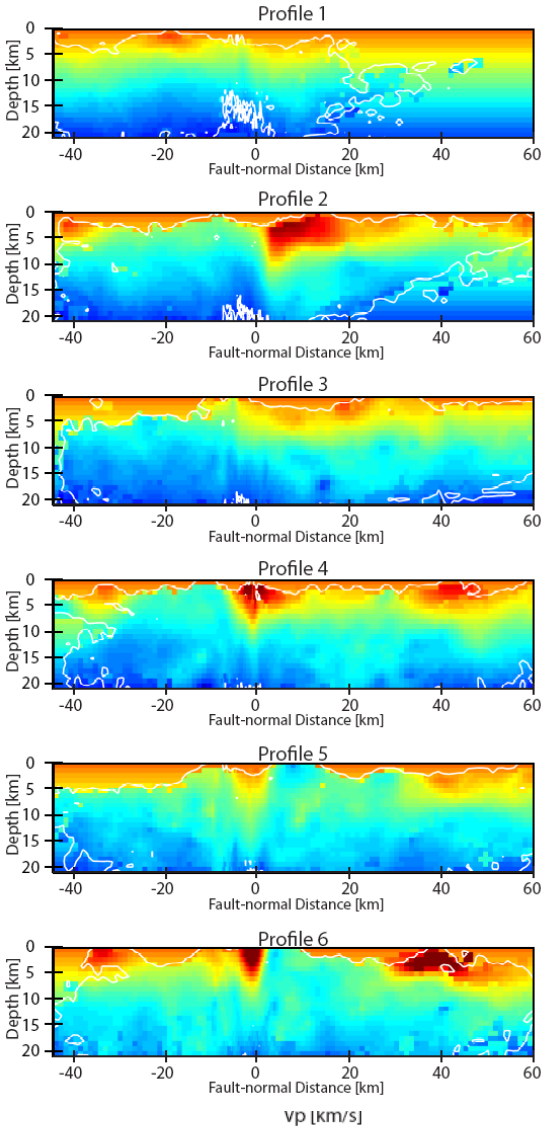

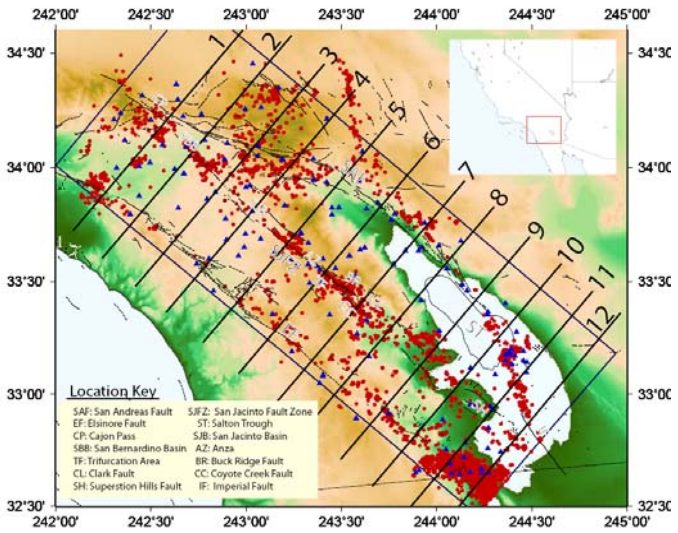

Location Key

SAF: San Andreas Fault SJFZ: San Jacinto Fault Zone EF: Elsinore Fault ST: Salton Trough CP: Cajon Pass SBB: San Bernardino Basin
SJB: San Jacinto Basin AZ: Anza TF: Trifurcation Area BR: Buck Ridge Fault CL: Clark Fault
CC: Coyote Creek Fault SH: Superstion Hills Fault IF: Imperial Fault

- 5493 earthquakes (2000-2011)
- 139 stations
- 360,000 *P*- and *S* arrival times
- grid cell size: 1km
- white contours > 10 rays/cell

central section

- Prominent generally in top 5 km

- Follow overall "flower" shape with depth

- Larger reductions of Vs (up to 40% in top 3-5 km) than Vp

Velocity contrasts along sections of the SJFZ

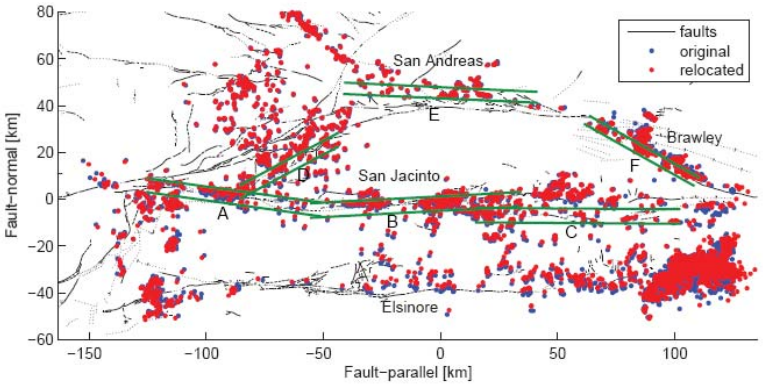

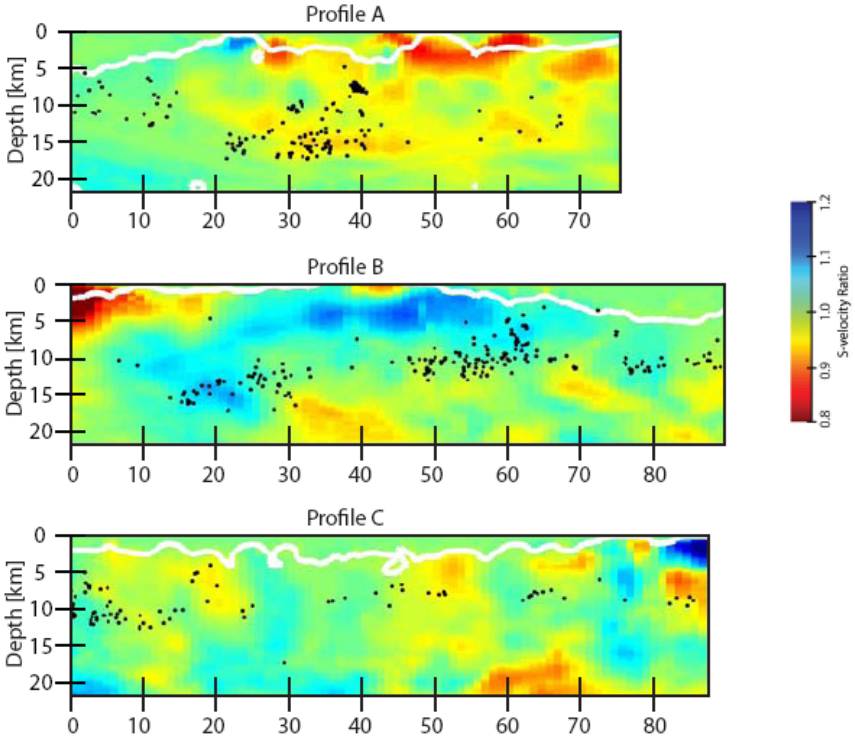

Profile B along the central SJFZ has significant velocity contrast (up to 20%) with NE side fast.

Profile C from the trifurcation to the SE has smaller and less persistent contrast.

Profile A from Cajon pass to the San-Jacinto basin has mild contrast with reversed polarity (slow NE)

Comments:

- **Higher resolution (250m^3 cells) TomoDD for the trifurcation areas** (Allam, Ben-Zion, Kurzon, Vernon, 2013)
- **Good resolution between 3-15 km; poor in top 3 km.**
- **Ambient noise imaging can resolve the structures in top 3 km (coming next)**
- **Fault zone head and trapped waves provide highest resolution of bimaterial interfaces and damage zones (coming later)**

Noise based Imaging of Southern California Plate Boundary Area

Dimitri Zigone, Yehuda Ben-Zion, Michel Campillo

with contributions from X. Briand, G. Hillers, P. Boué, L. Sthely, P. Roux, X. Liu

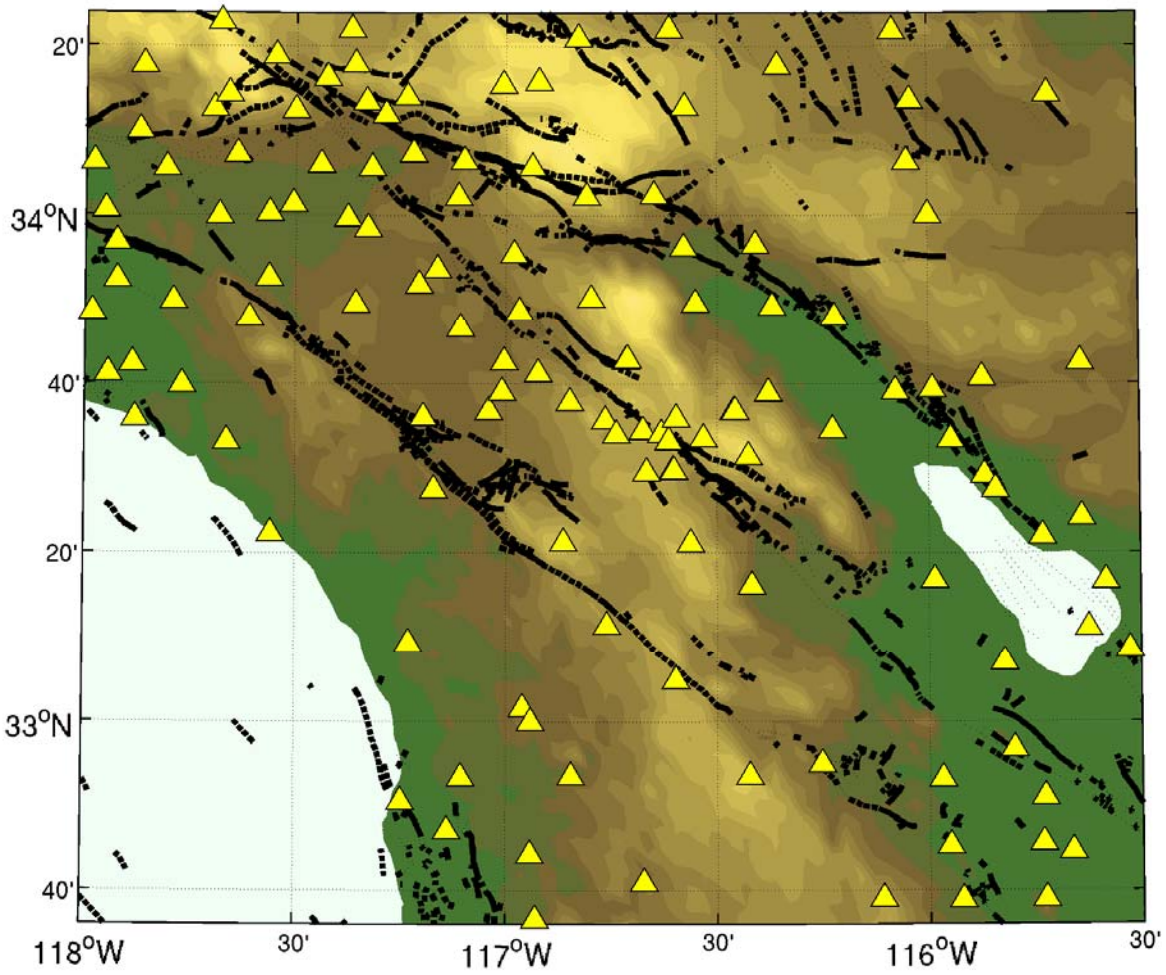

140 Stations

1 year of data
2012

Both 3 components
(66%) and short period
(33%) sensors

Cross-correlations : processing

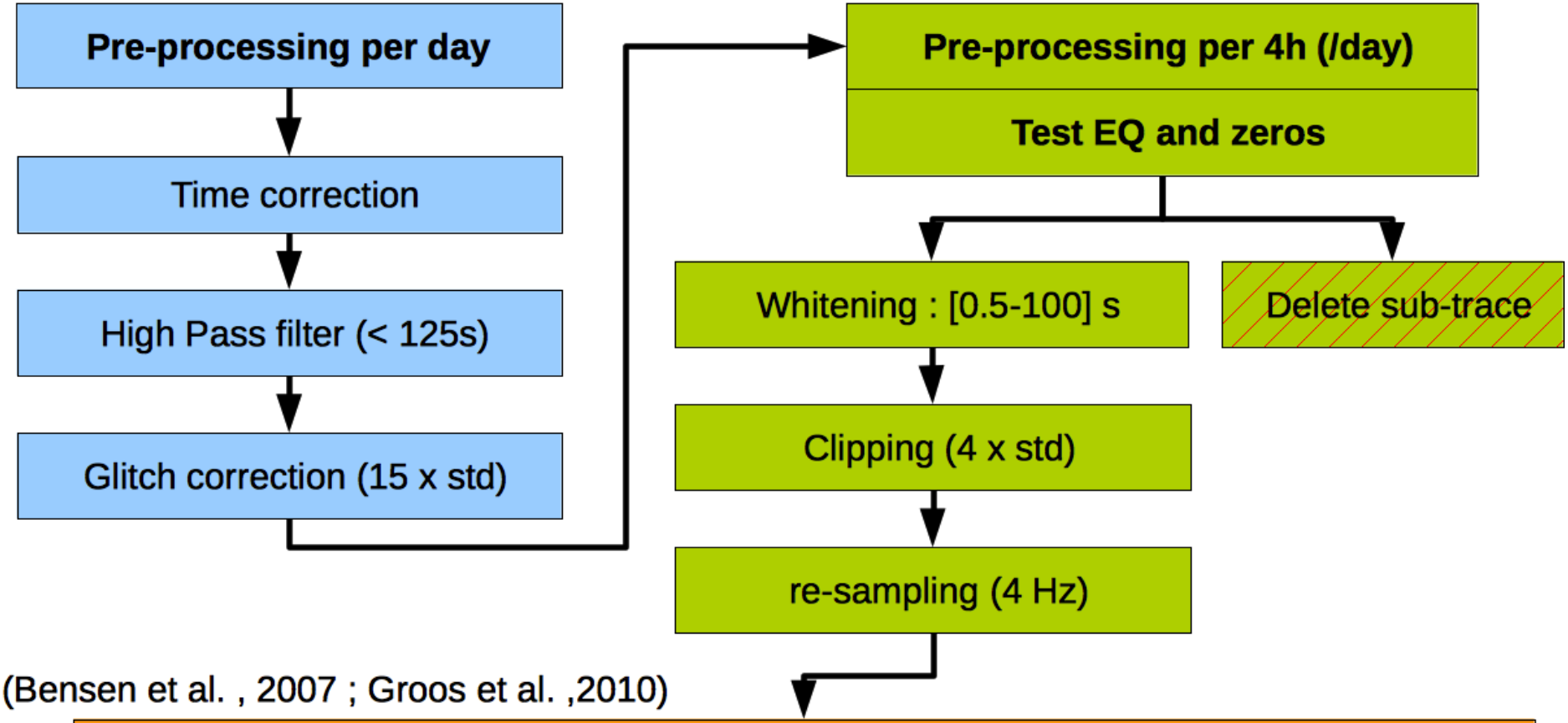

(Bensen et al. , 2007 ; Groos et al. ,2010)

Correlations per 4h (stacked per day)

9 components
Maxlag = 300 s

$$[C_{AB}(t)]_{ij} = \frac{\int_0^T S_{A,i}(\tau)\, S_{B,j}(t+\tau)\, \mathrm{d}\tau}{\sqrt{\int_0^T S_{A,i}^2(\tau)\, \mathrm{d}\tau \int_0^T S_{B,j}^2(\tau)\, \mathrm{d}\tau}}$$

Surface Waves Green's functions and Velocity Measurements

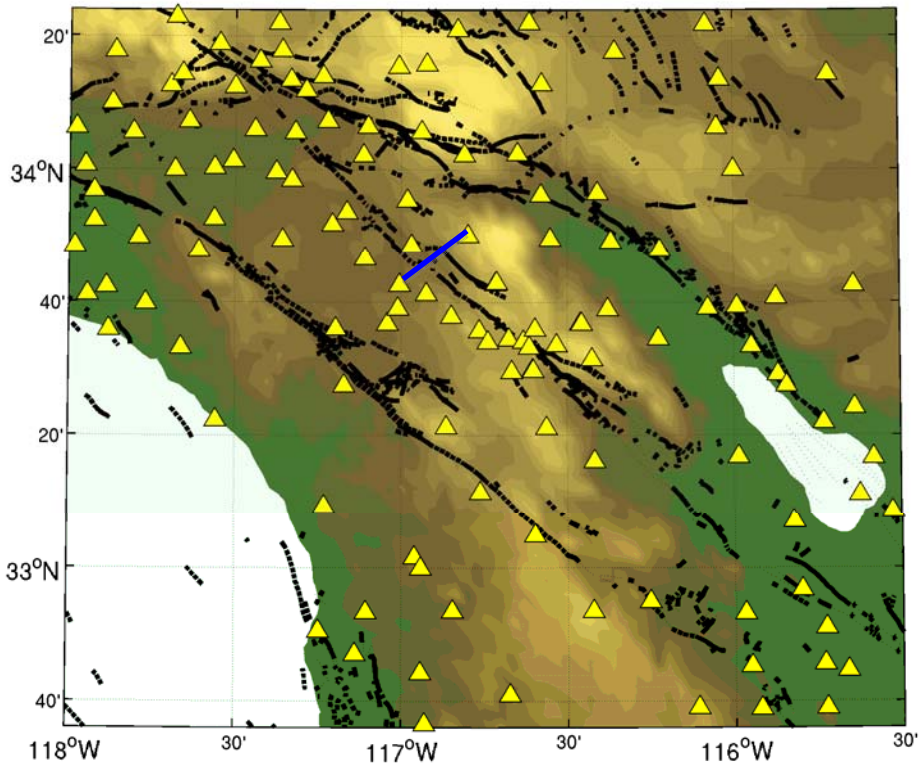

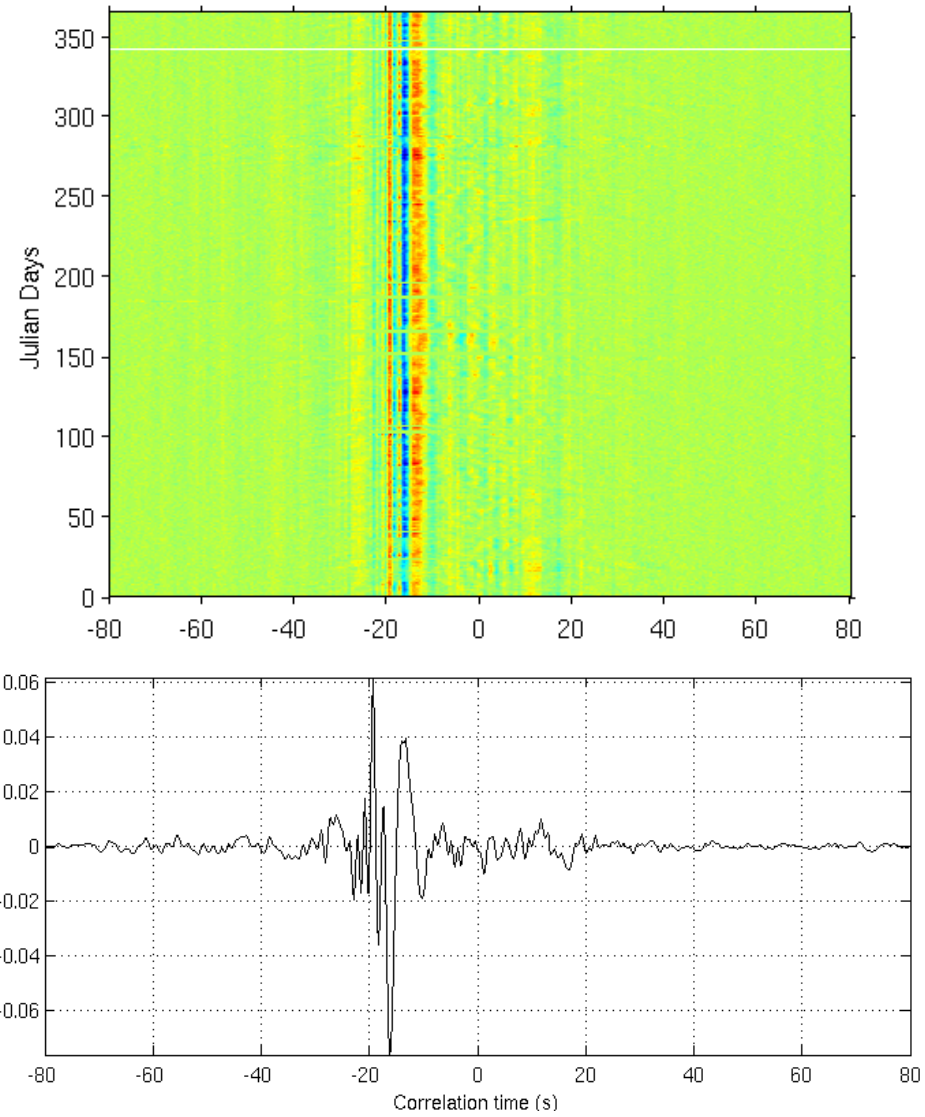

Asymmetric correlogram with clear dispersive surface waves

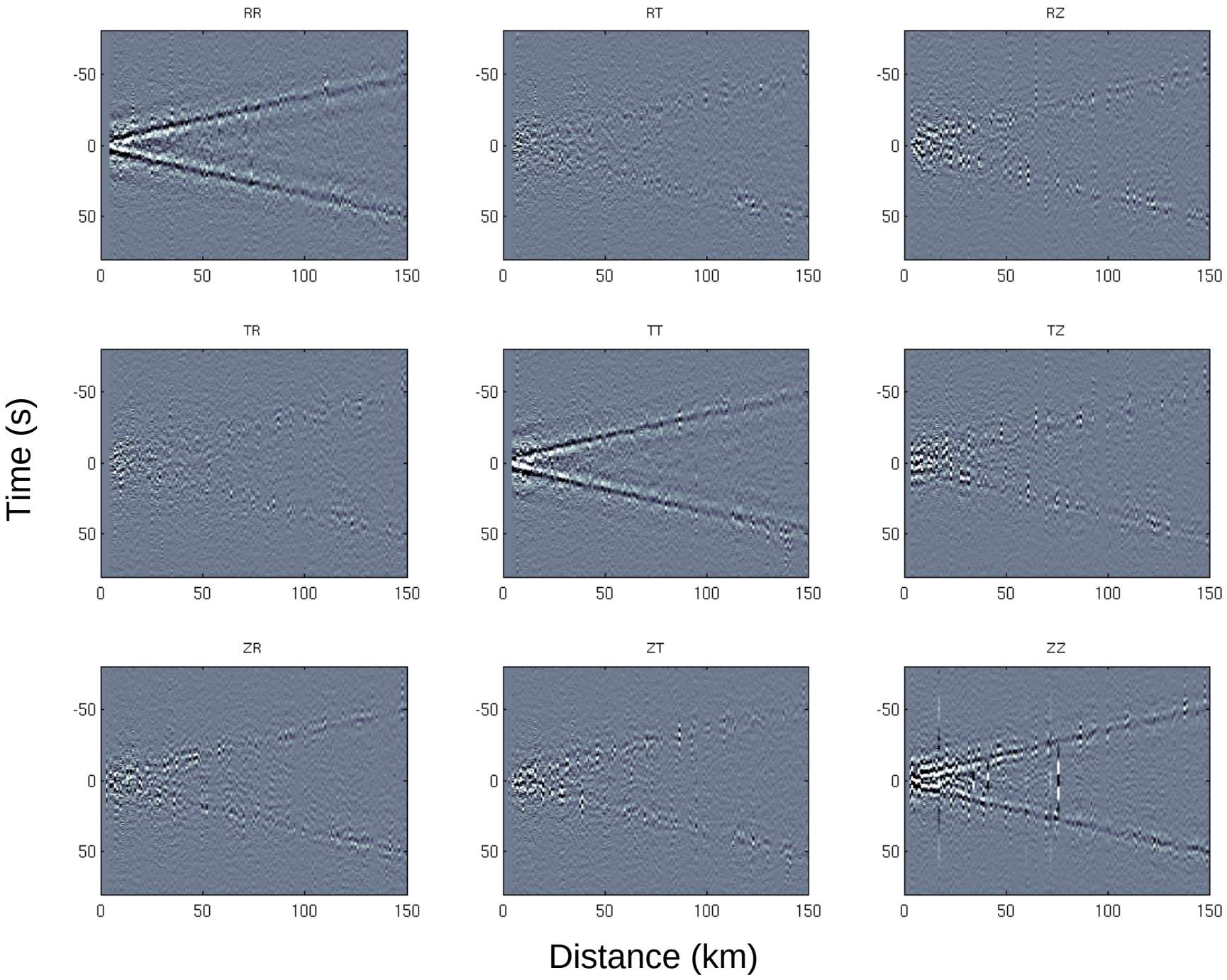
RR
RT
RZ
TR
TT
TZ
ZR
ZT
ZZ
-50
0
50
0
50
100
150
Time (s)
Distance (km)

6734 paths with SNR>10

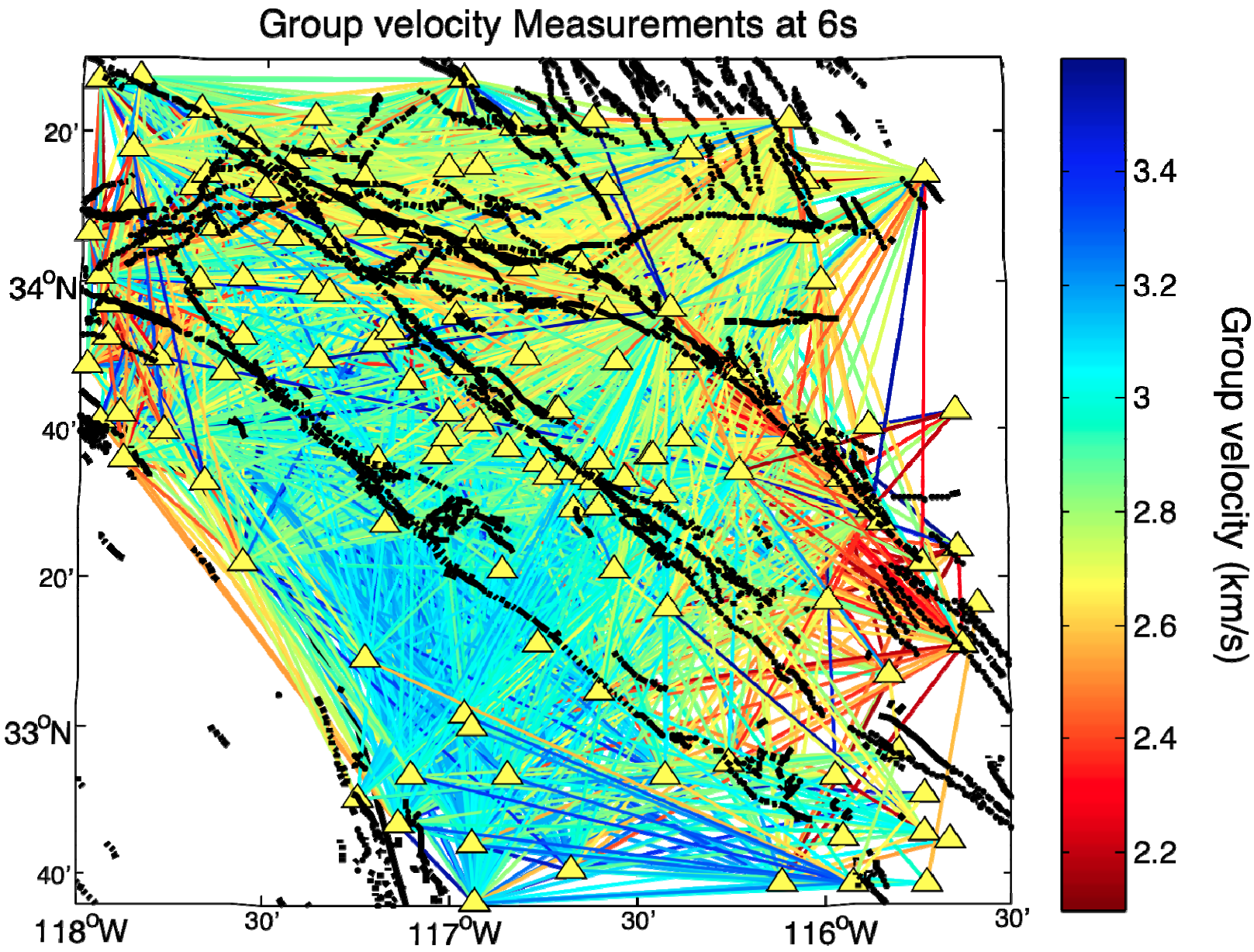

Vs from Love waves
(linearized Inversion of
Hermann and Ammon, 2002)

The results show flower-type damage structures in the top 3 km (connect nicely to the deeper images of Allam & Ben-Zion 2012)

High-resolution results in the top 500-1000m can be obtained by cross correlating earthquake waveforms (work in progress with P. Roux)

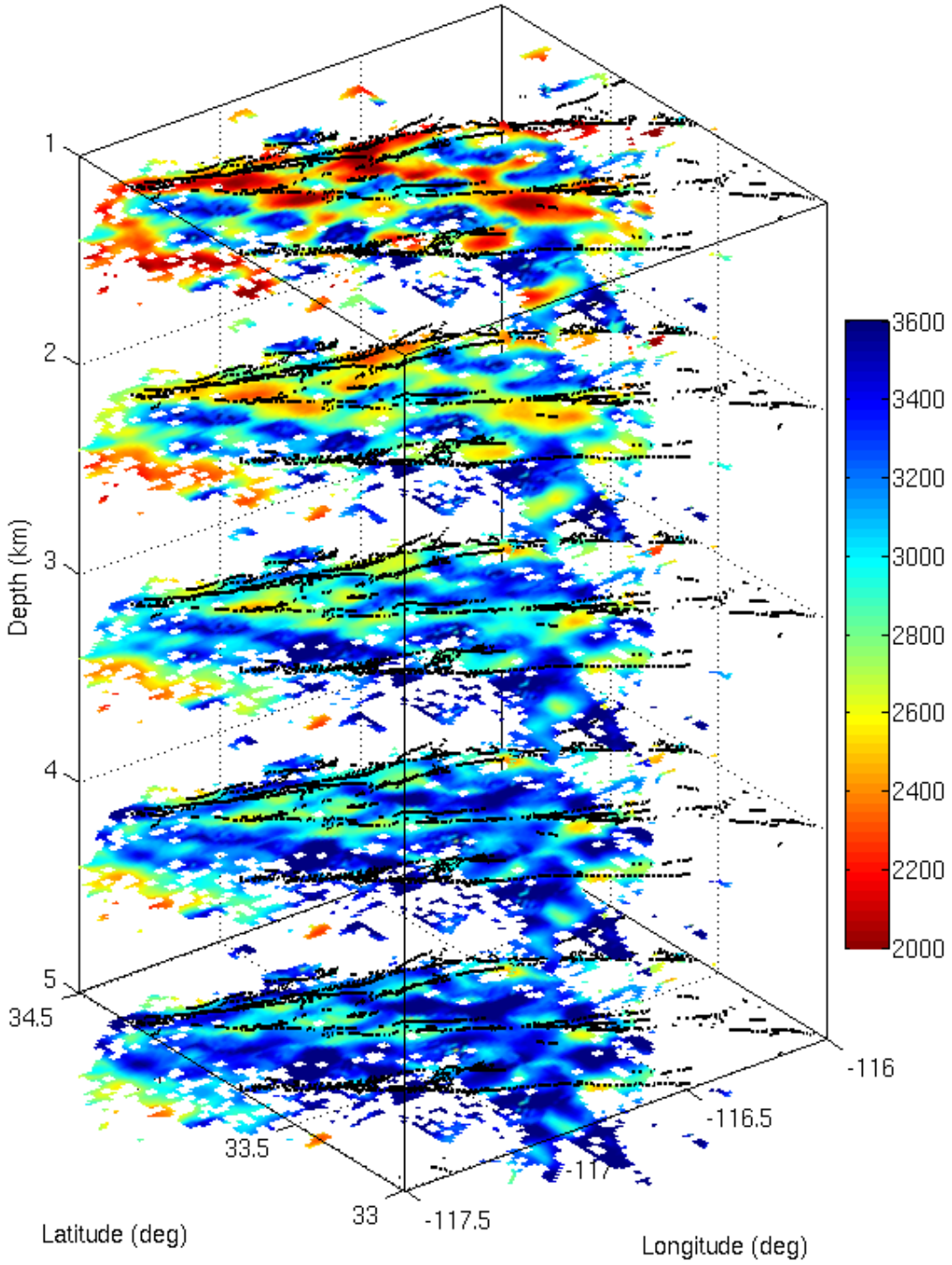

Imaging bimaterial fault interface with Head Waves

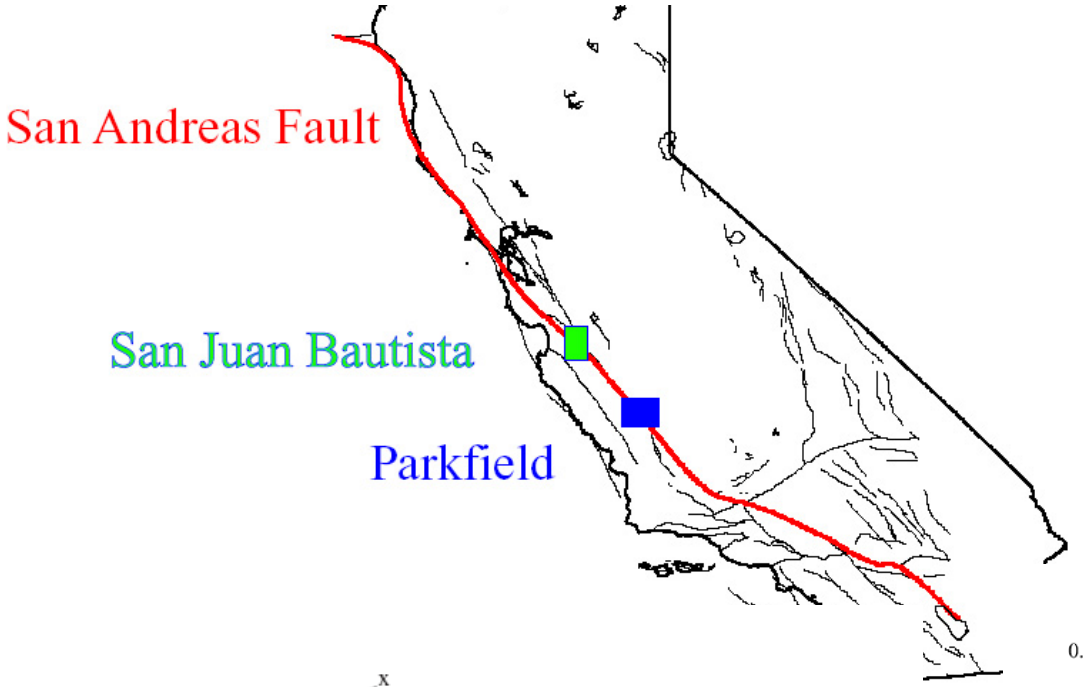

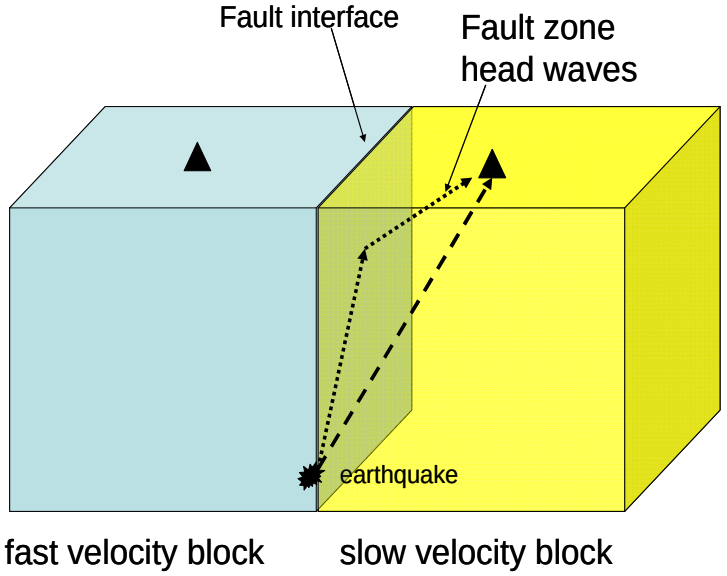

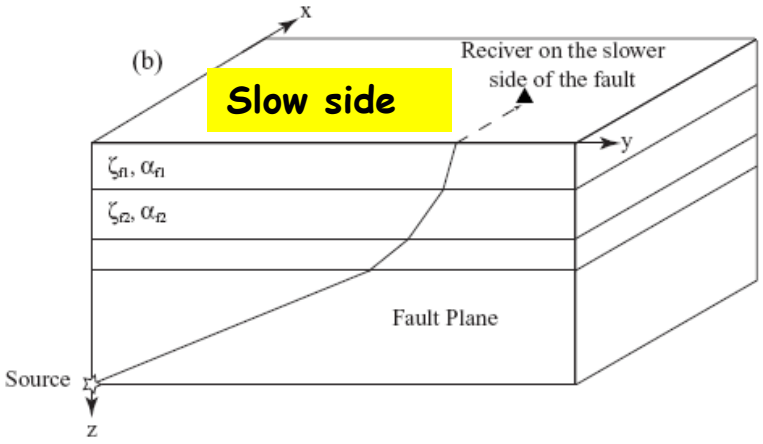

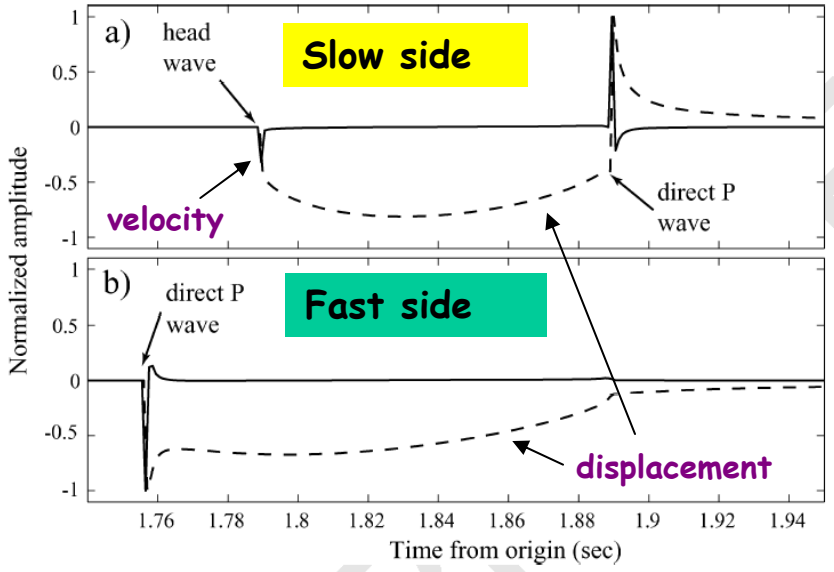

The head waves are first arrivals at stations on the slower side of the fault with normal distance $x < x_c = r \tan [\cos^{-1}(\alpha_2/\alpha_1)]$ and have opposite polarity than the direct *P* wave (Ben-Zion, 1989, 1990)

Imaging bimaterial fault interface with Head Waves

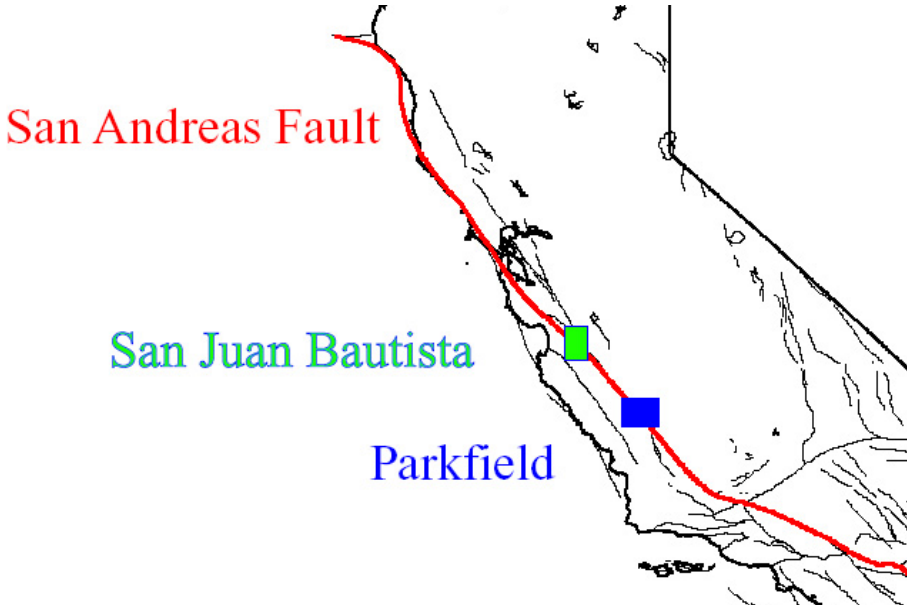

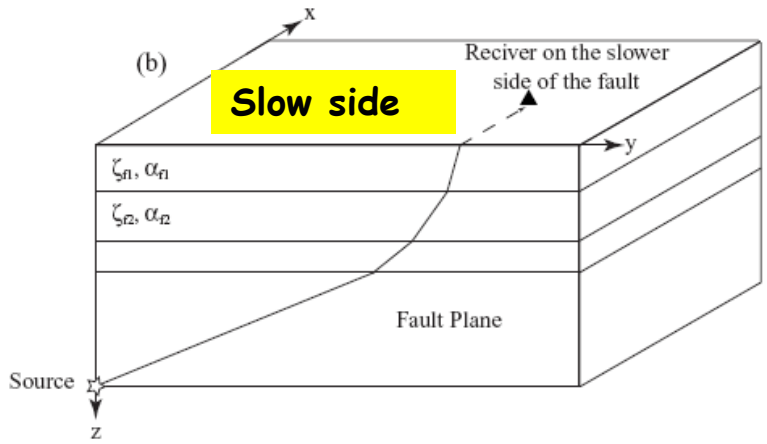

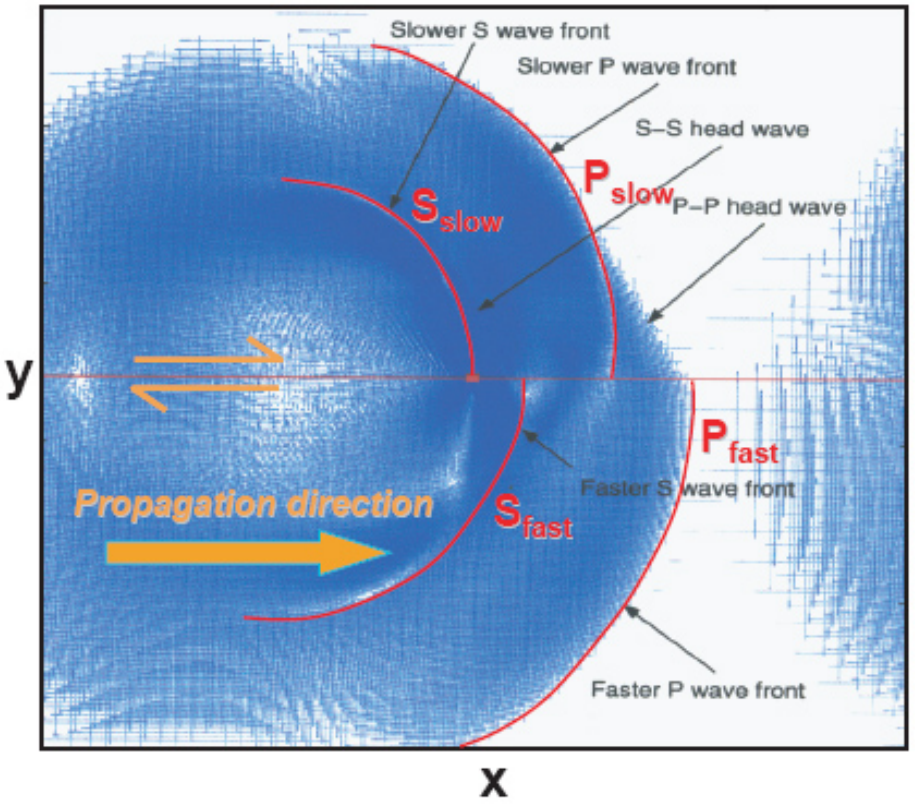

The head waves are <u>first arrivals</u> at stations on the slower side of the fault with normal distance $x < x_c = r \tan [\cos^{-1}(\alpha_2/\alpha_1)]$ and have <u>opposite polarity</u> than the direct *P* wave (Ben-Zion, 1989, 1990)

Analysis of fault zone trapped waves

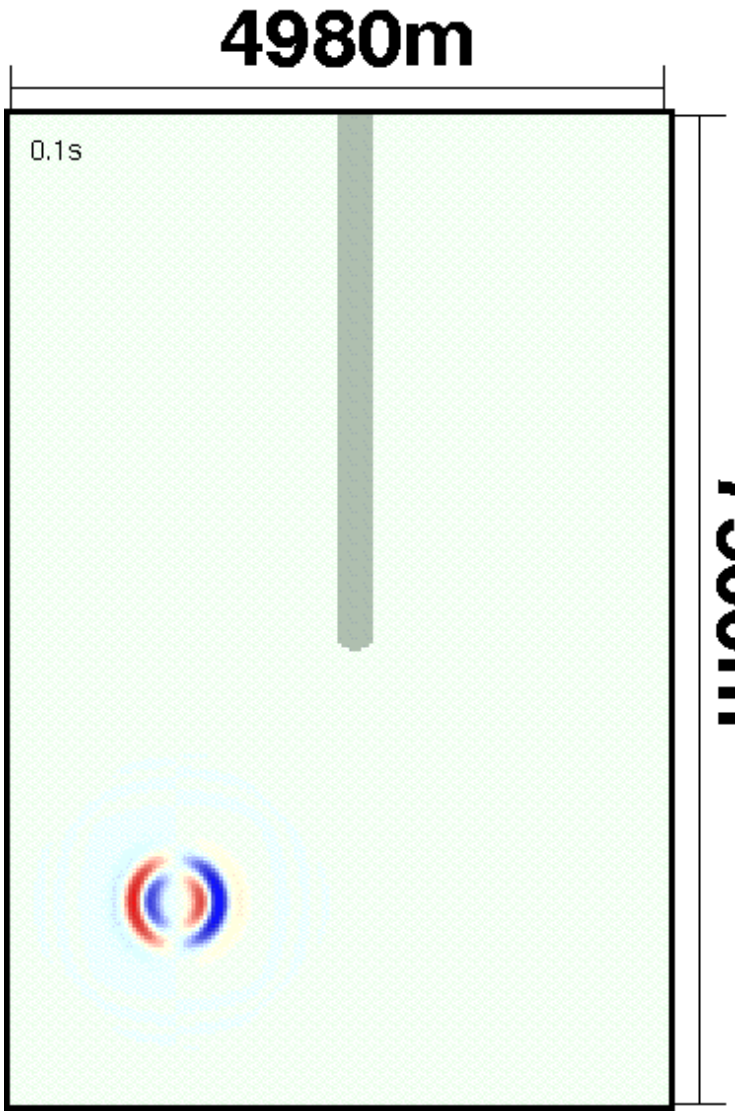

Fohrmann, Igel, Jahnke, Ben-Zion (2004)

Ben-Zion and Aki, 1990

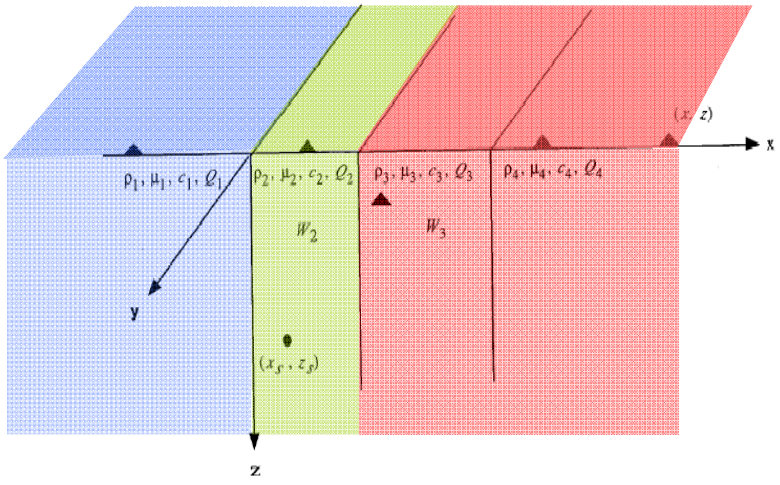

Direct body waves

Head waves

Trapped waves

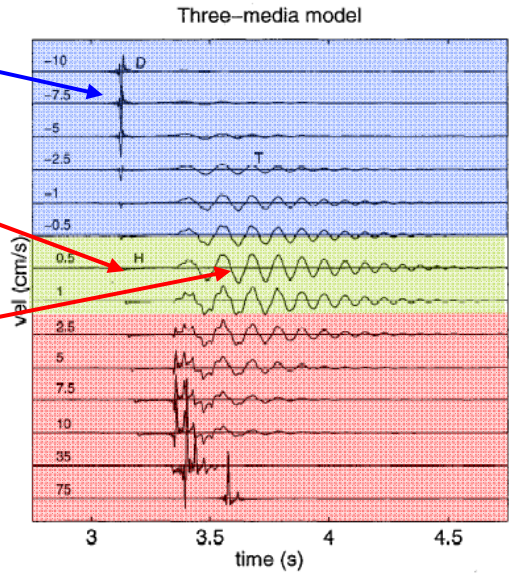

Trapped waves depends strongly on

$N = r/[W \tan(\theta_c)] = r/[W \tan(\sin^{-1}(\beta_2/\beta_1))]$

Volumetric sensitivity kernels of fault zone waves

(Allam, Tape and Ben-Zion)

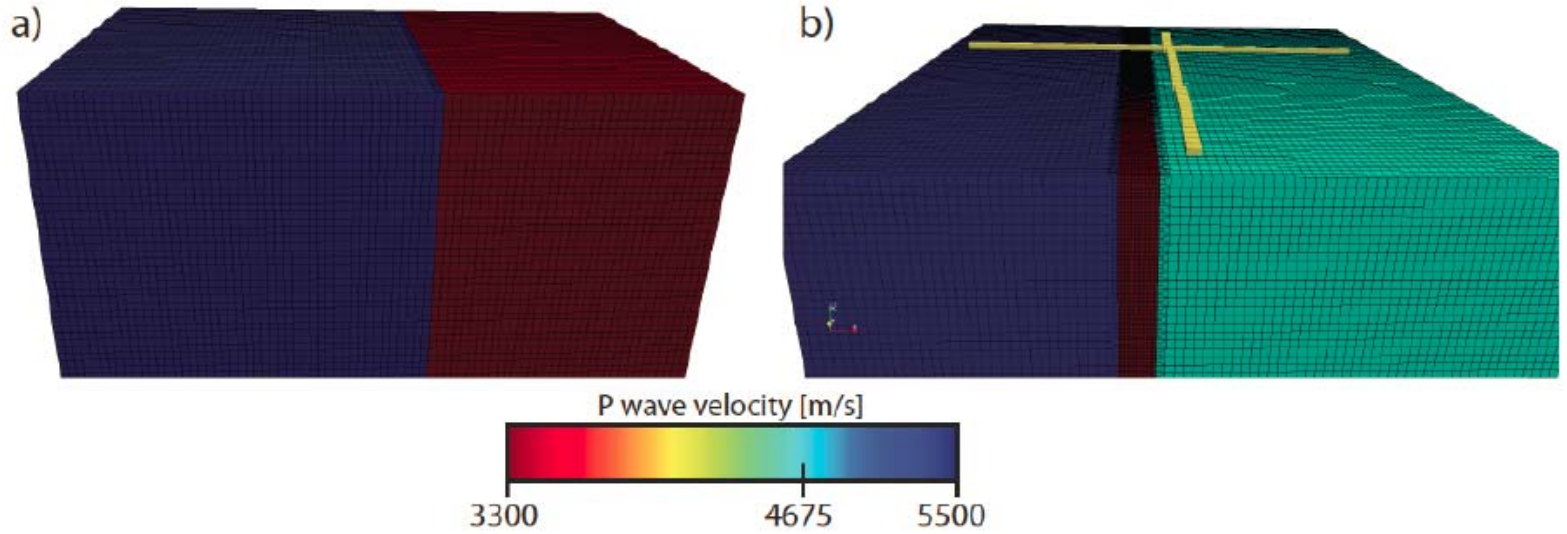

3D spectral element calculations

(Komatitsch & Tromp, 1999, and later works)

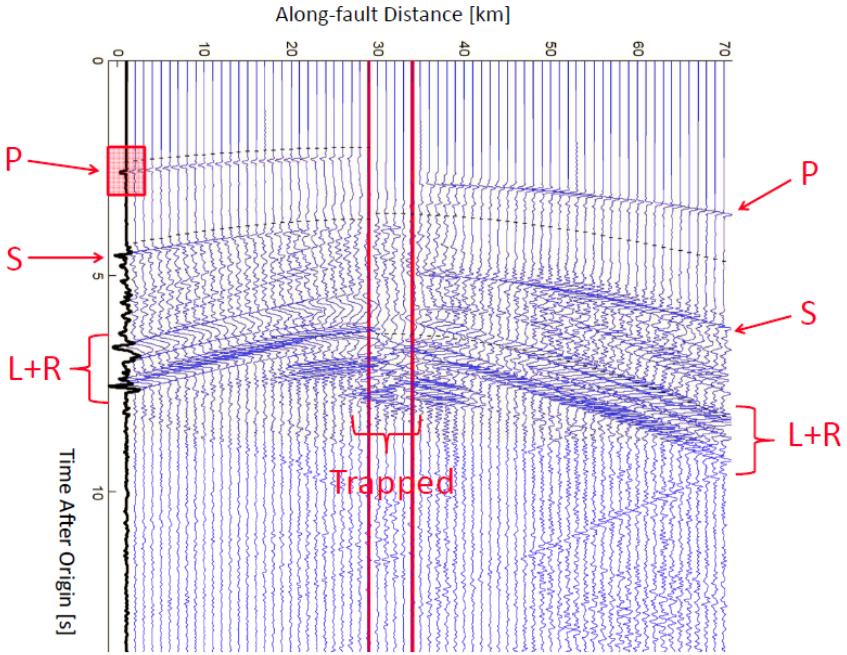

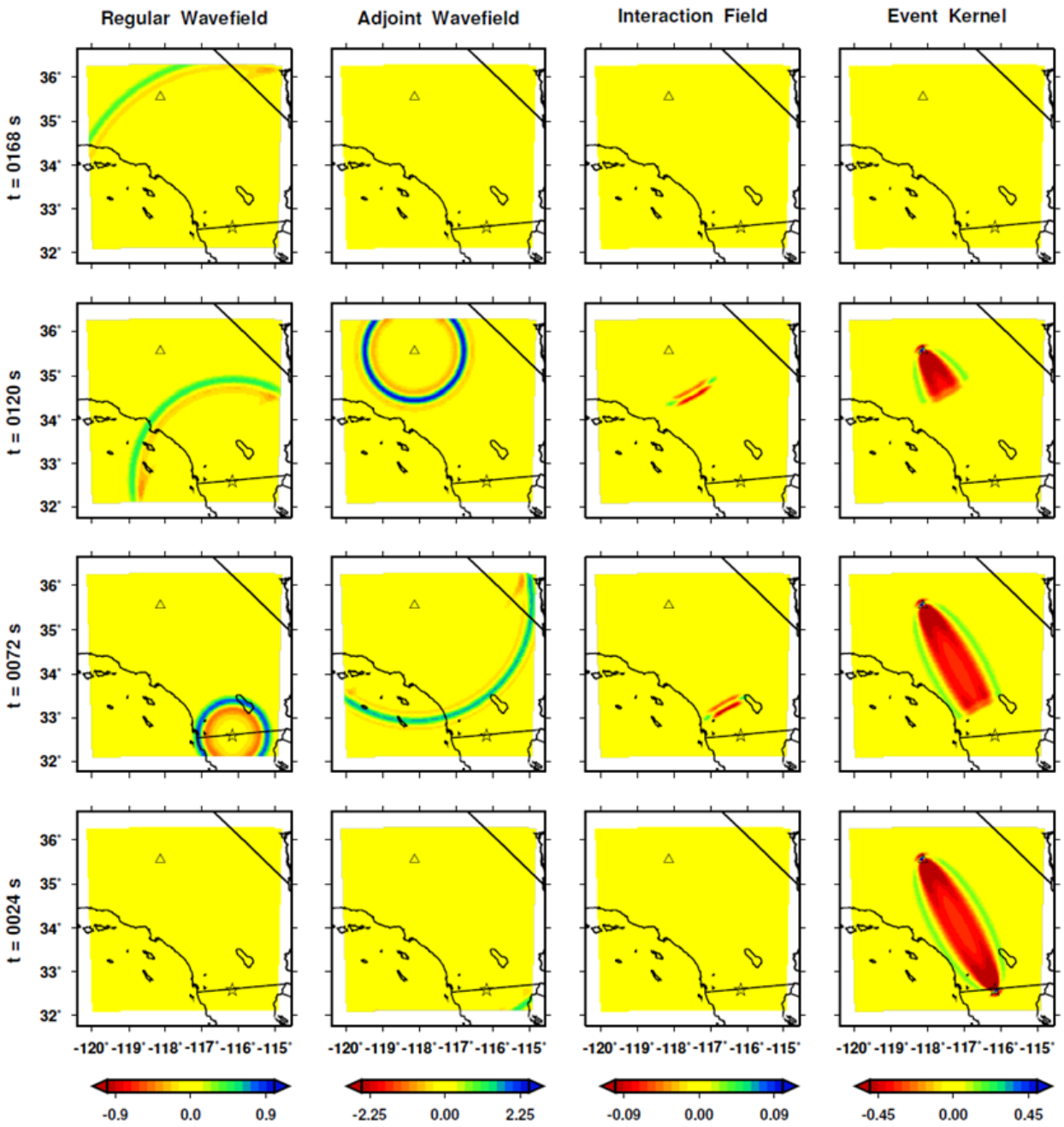
Regular Wavefield
Adjoint Wavefield
Interaction Field
Event Kernel
t = 0168 s
t = 0120 s
t = 0072 s
t = 0024 s
36°
35°
34°
33°
32°
-120°-119°-118°-117°-116°-115°
-0.9 0.0 0.9
-2.25 0.00 2.25
-0.09 0.00 0.09
-0.45 0.00 0.45

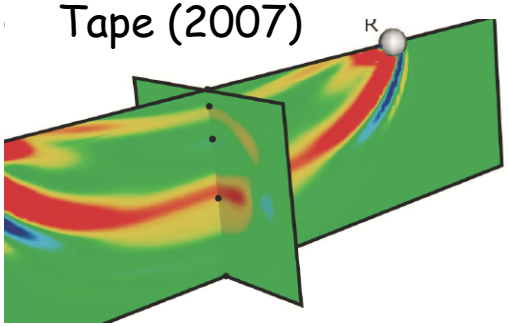
Tape (2007)

Two quarter spaces

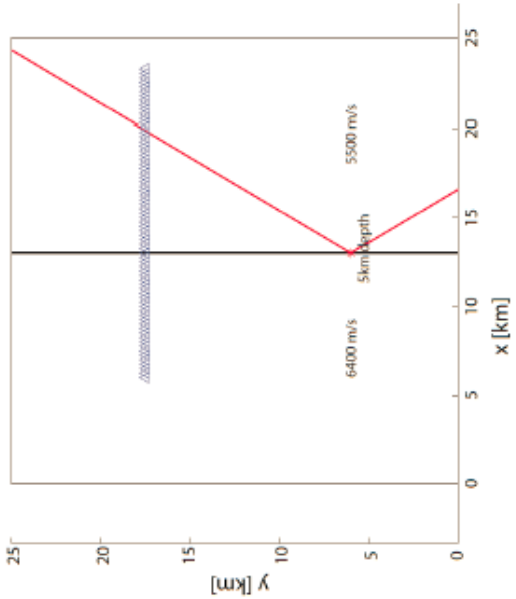

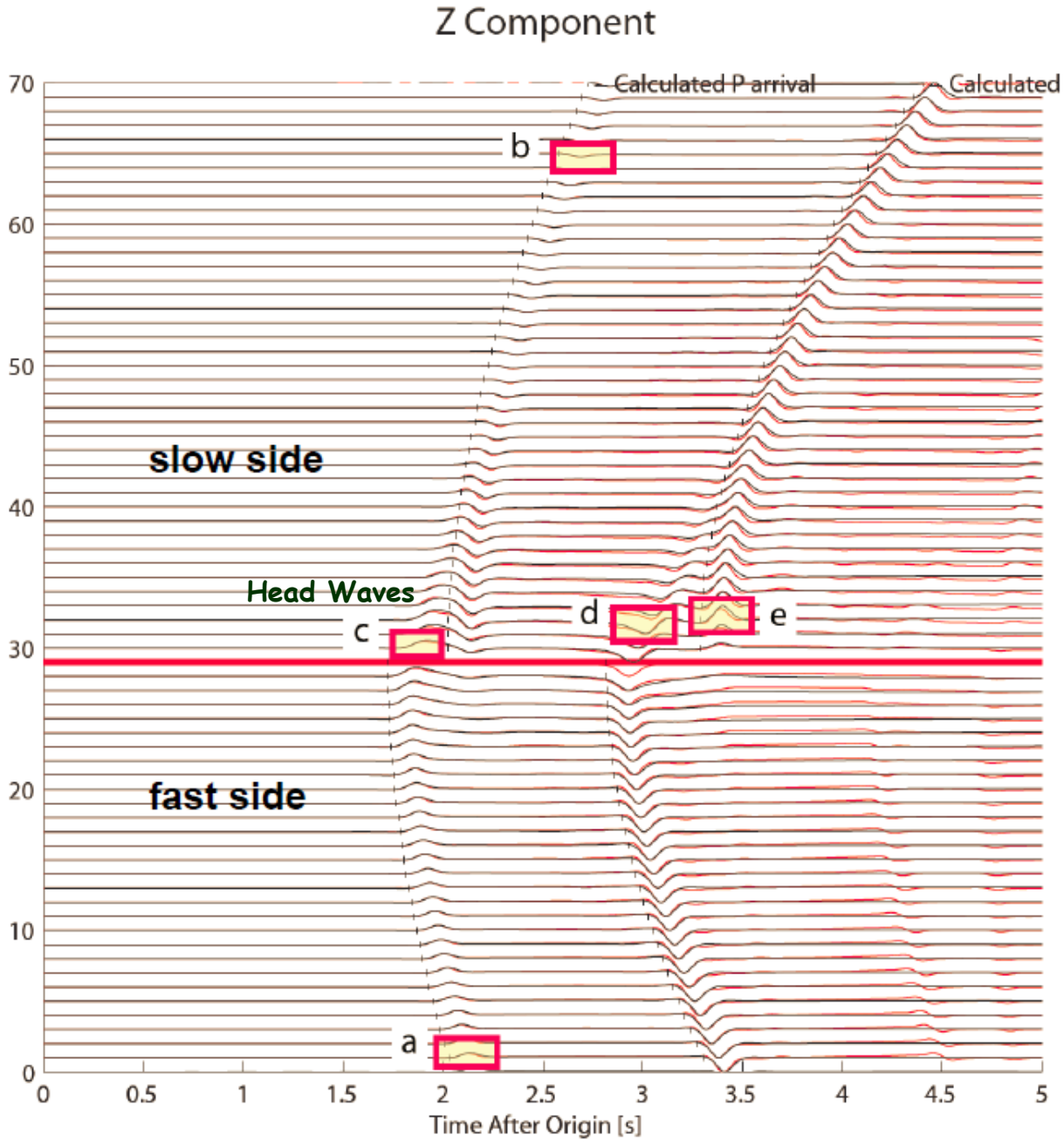

P wave

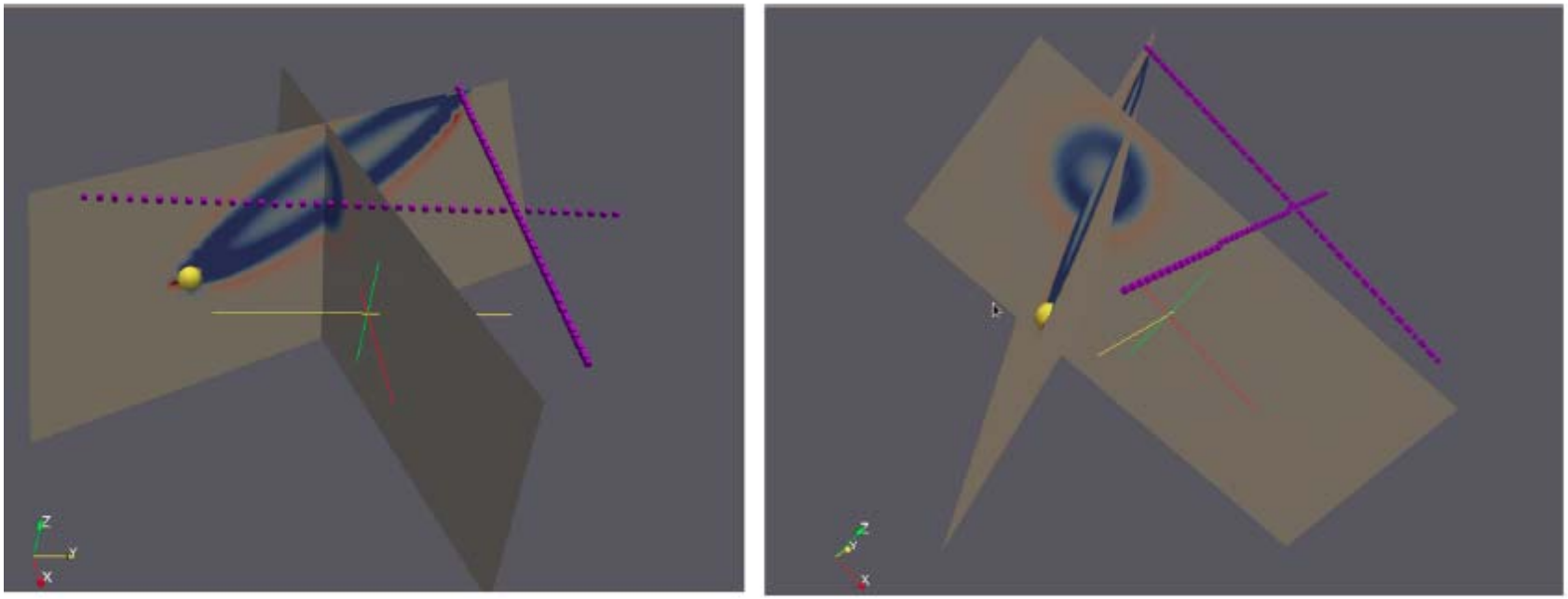

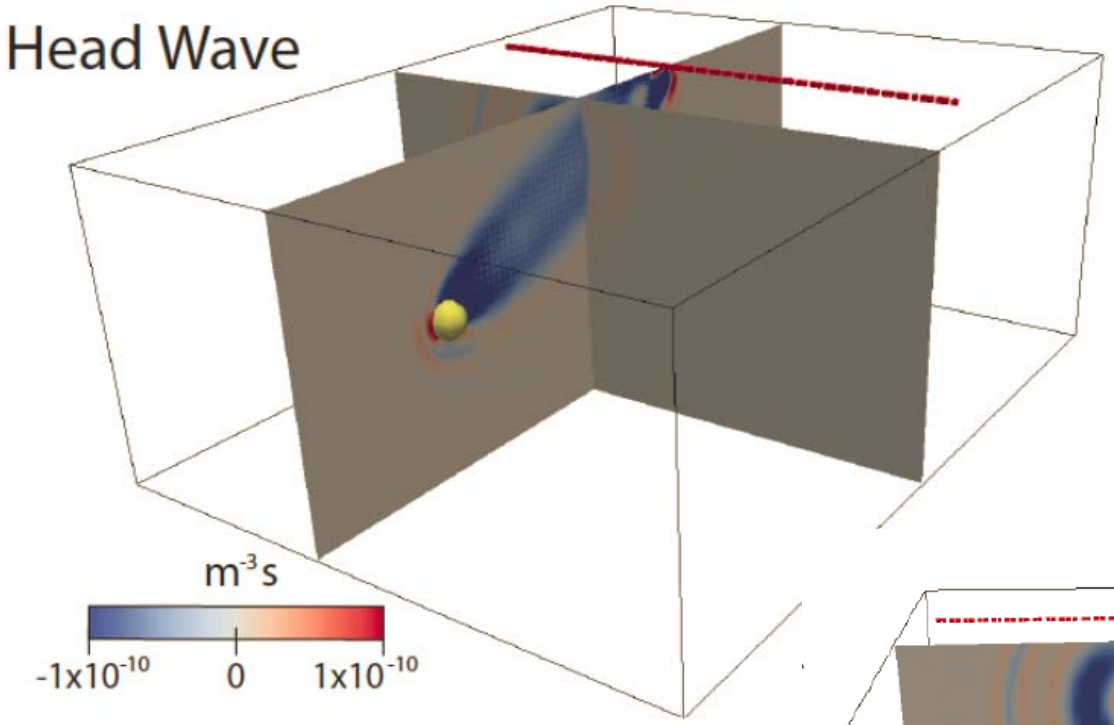

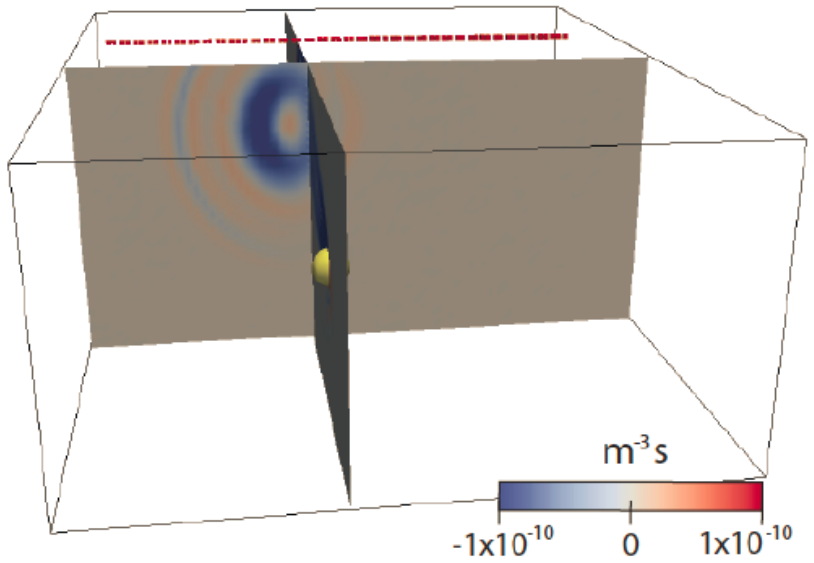

Half banana or canoe

Two quarter spaces with LVZ in between

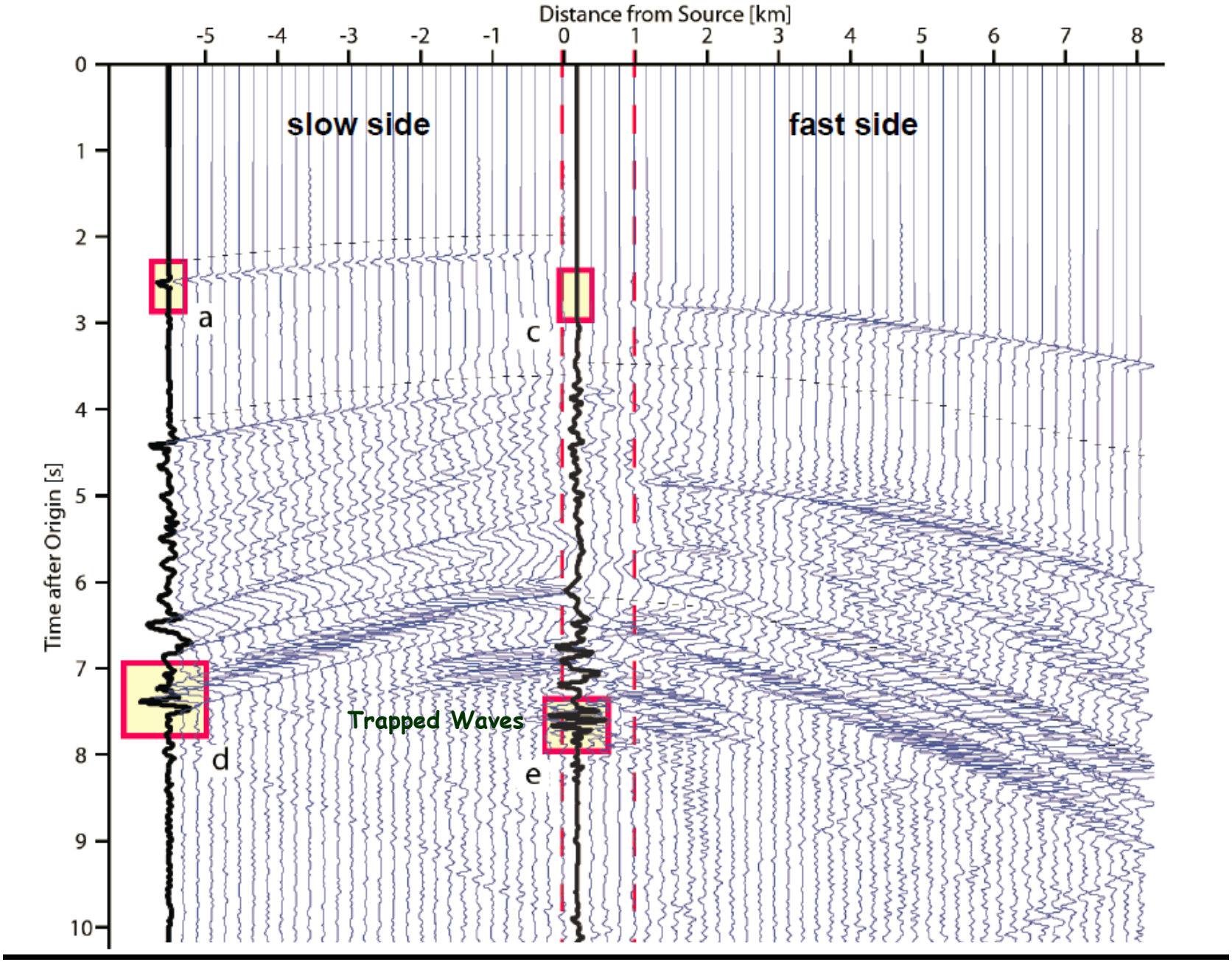

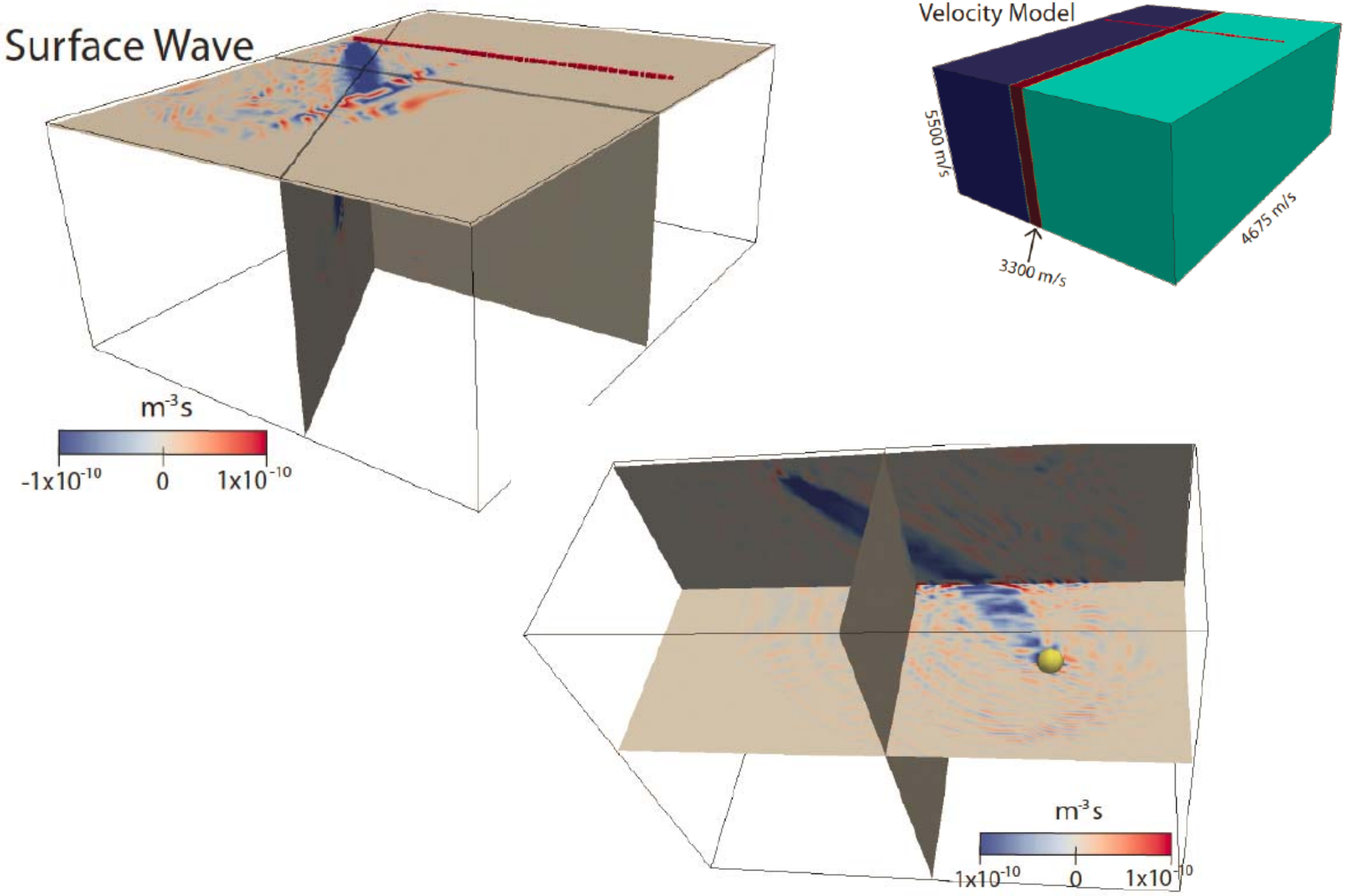
Surface Wave
m-3s
-1x10-10
0
1x10-10
Velocity Model
5500 m/s
3300 m/s
4675 m/s
m-3s
-1x10-10
0
1x10-10

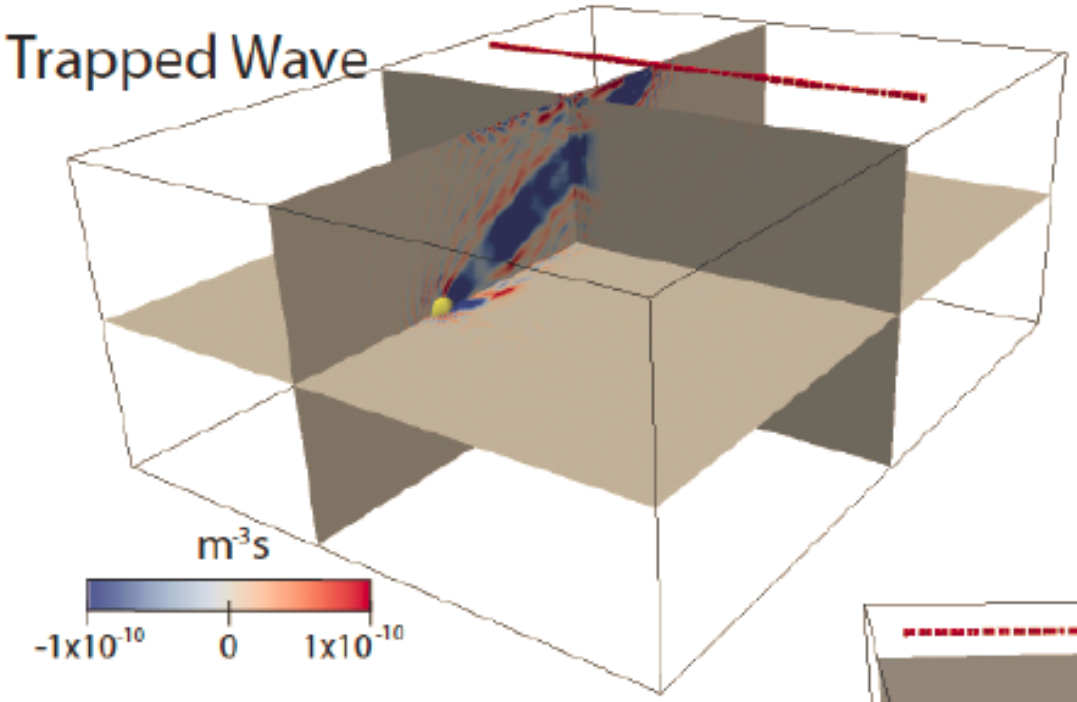

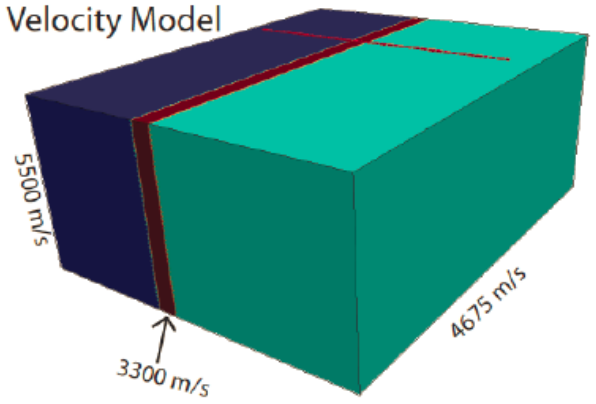

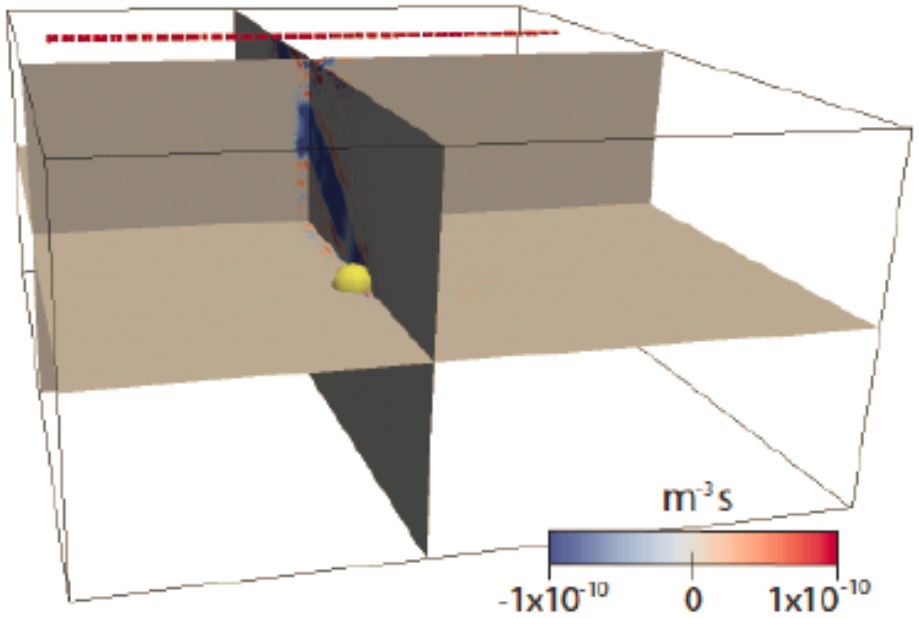

Narrow disk or pancake

Observational results using fault zone head and trapped waves

Ben-Zion and Malin (Sci., 1991)

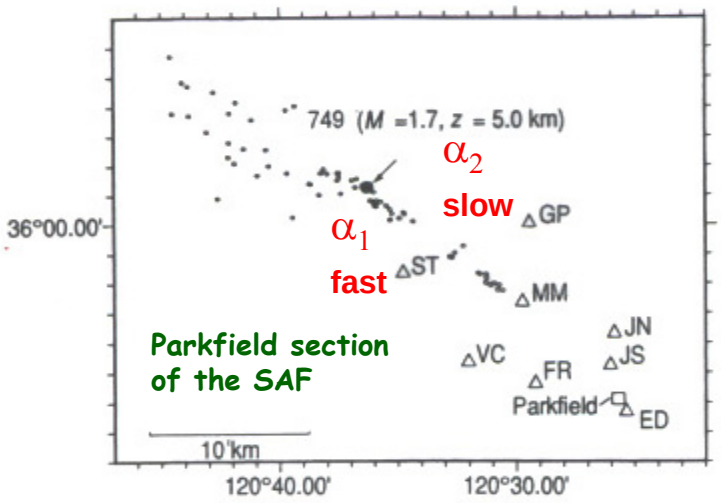

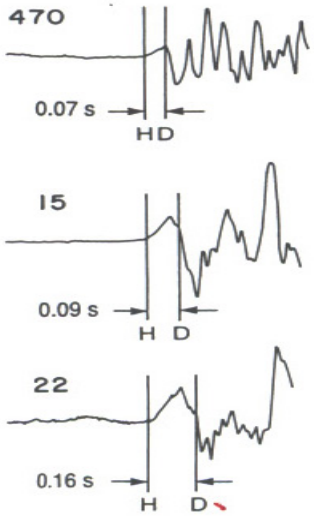

$\Delta t \sim r\,[1/\alpha_2 - 1/\alpha_1] \sim r\,(\Delta\alpha/\alpha^2)$

$X_c = r \tan[\cos^{-1}(\alpha_2/\alpha_1)]$

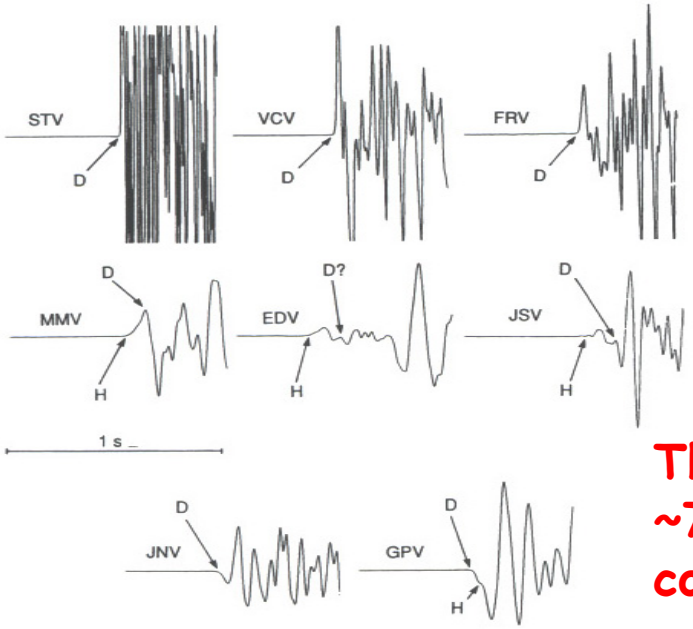

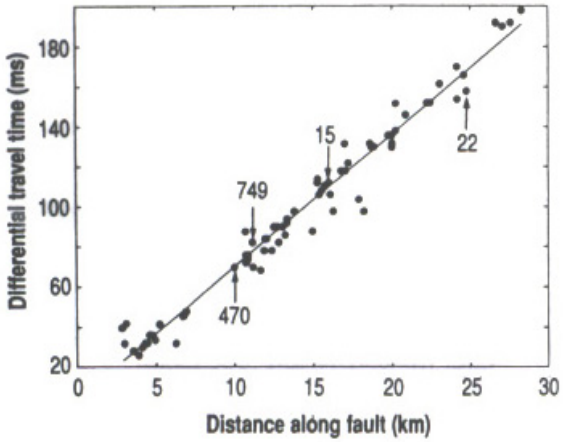

The SAF at Parkfield has a material contrast of ~7% that extends to a depth of ~10 km and is continuous along strike for 10's of km.

Fault Zone Head Waves south of Hollister
(McGuire and Ben-Zion, 2005)

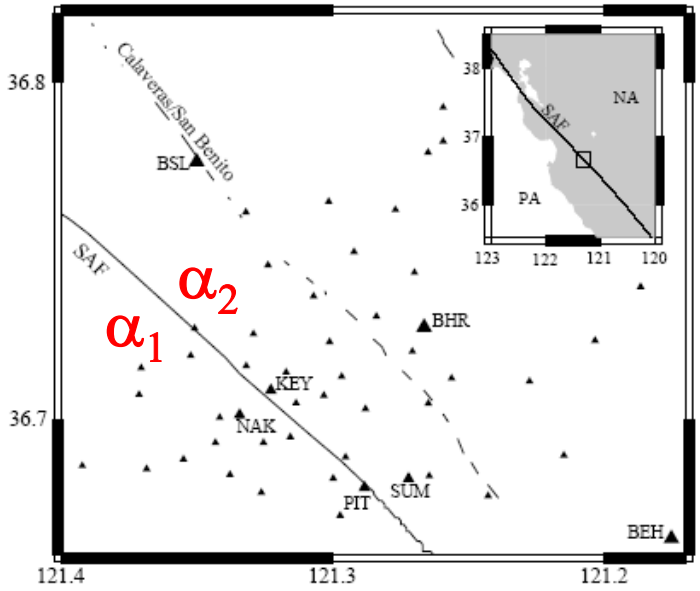

α_2

α_1

$X_c = r \tan [\cos^{-1}(\alpha_2/\alpha_1)]$

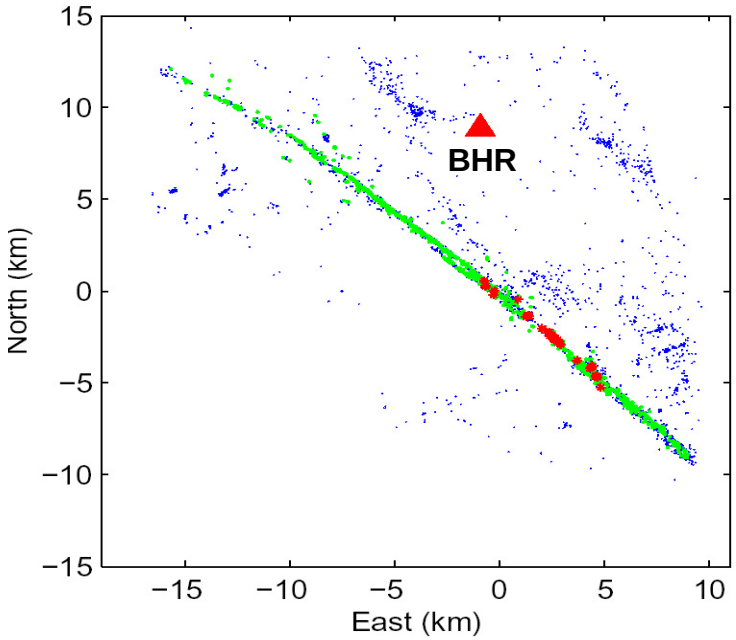

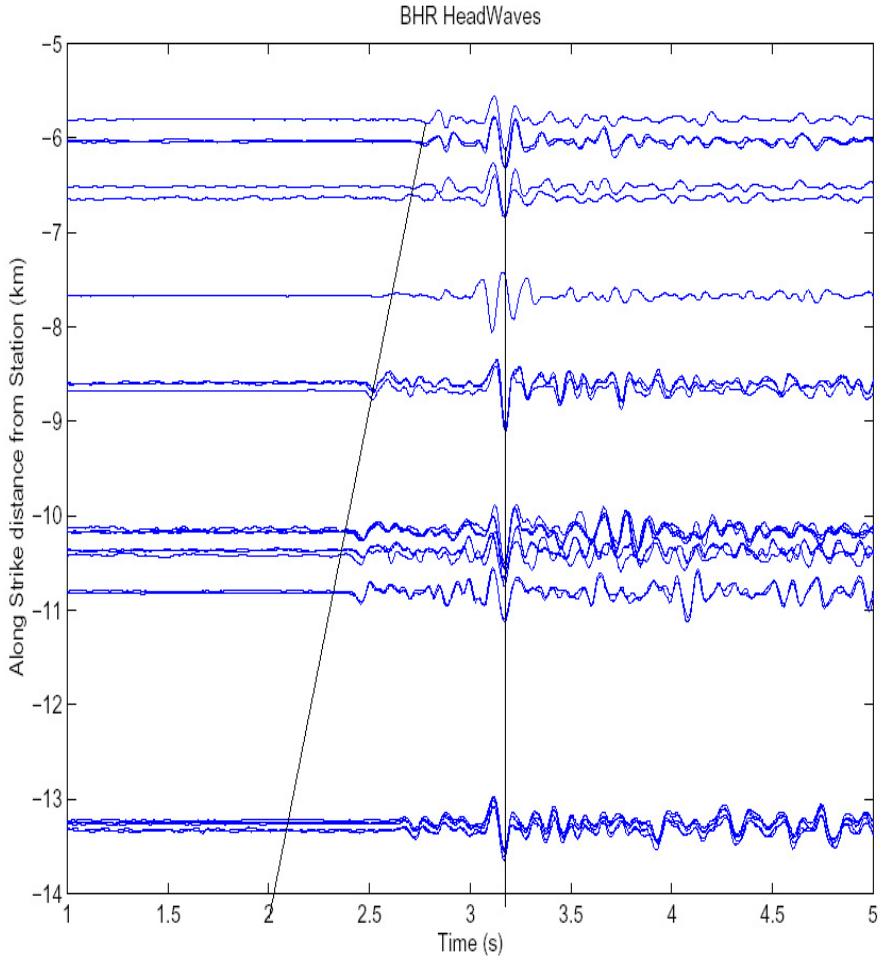

$\Delta t \sim r [1/\alpha_2 - 1/\alpha_1] \sim r (\Delta\alpha/\alpha^2)$

The SAF at this location has average velocity contrast of 10-20% to ~10 km depth

Local Tomography results

Eberhart-Phillips & Michael (1993)

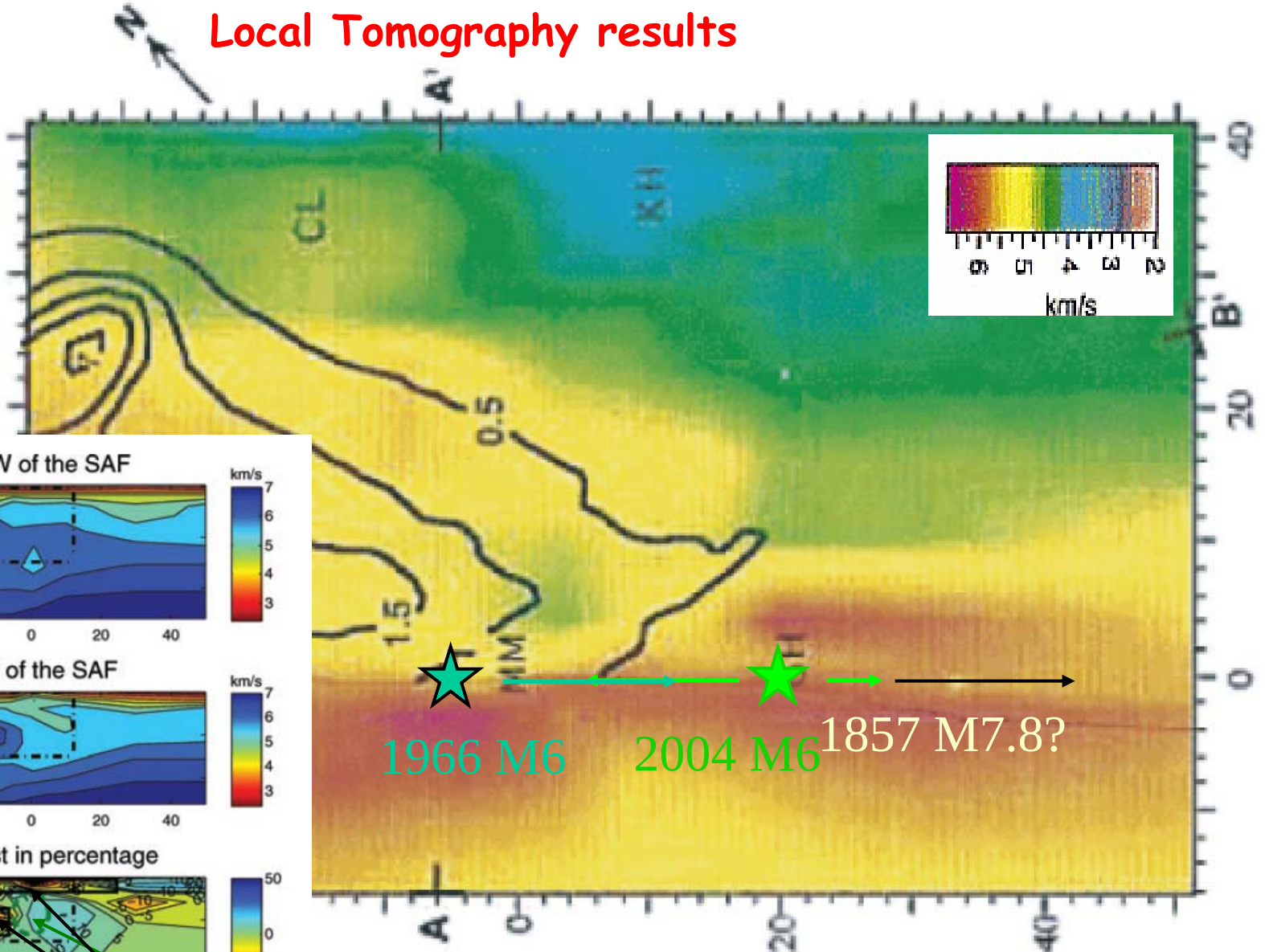

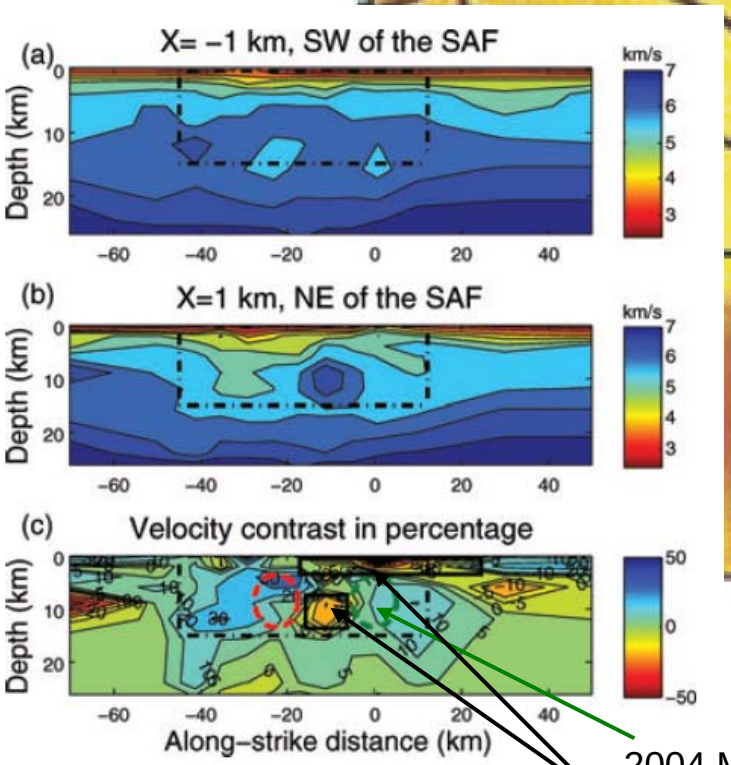

Thurber et al (2006)

2004 M6 velocity contrast reversals

"The previously reported strong wavespeed contrast across the SAF (southwest side fast) is imaged in most places, with the primary exception being the general region of the 2004 Parkfield rupture zone, where a high Vp body is present northeast of the fault."

Zhao et al. (GJI, 2010)

Station to the north

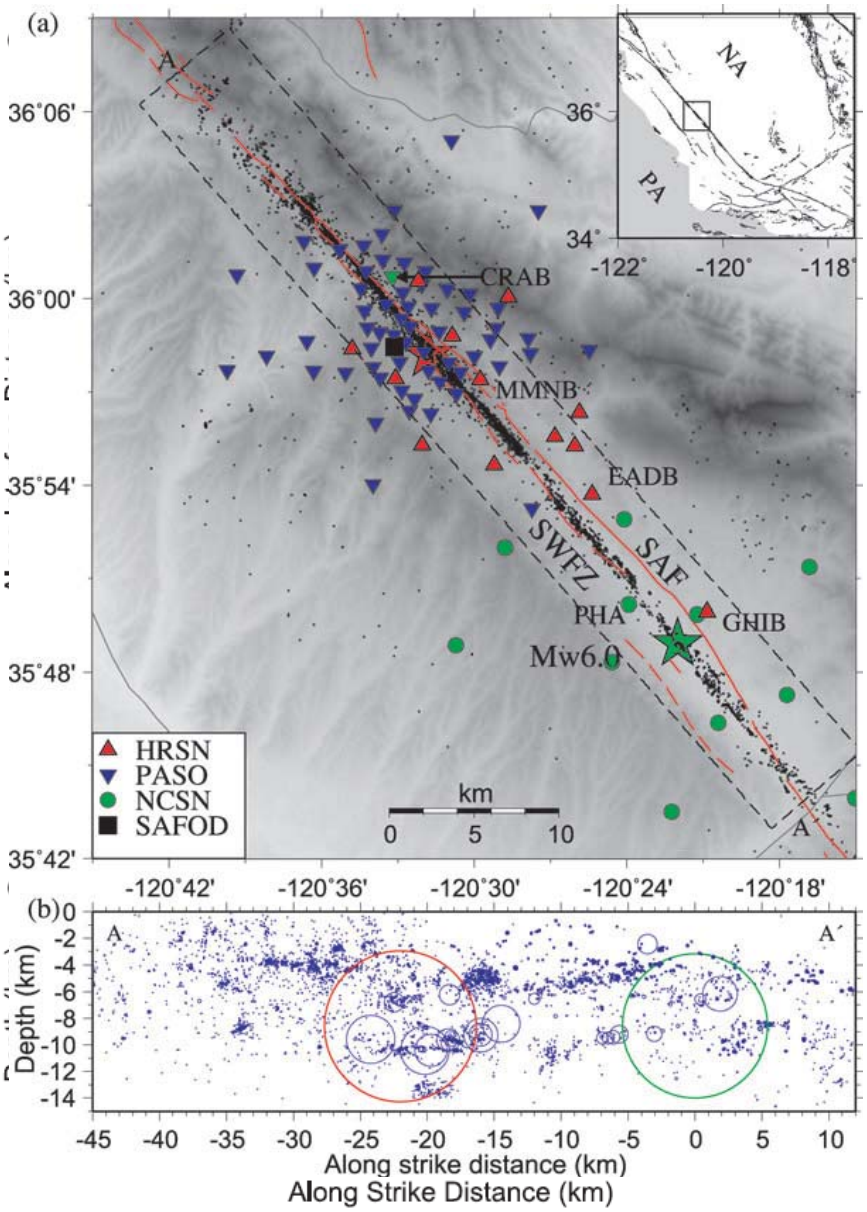

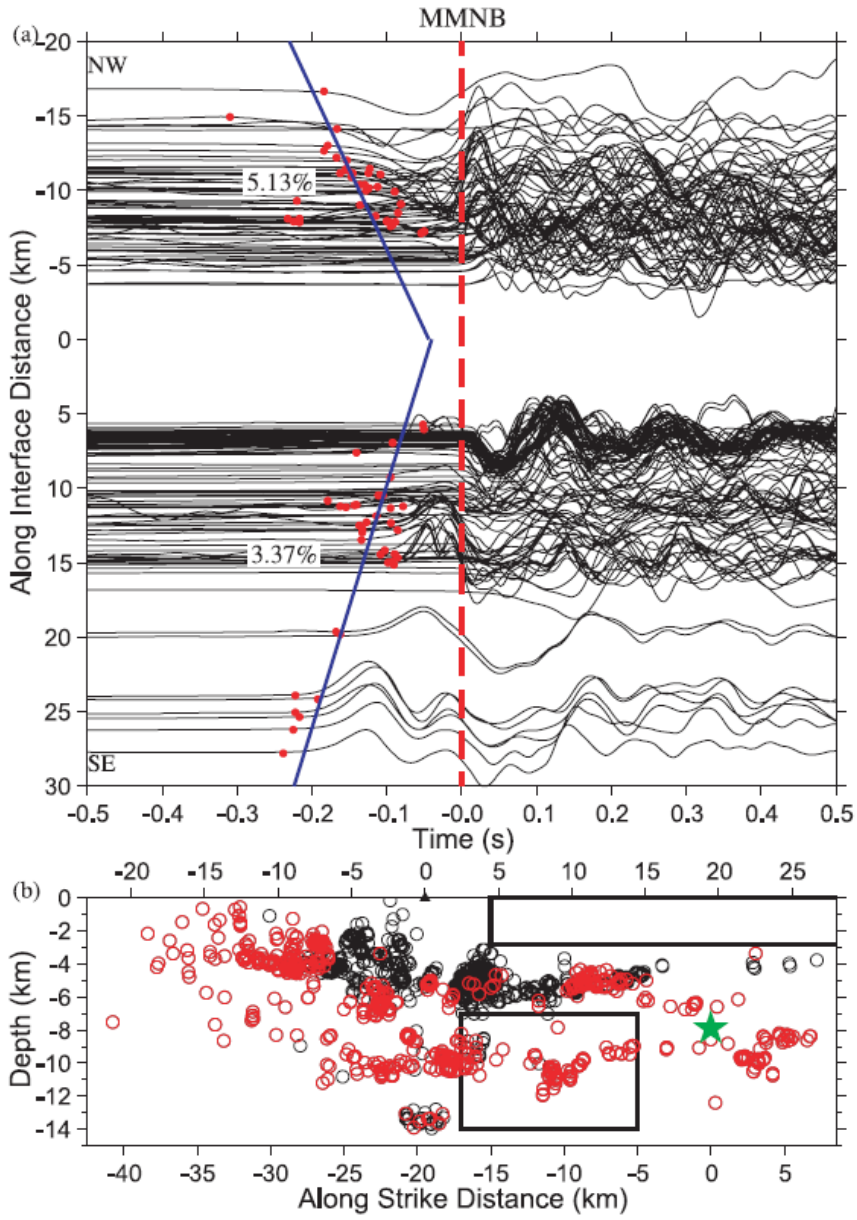

Stations to the south

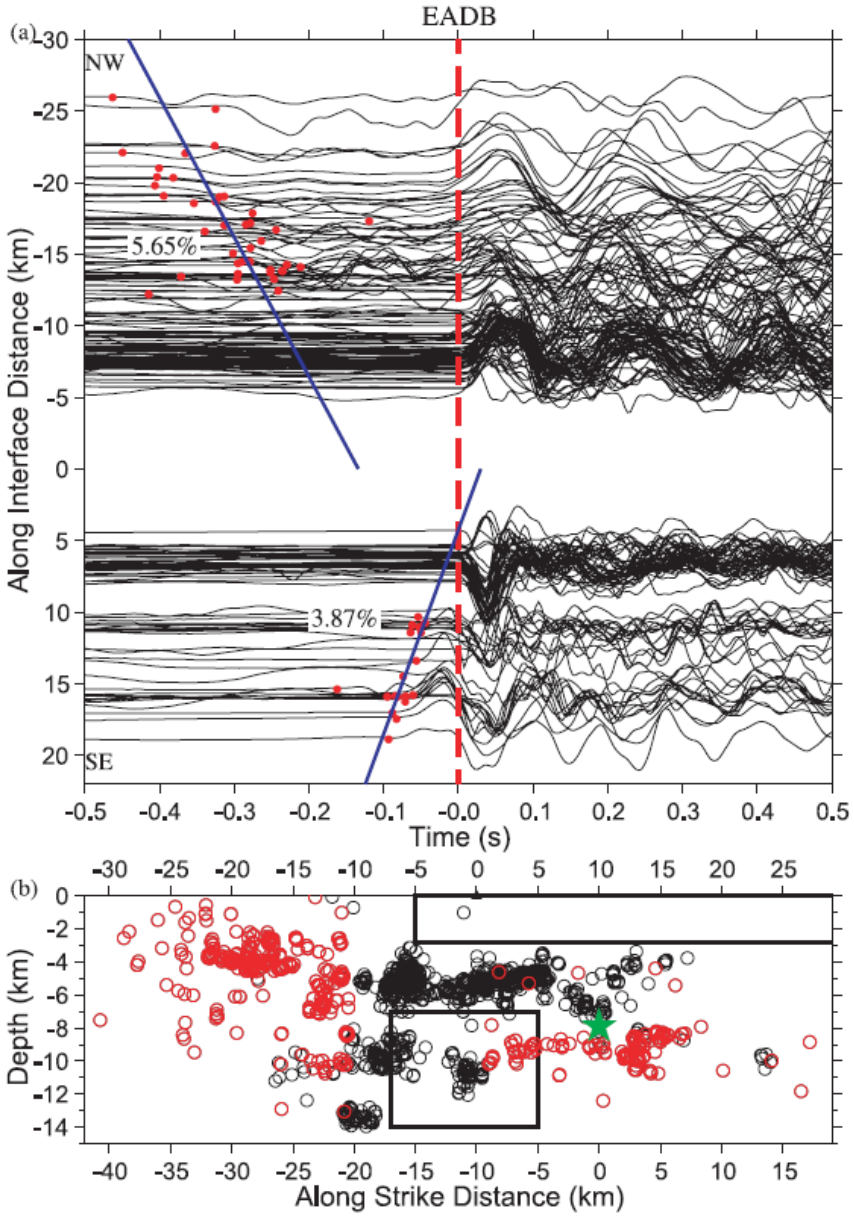

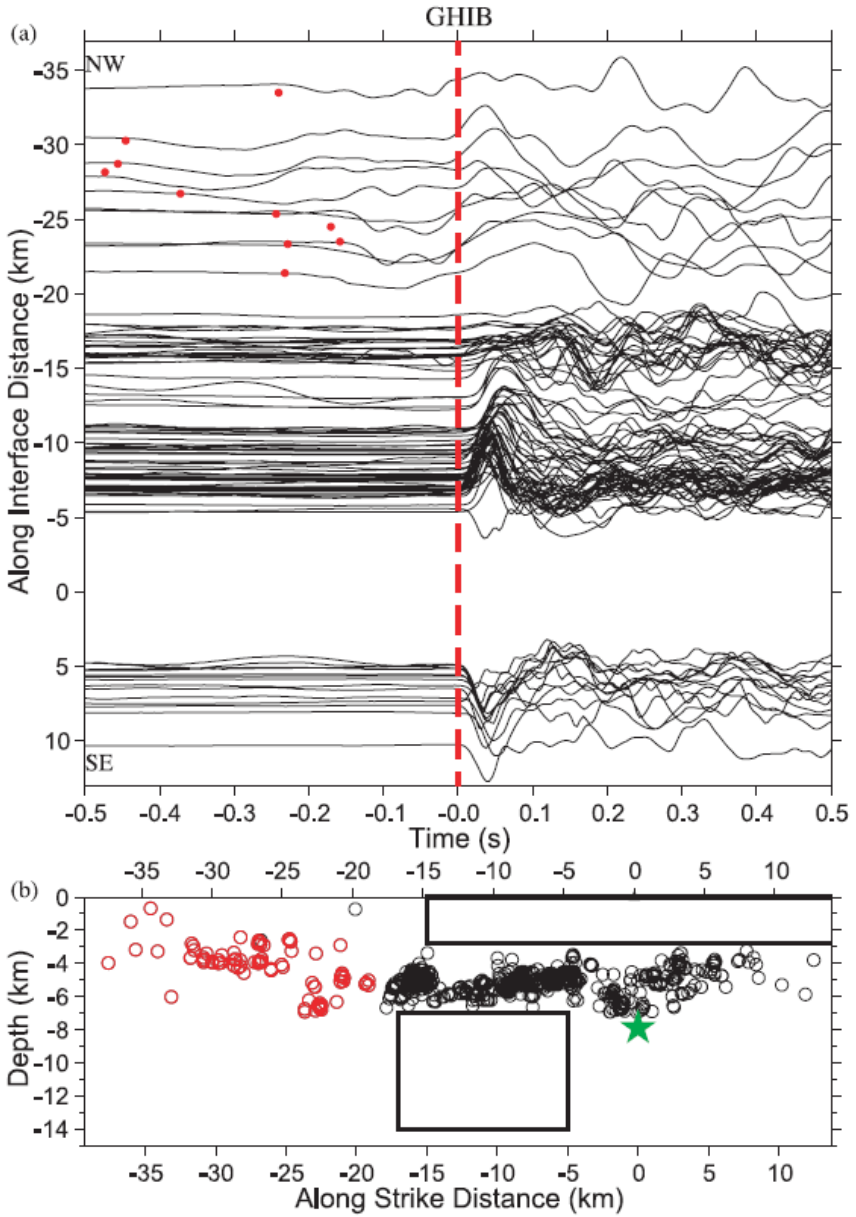

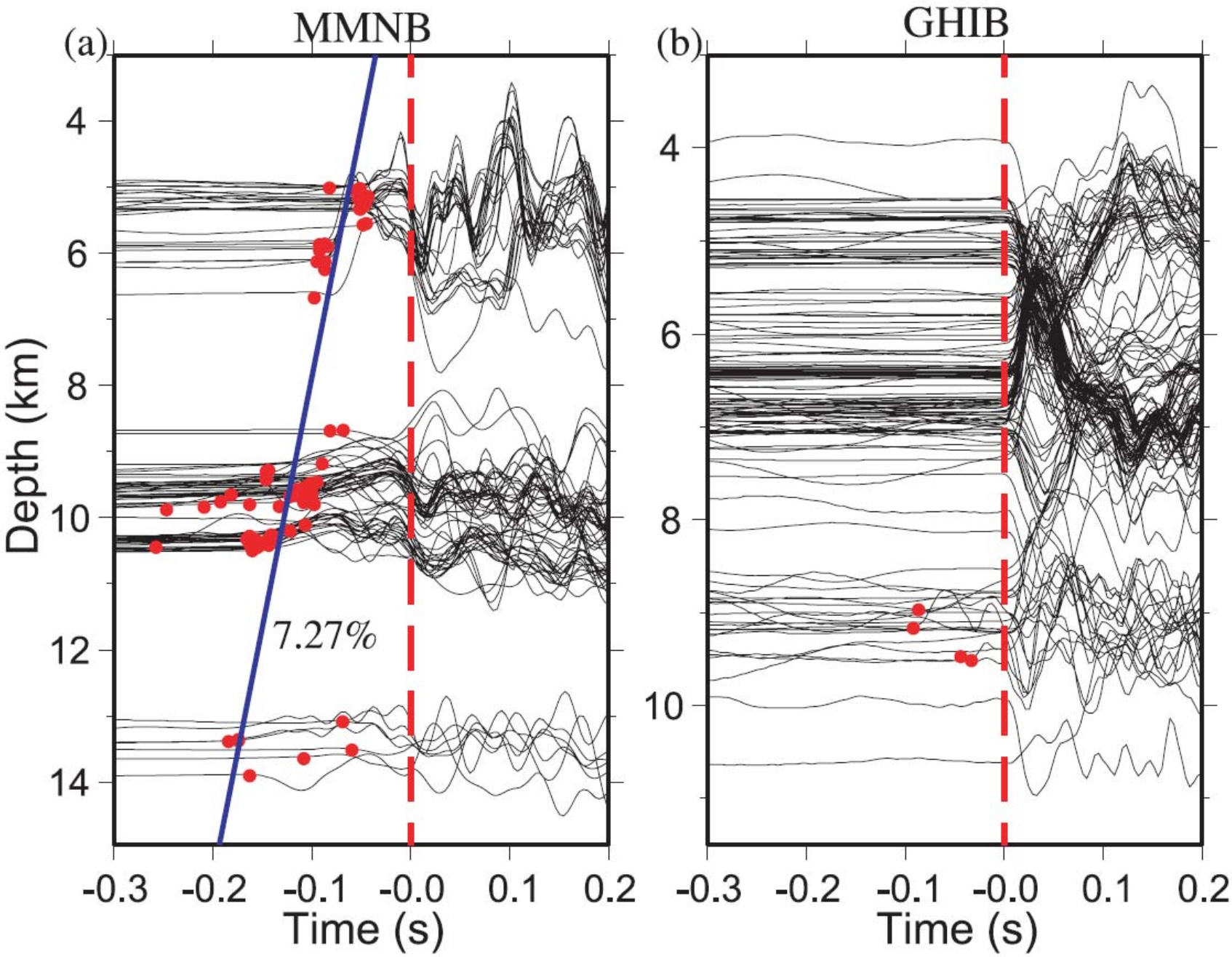
(a)
MMNB
(b)
GHIB
Depth (km)
4
6
8
10
12
14
7.27%
-0.3
-0.2
-0.1
-0.0
0.1
0.2
Time (s)

Evidence for a bimaterial interface along the Mudurnu segment of the North Anatolian Fault Zone from polarization analysis of P waves

Fatih Bulut, Yehuda Ben-Zion and Marco Bohnhoff (EPSL, 2012)

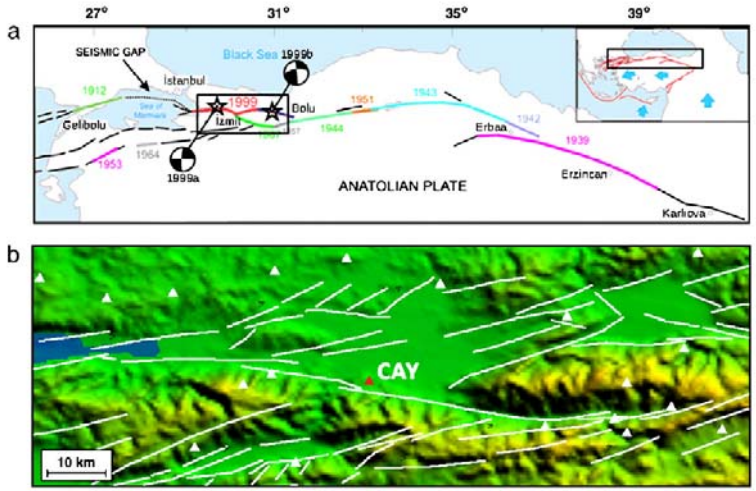

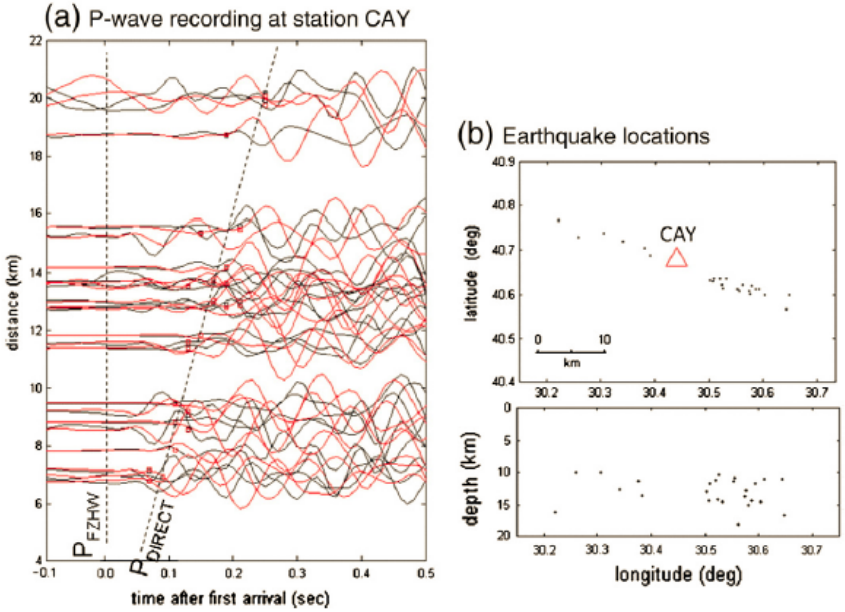

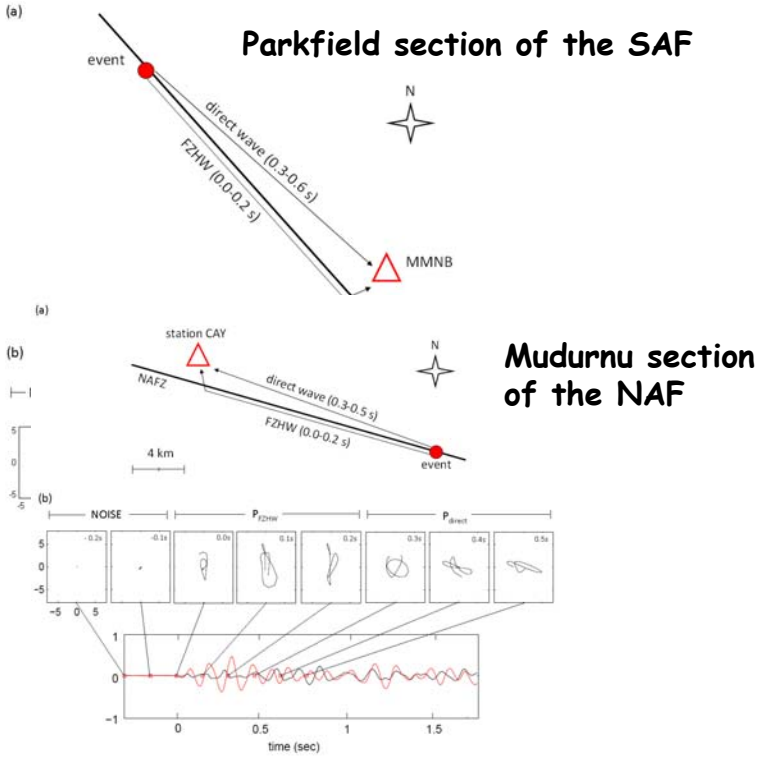

The moveout analysis indicates average velocity contrast of ~6% over the top 15 km of the Mudurnu segment of the NAFZ

Bimaterial interface along the Hayward fault

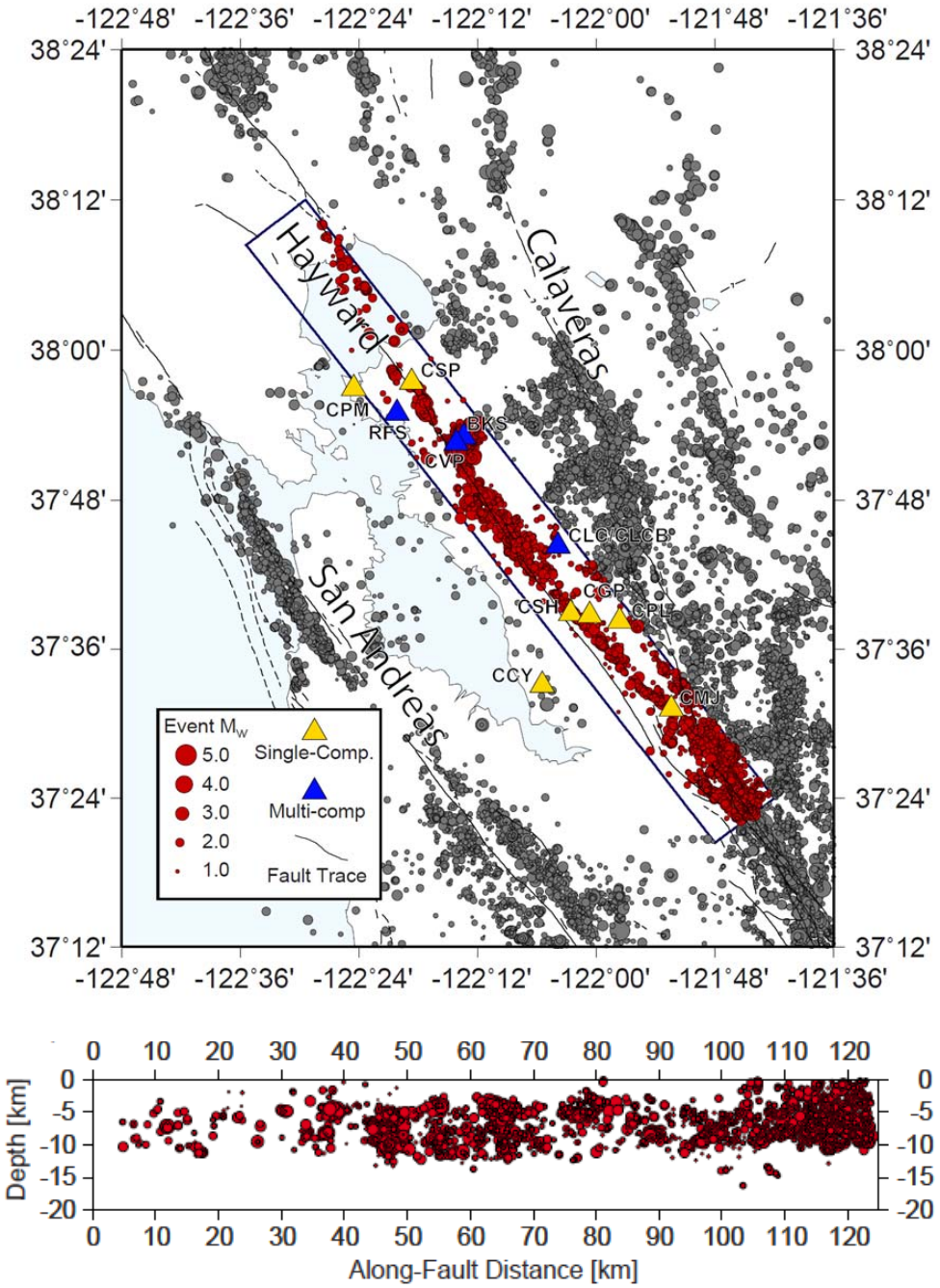

Allam, Ben-Zion & Peng (2013)

- 5834 Events > M_w 1.0
- DD relocated catalog (Waldhauser & Schaff, 2008)
- From 1984-2009
- 9 station on NE side
- 3 stations on SW side
- Wide variety of instruments (broadband, strong motion, single-component, etc…)
- Bandpass 1Hz < X < 15Hz

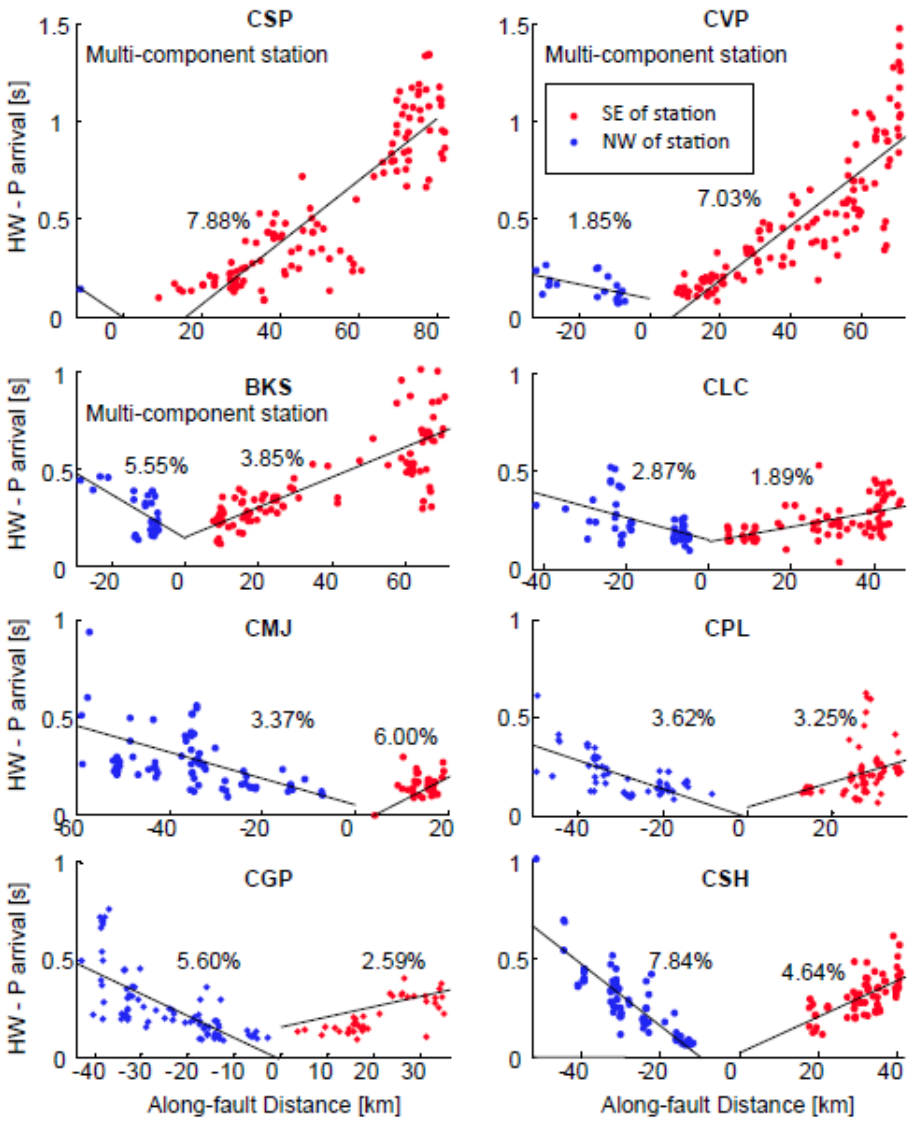

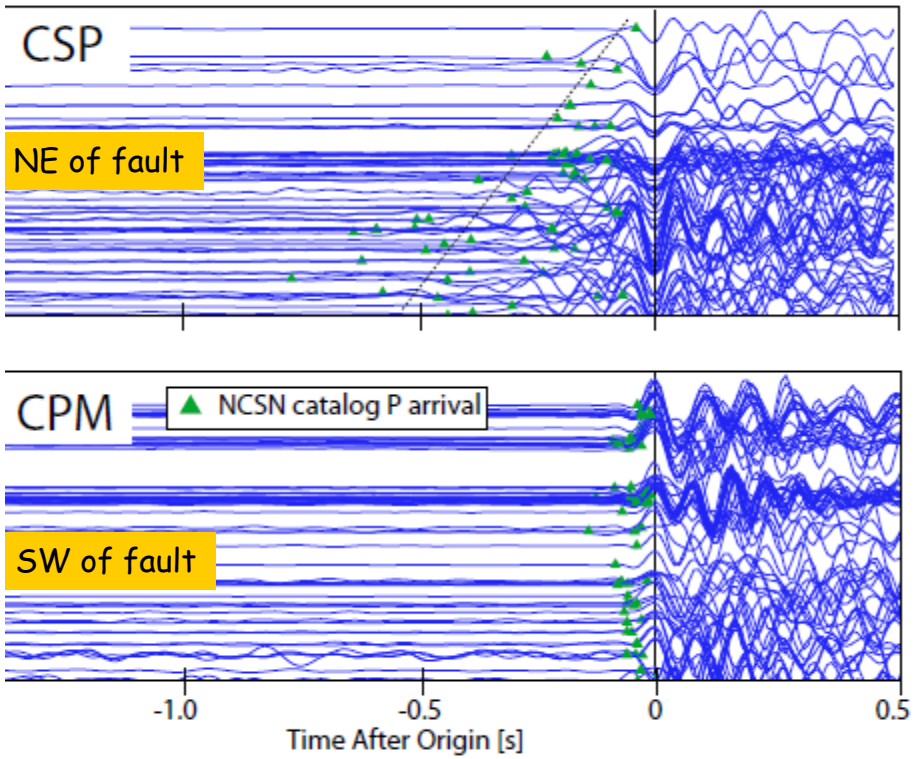

There is a continuous bimaterial interface for ~80km along the Hayward fault with variable velocity contrast

Seismic observations associated with damaged fault zone rocks

(Ben-Zion et al., 03; Peng and Ben-Zion, 04, 05, 06; Wu et al., 09, 10; Lewis & Ben-Zion, 10)

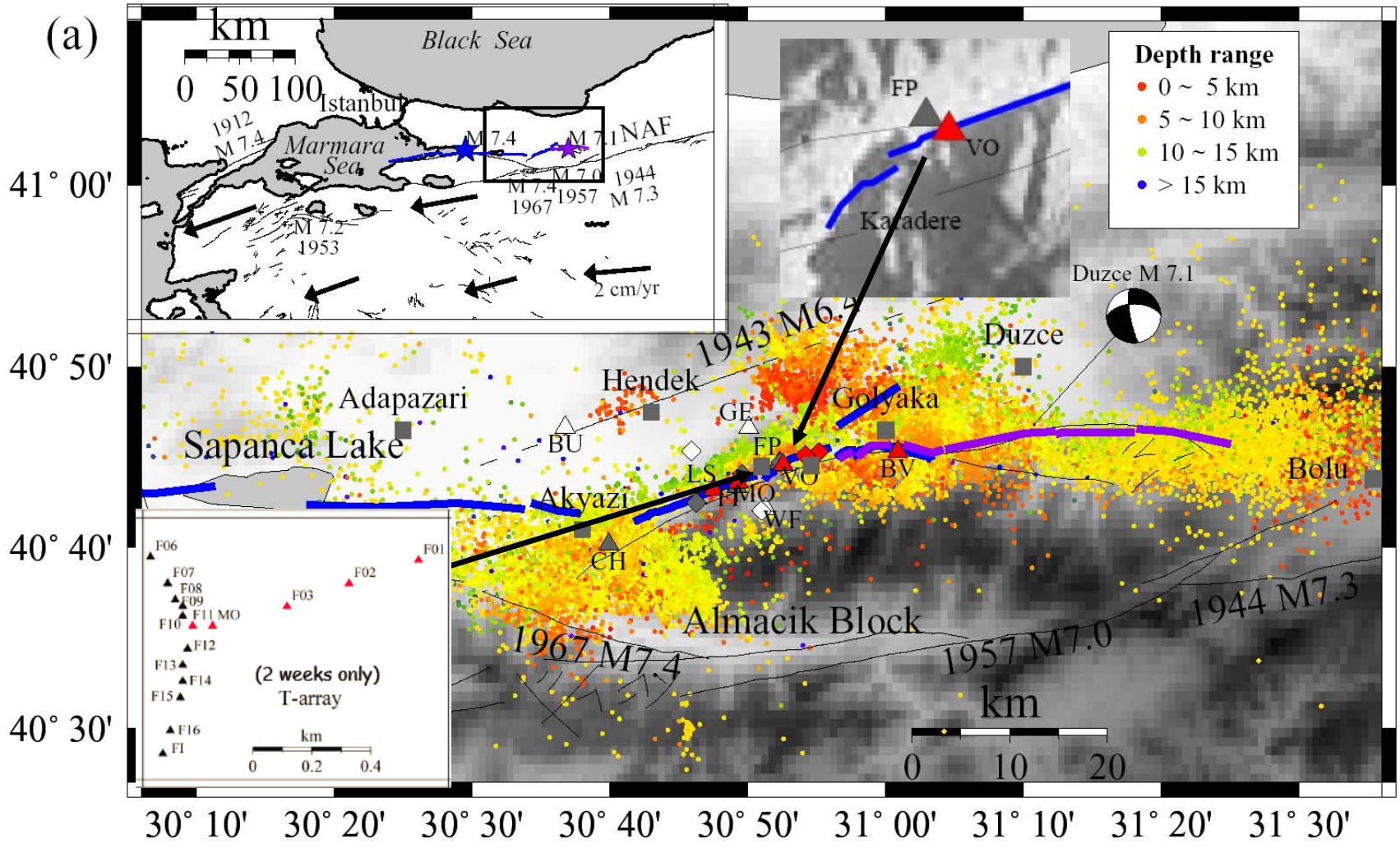

A PASSCAL network along the Karadere-Duzce branch of the NAF recorded ~26000 earthquakes in the 6-months following the 1999 Izmit earthquake

Fault zone trapped waves

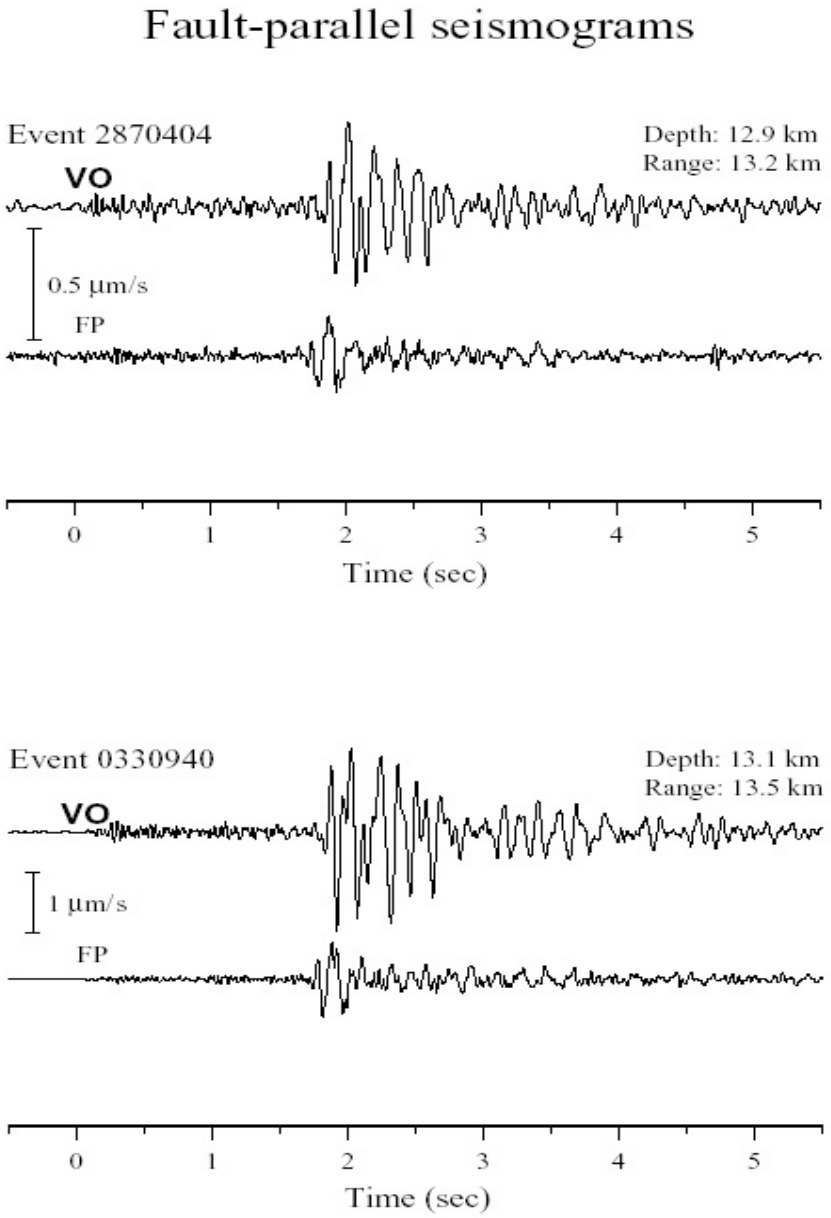

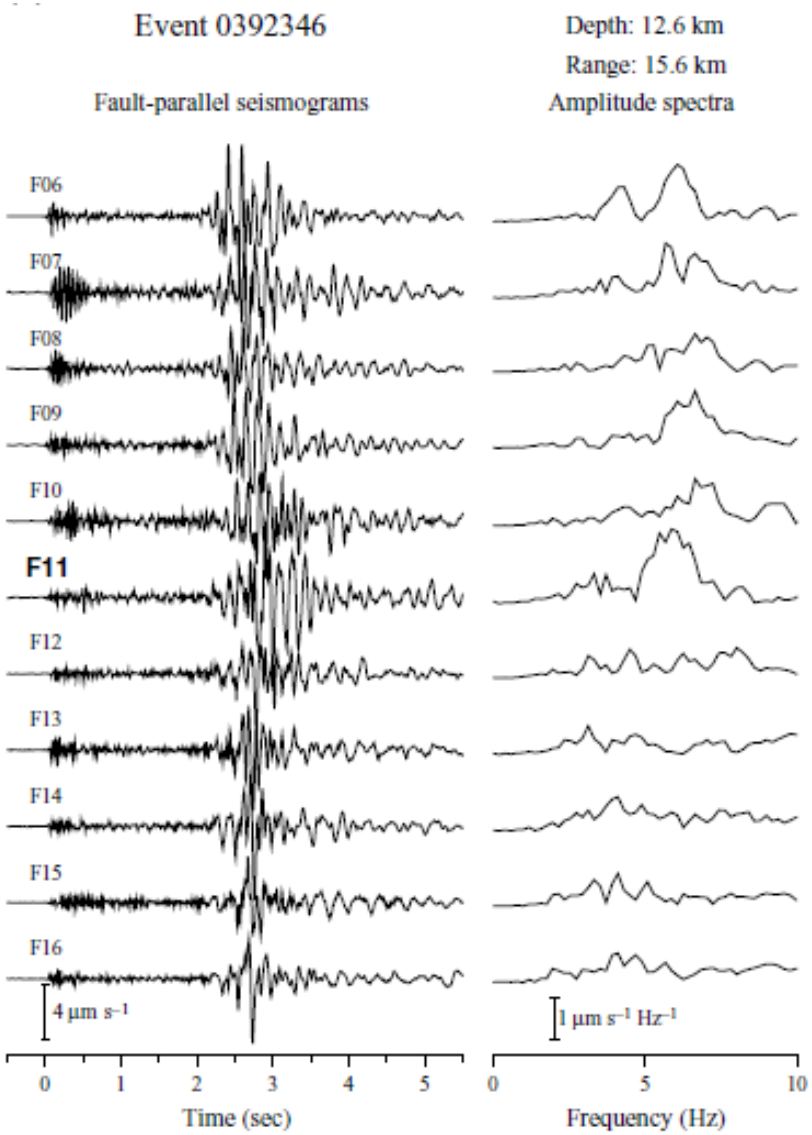

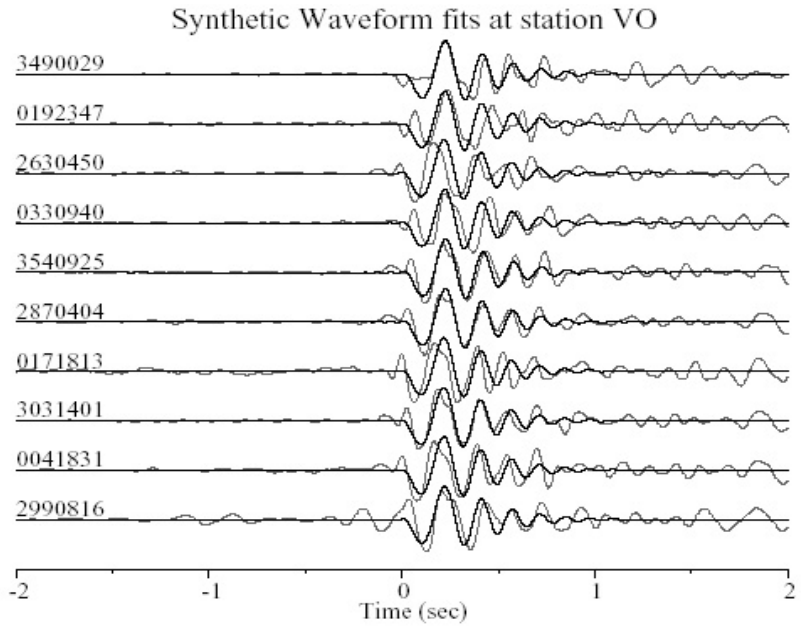

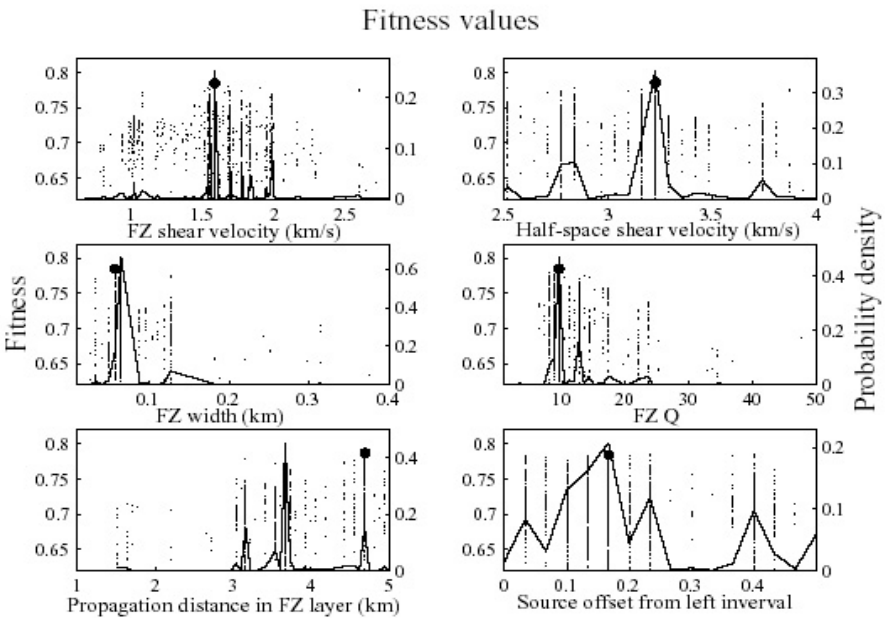

The damaged fault zone layer is most likely characterized by:

width ~75 m,
depth ~3.5 km,
S-wave velocity reduction ~50%,
Q-value ~10.

Similar results are obtained from analyses of trapped waves also at the:

- **Nocera Umbra fault in Italy** (Roveli et al., 2002)
- **Rupture zone of the 1992 Landers, CA, earthquake** (Peng et al., *GJI*, 2003)
- **Trifurcation area of the San Jacinto Fault** (Lewis et al., *GJI*, 2005; Yang and Zhu, 2010)
- **Parkfield section of the San Andreas Fault** (Lewis and Ben-Zion, *GJI*, 2010)
- **Calico fault, ECSZ, CA** (Yang et al., 2011)

Analyses of subsets of data imply strong along-strike variations and discontinuities of the trapping structures! (Lewis & Ben-Zion, GJI, 2010)

Rupture zone of the 1992 Landers, CA, earthquake (Peng et al., *GJI*, 2003)

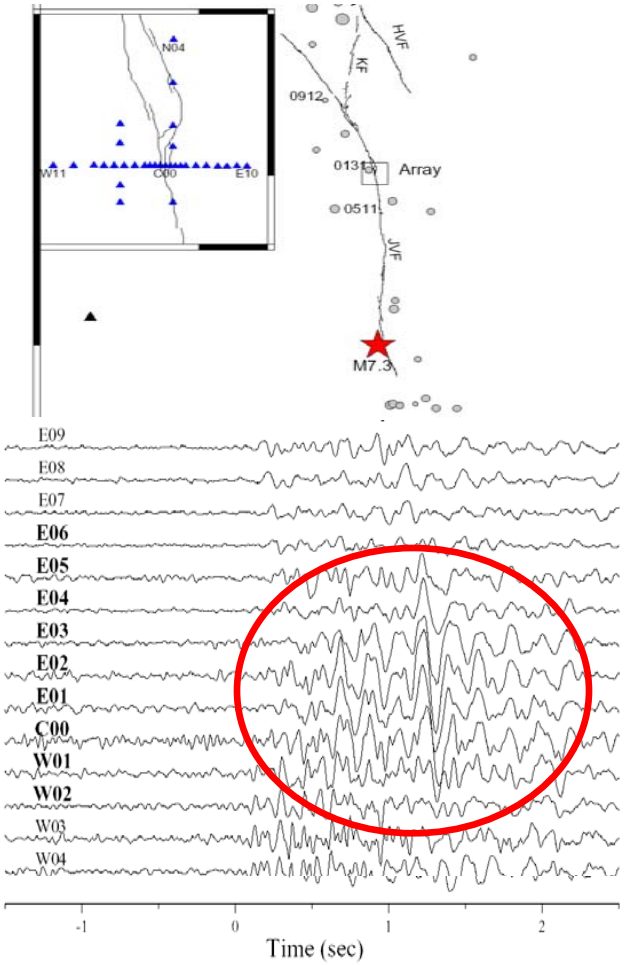

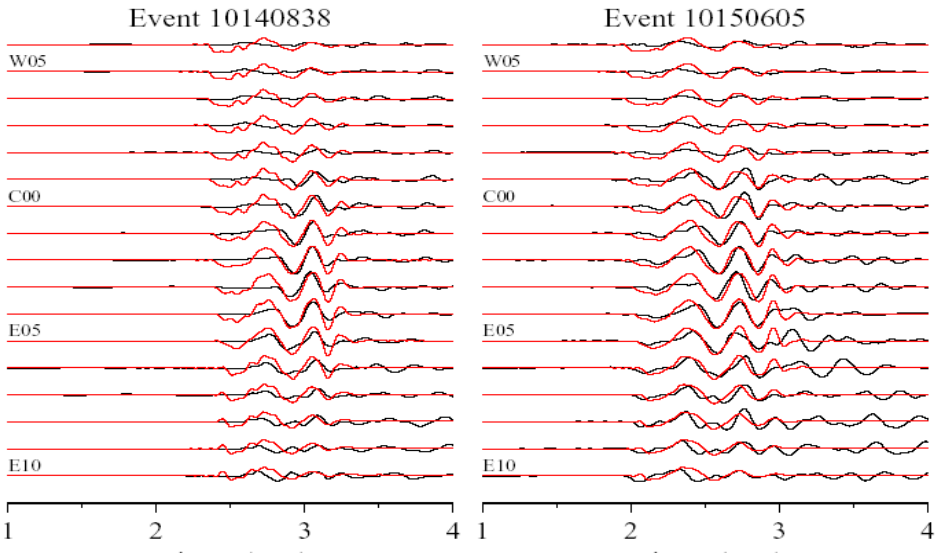

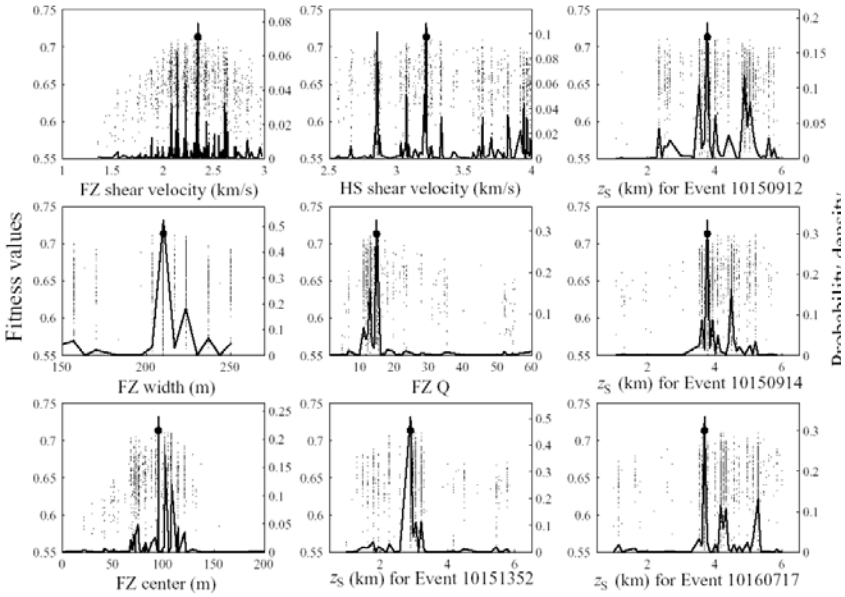

Most likely damage zone parameters:

width ~200 m,
depth ~3.5 km,
S velocity reduction ~50%,
Q-value ~15.

Trifurcation area of the San Jacinto fault zone (Lewis et al., *GJI*, 2005)

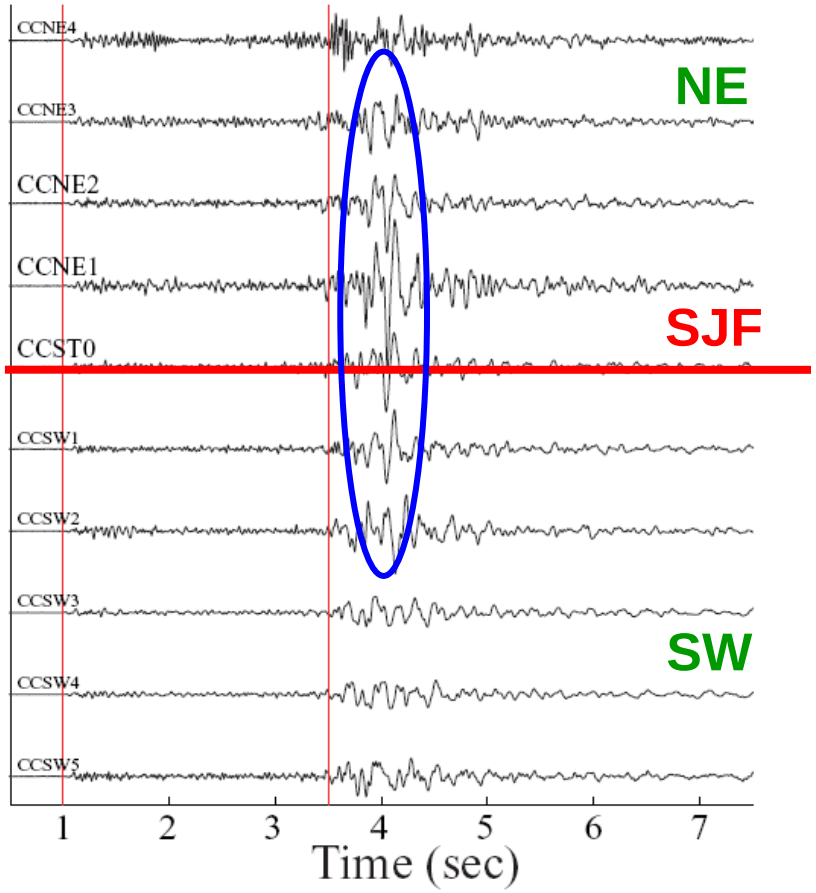

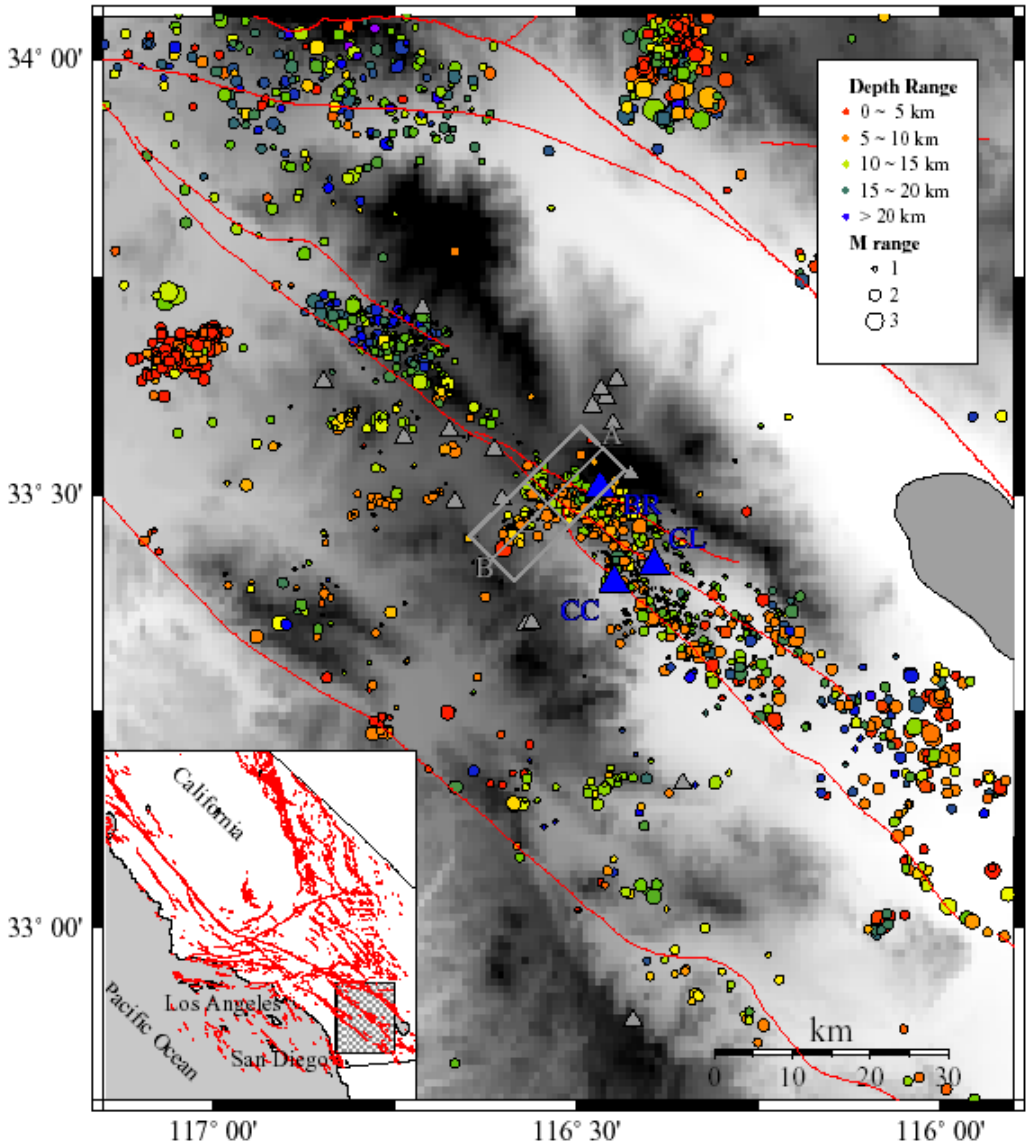

Most likely damage zone parameters:
width ~125 m,
depth ~3.5 km,
S velocity reduction ~40%,
Q-value ~30.

The da
seismic
direction of ruptures on a bimaterial interface in the core structure of the SJF.

Expected damage patterns generated by many earthquakes

Dynamic rupture on a frictional fault with off-fault plastic yielding

Homogenous solid

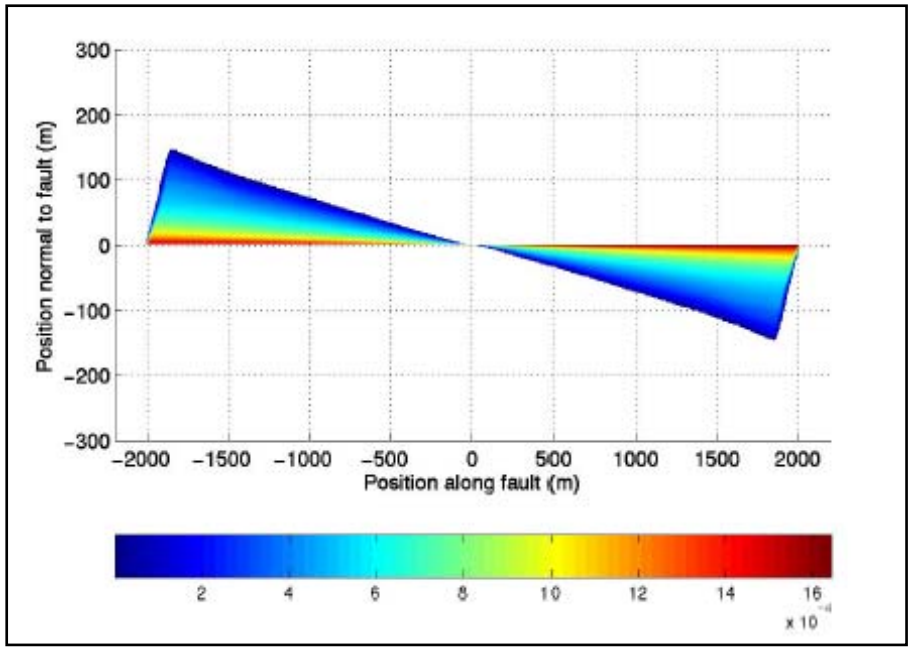

Andrews, 2005

Bimaterial

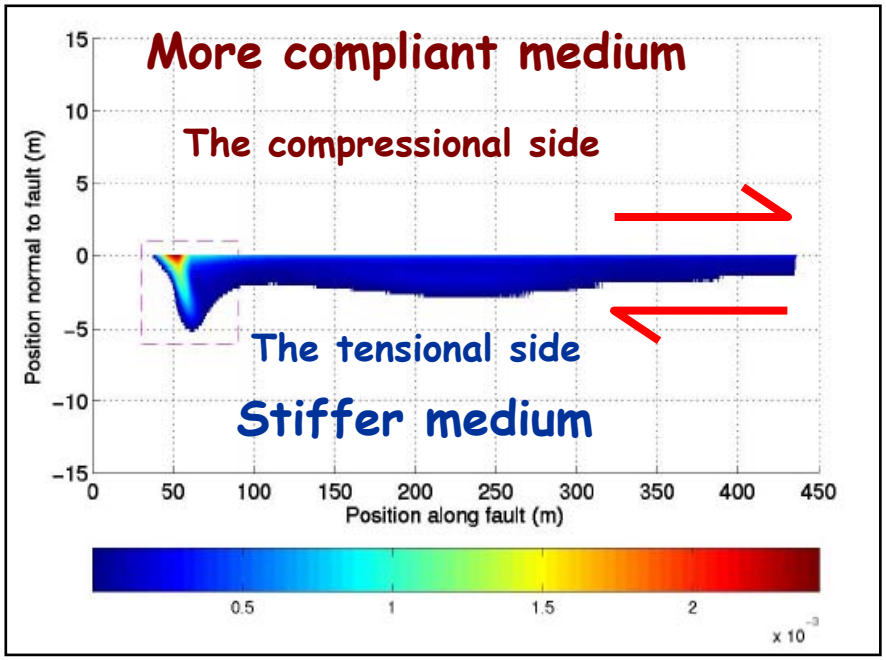

Ben-Zion and Shi, 2005

Analyses of seismic fault zone waves and geological data in several large structures show strongly asymmetric damage zones, as expected for ruptures along a bimaterial interface
(Lewis et al. 2005, 07; Dor et al. 06, 08; Wechsler et al. 09; Mitchell et al. 2011; Rempe et al. 2013)

Geological mapping of rock damage in large fault zones

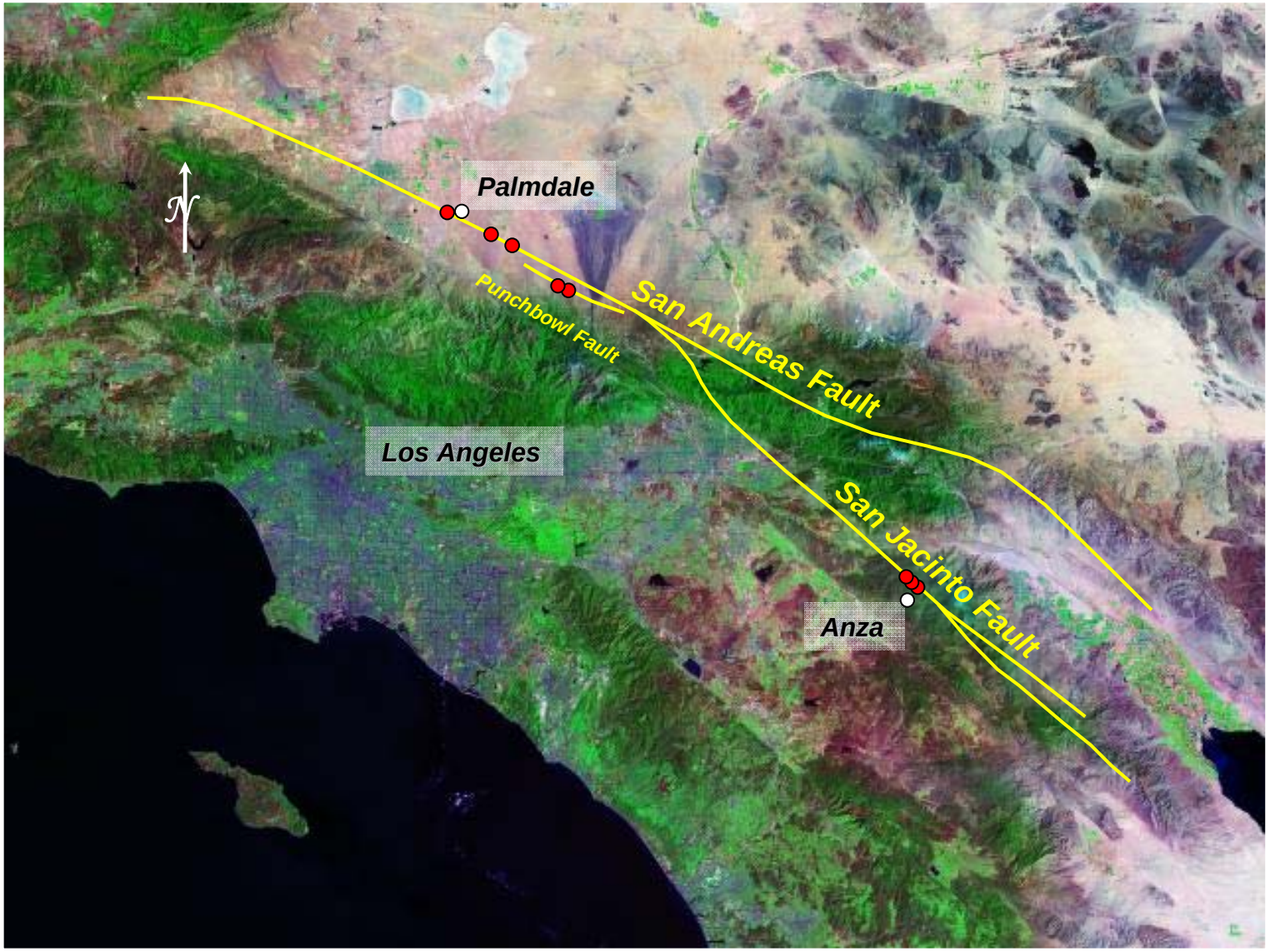

Dor, Ben-Zion, Rockwell, Brune (PAGEOPH, 2006, EPSL, 2006)

SJF near Anza

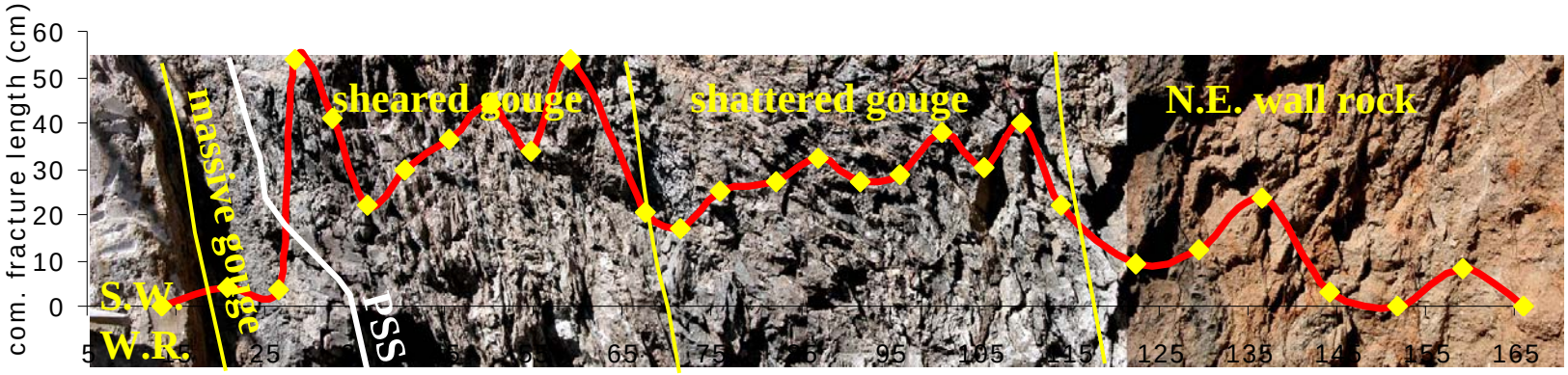

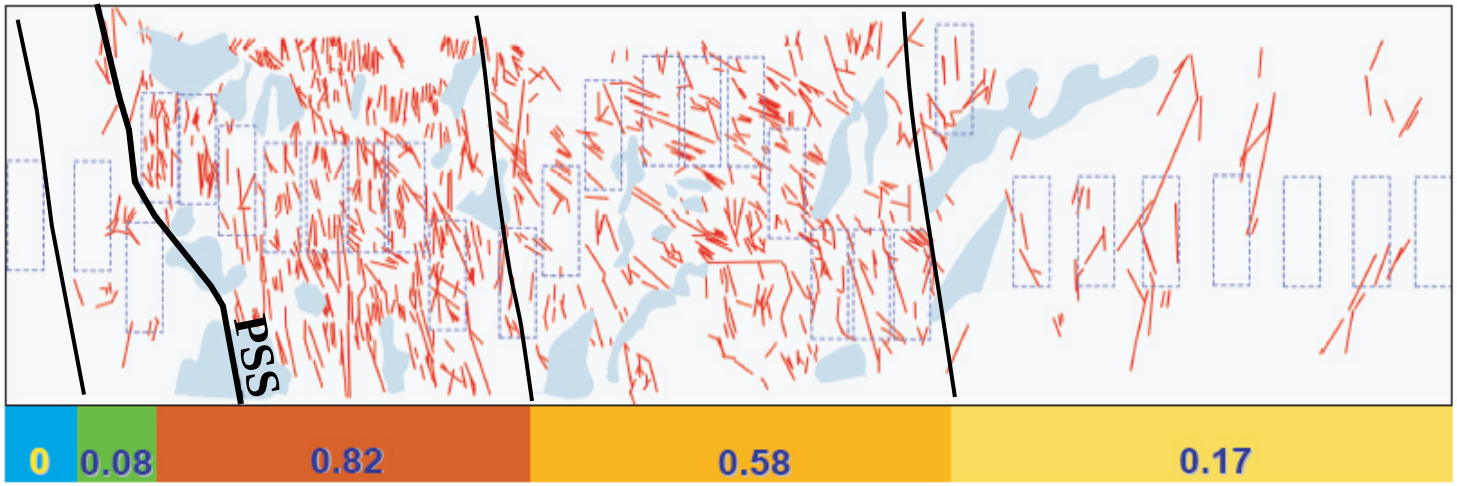

Gouge scale ~1m

Dor et al. (PAGEOPH, 2006)

SAF near Palmdale

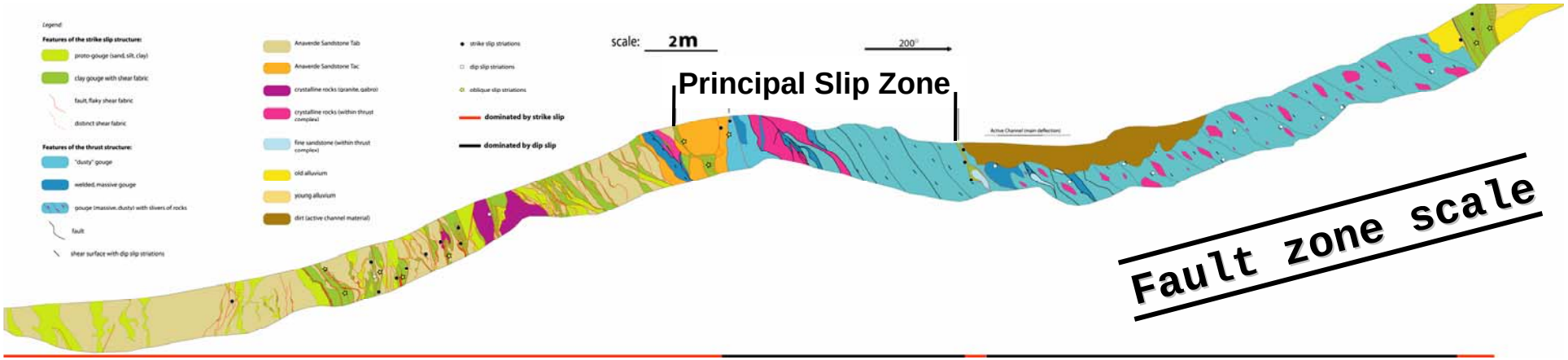

Dor et al., PAGEOPH, 2006

Pulverized rocks in the Mojave section of the SAF

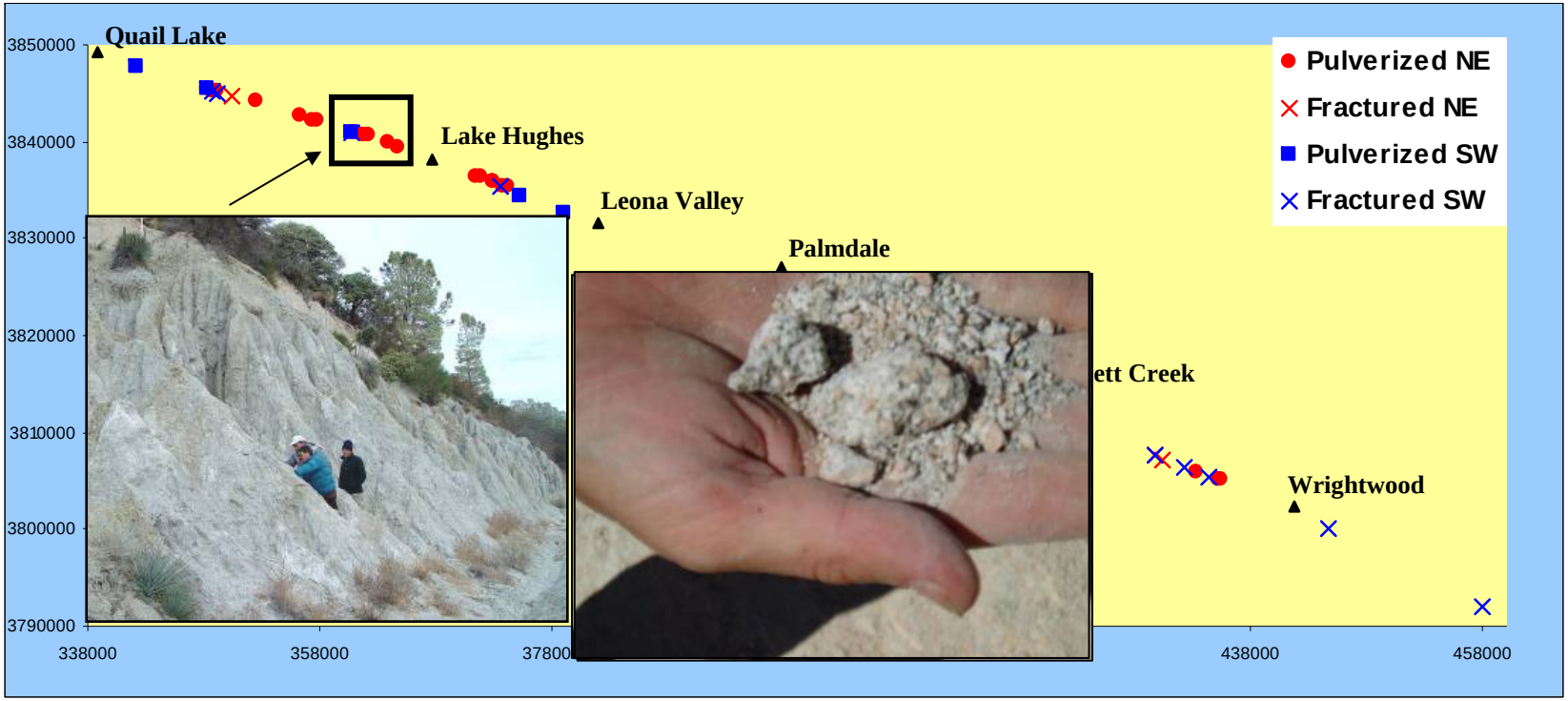

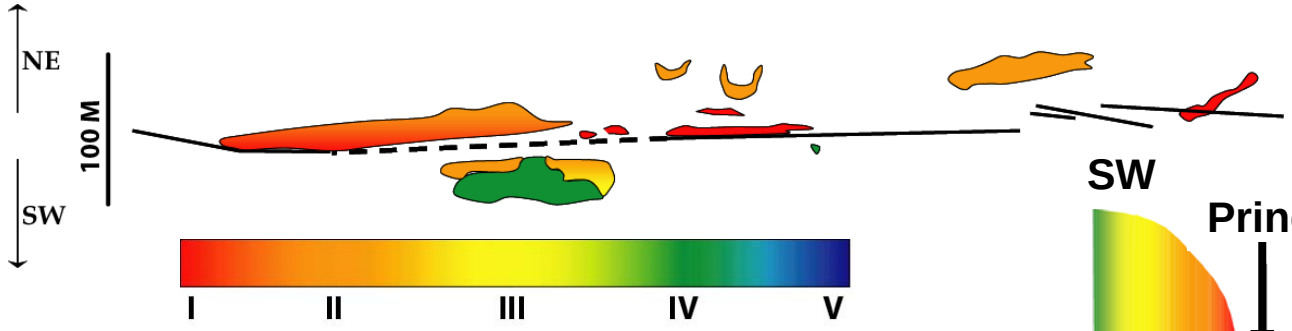

Damage intensity scale

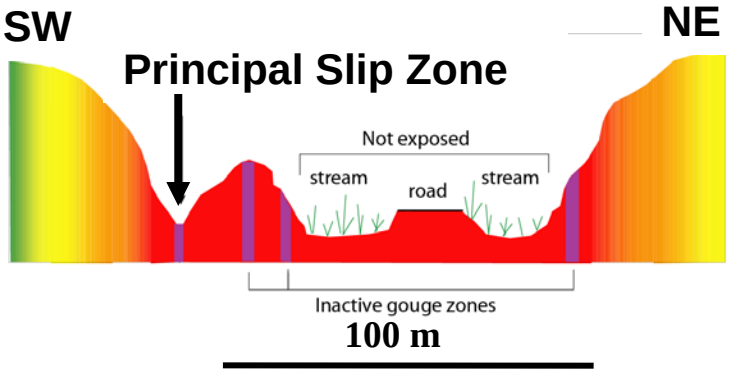

Dor et al., EPSL, 2006

4D analysis of anisotropy and scattering along the Karadere-Duzce branch of the NAF (Peng and Ben-Zion, 2004, 2005, 2006)

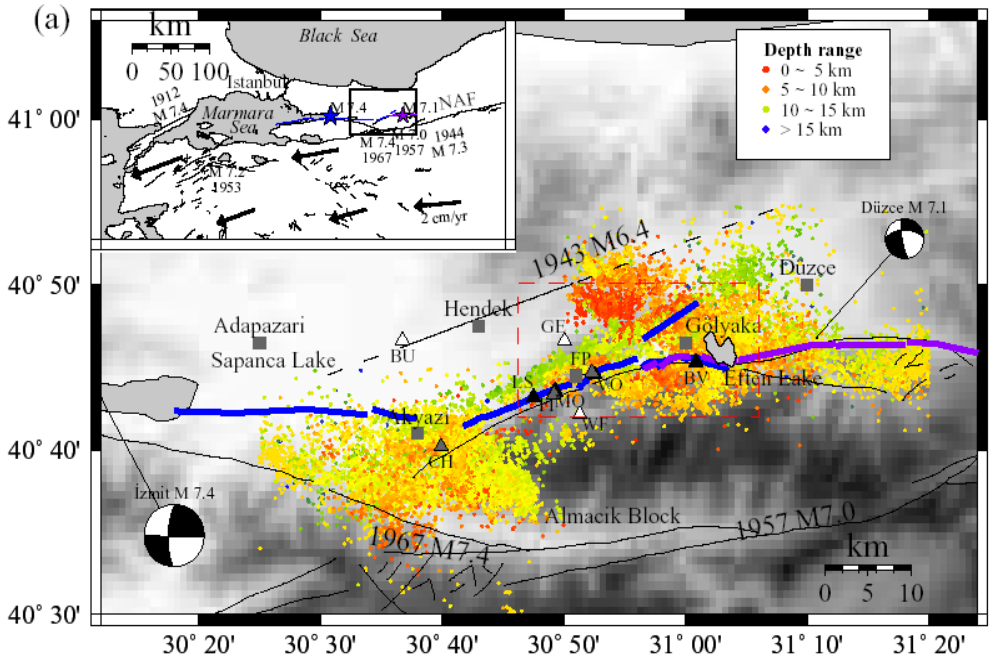

cluster C04, station FP

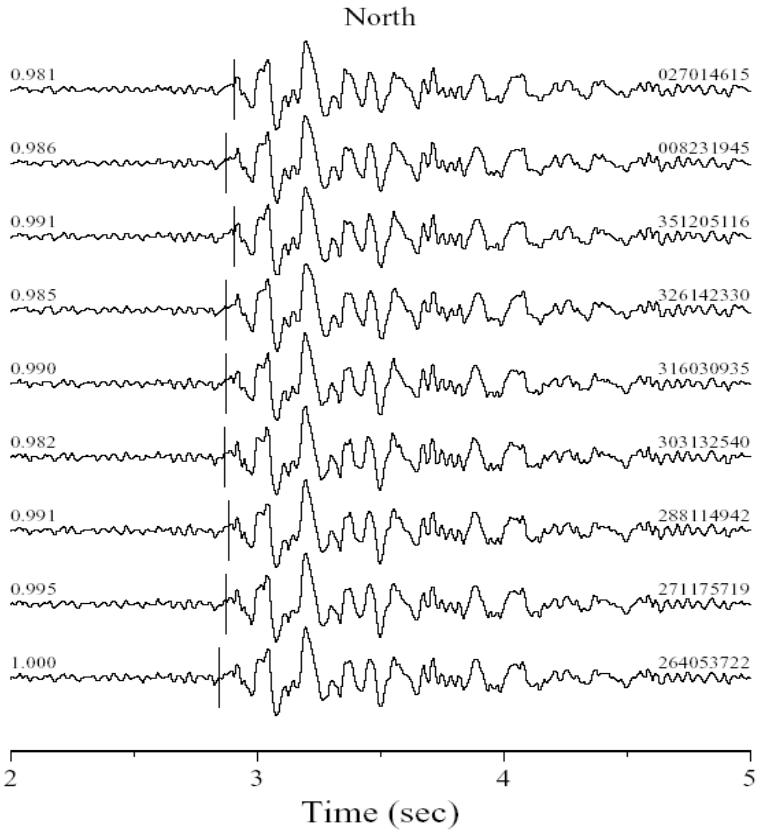

Temporal changes of delay times based on evolving de-correlation analysis

(Peng and Ben-Zion, 2006)

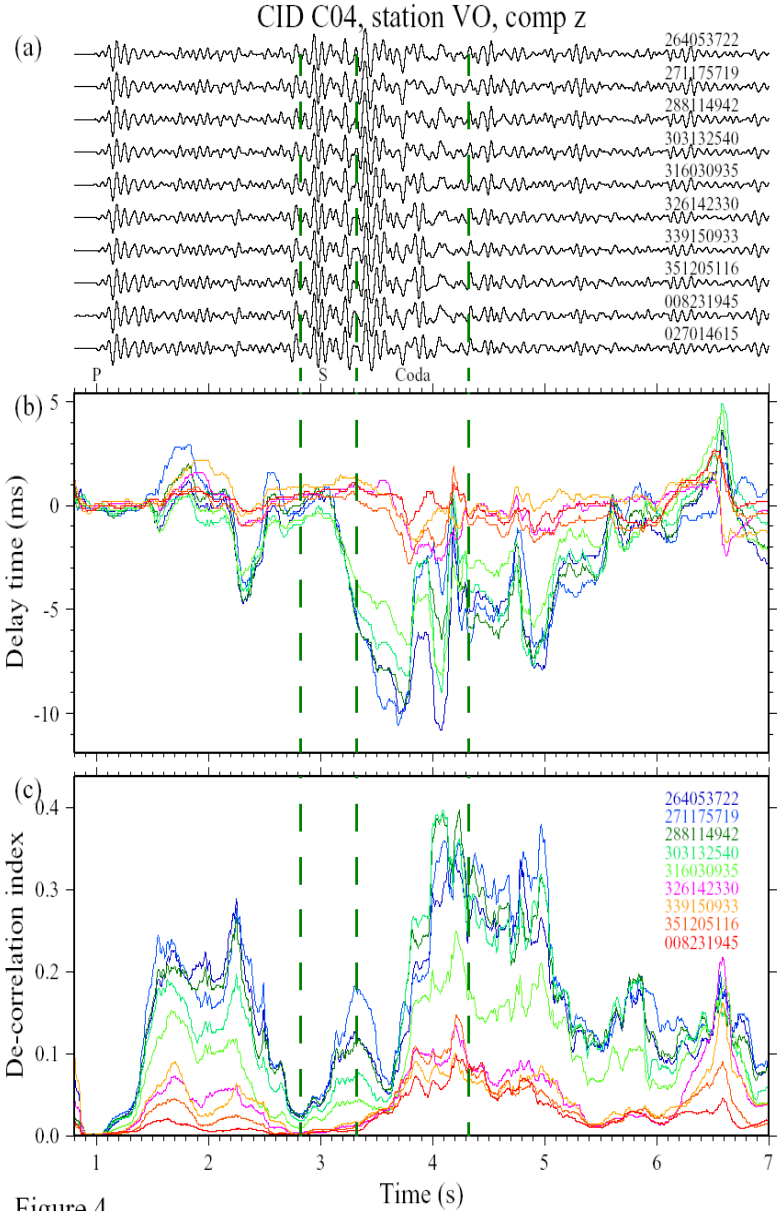

Figure 4

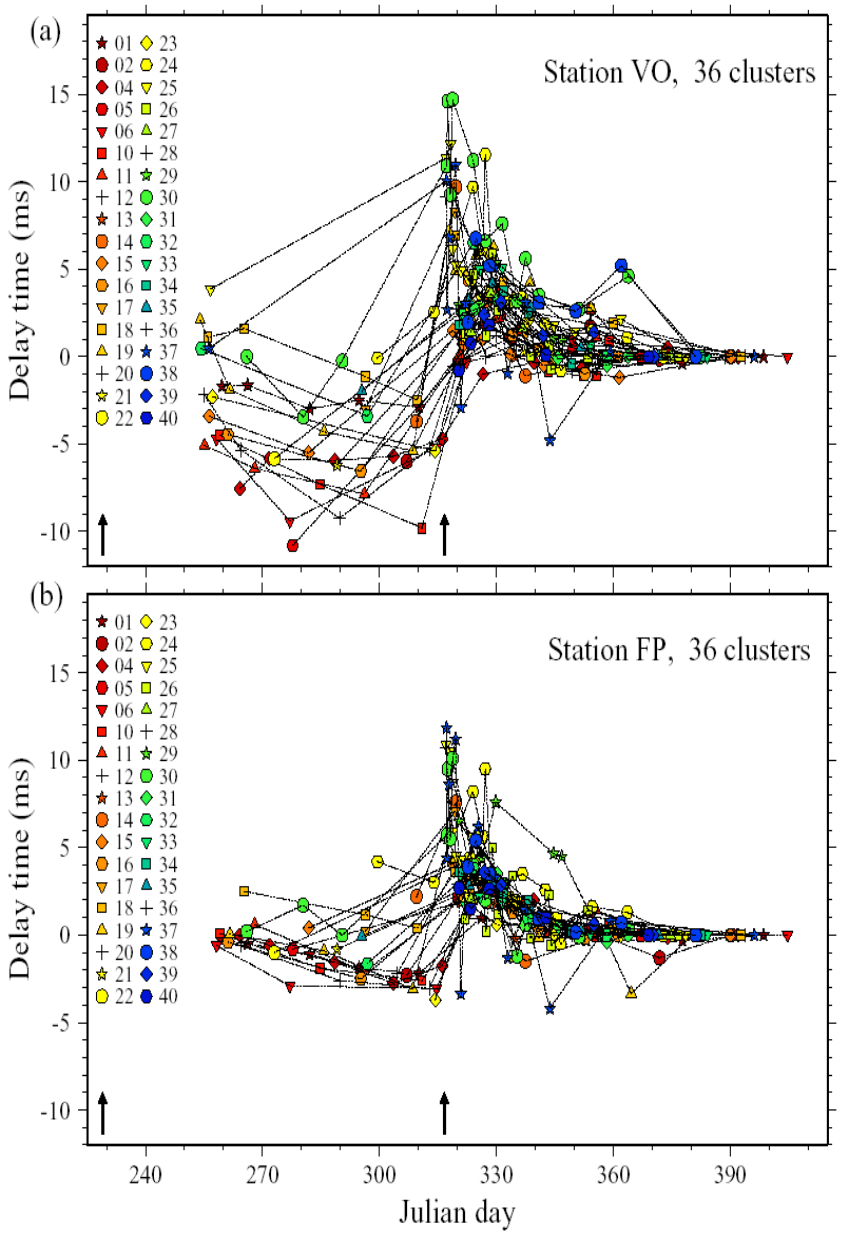

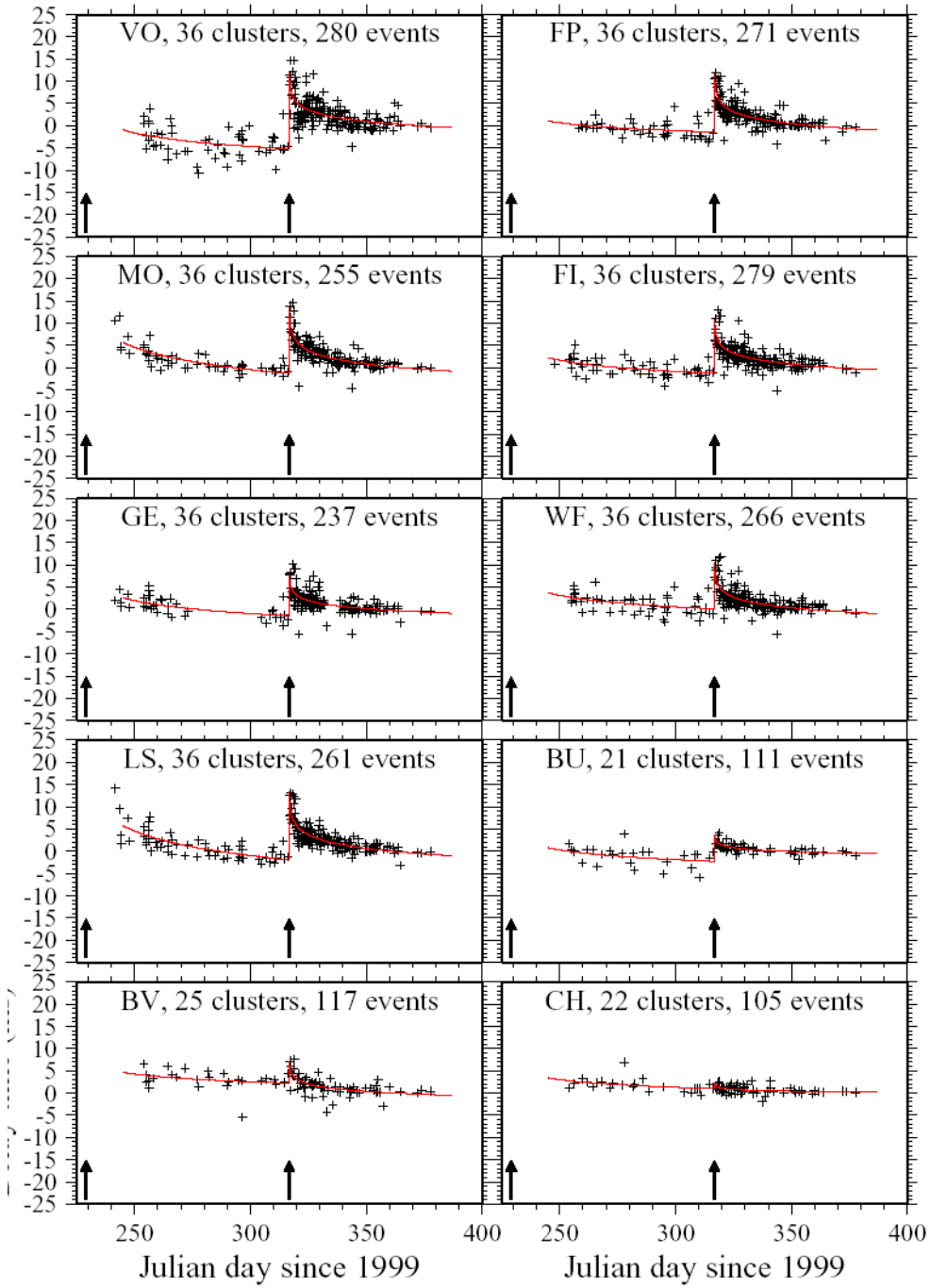

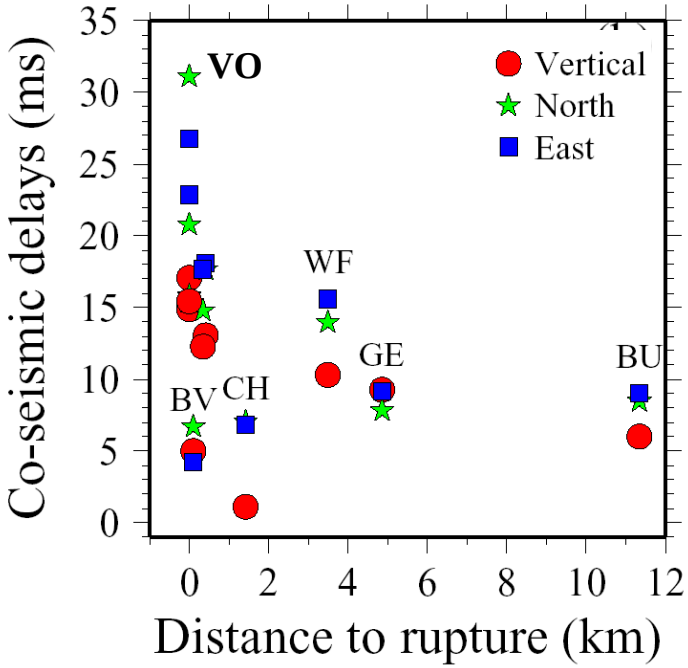

- The changes are strongest in the vicinity of the damaged FZ rock, but exist at all stations and do not change with source location (including depth).

- The effects reflect changes in the top damaged surface layer and shallow FZ damaged rock (e.g., 200-500 m)

- Similar results were obtained by others (e.g., Rubenstein and Beroza, 04, 05) for earthquakes in California and Japan.

Non-linearity and temporal changes of fault zone site response

(Wu, Peng and Ben-Zion, GJI, 2009, 2010)

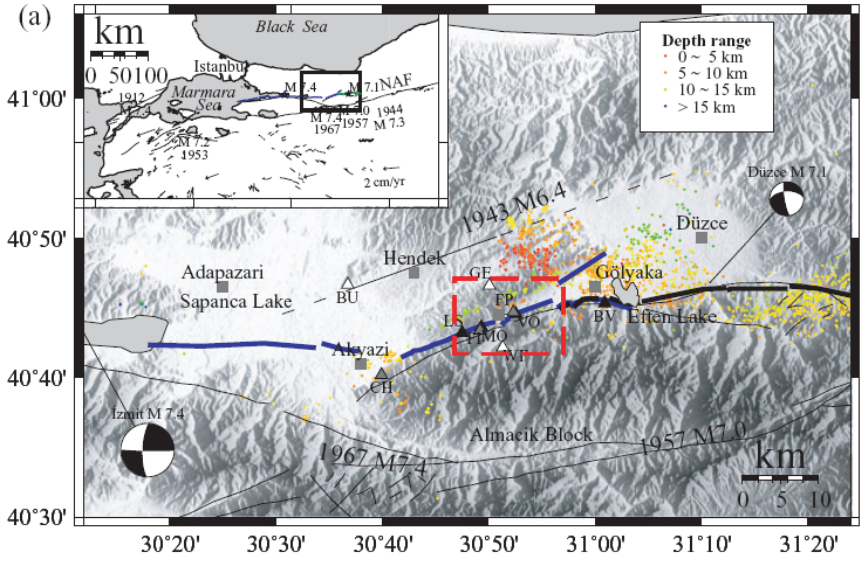

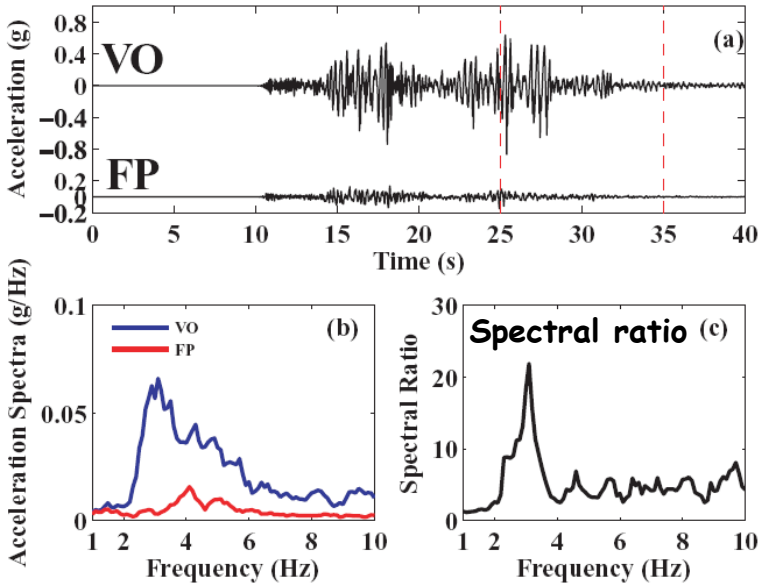

Spectral ratios of 15 events

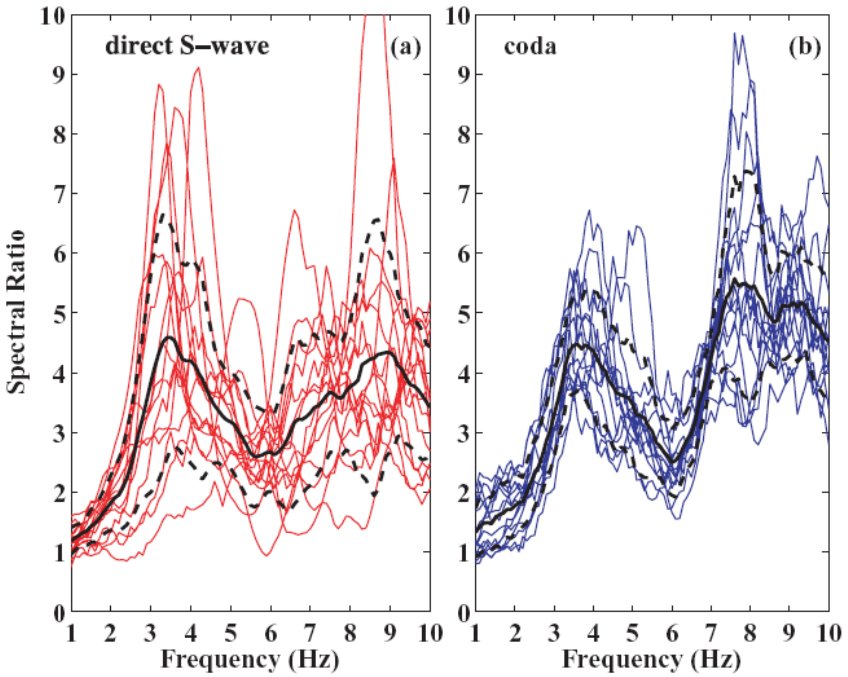

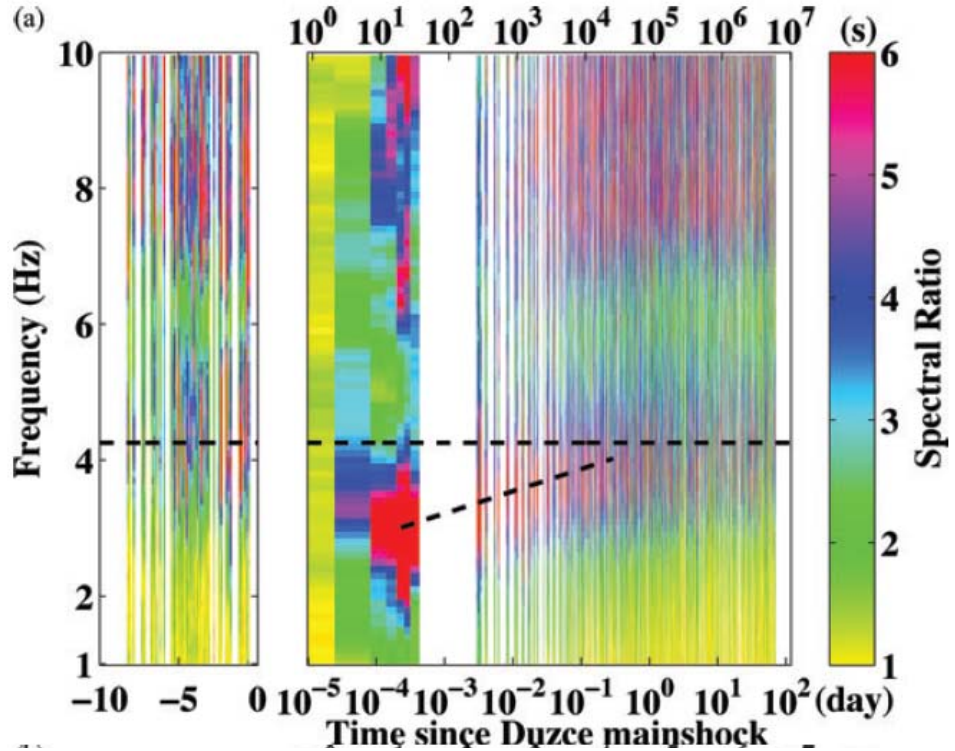

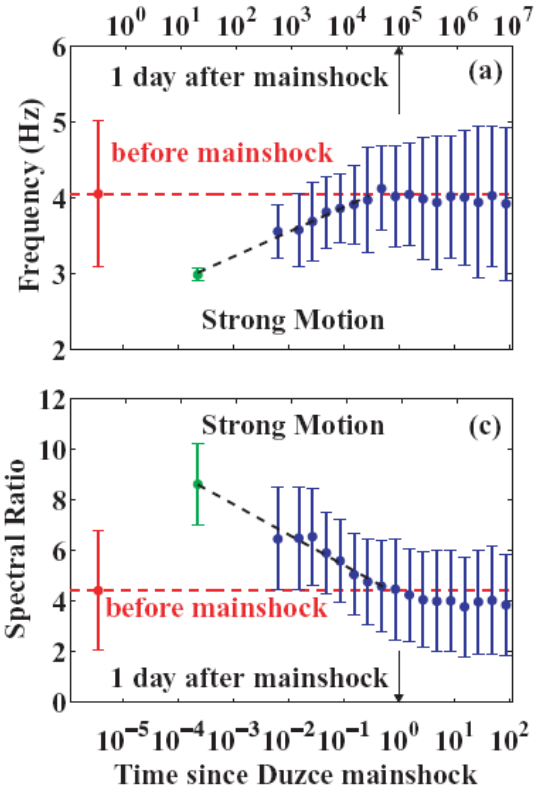

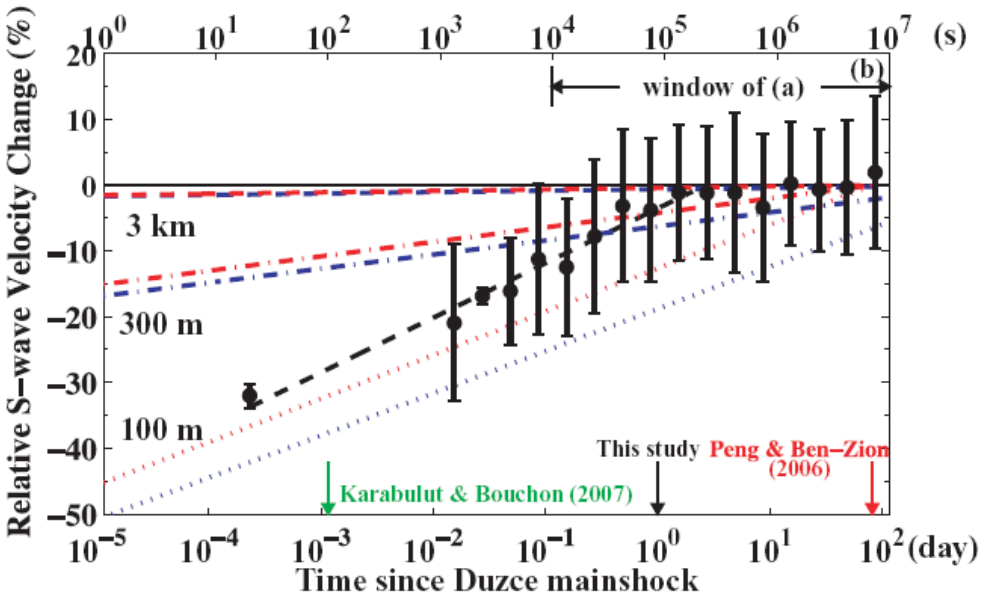

·The results suggest 30-50% S velocity reduction in the top 100-300 m, and logarithmic healing with strong effects over ~1 day but ~3 months or longer duration.

·Similar results were obtained by Karabulut and Bouchon (07), Rubenstein et al. (04, 05, 07), Sawazaki et al. (06, 08), and others for earthquakes in the US and Japan.

Schematic Summary

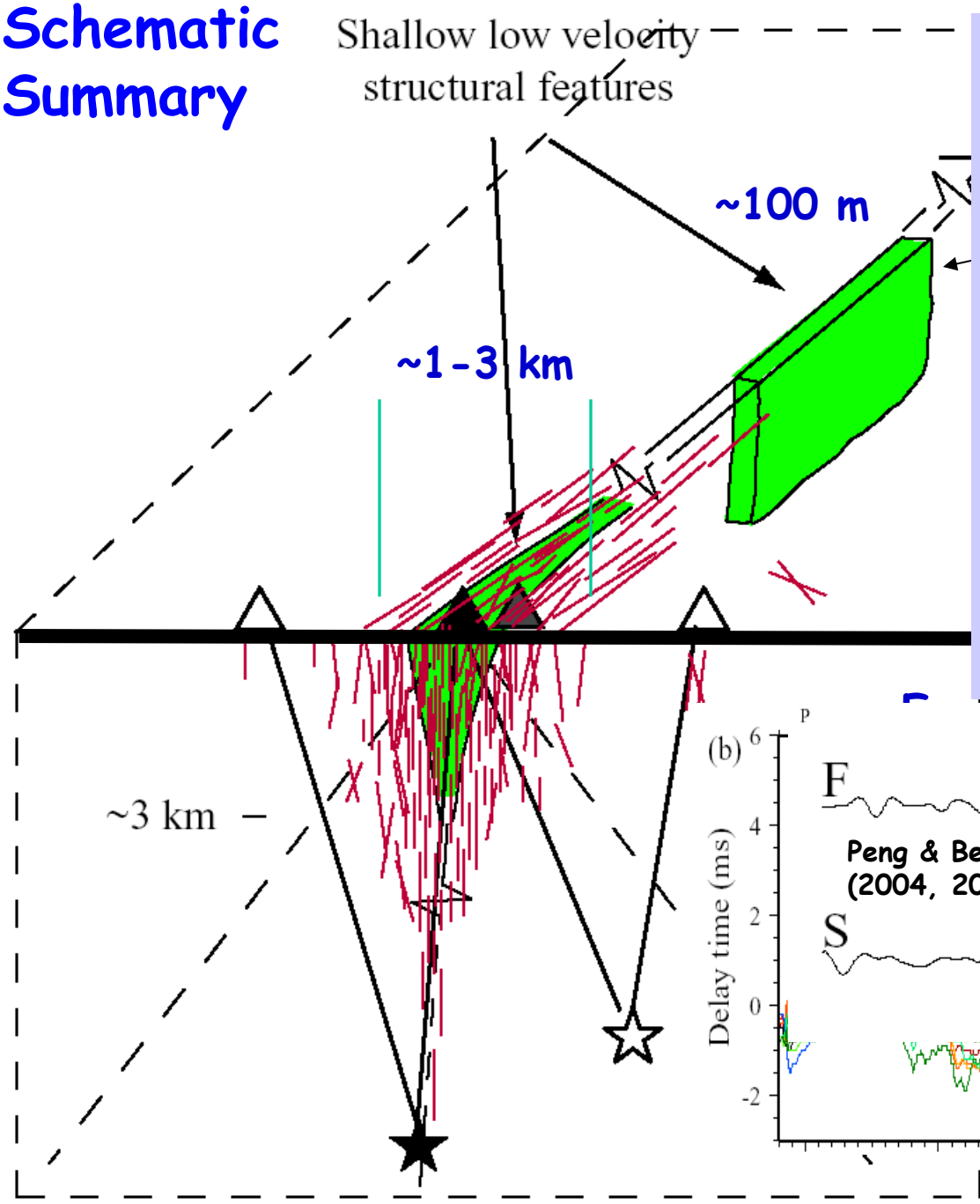

The trapping structures are ~100 m wide, have ~50% reduction of S-wave velocity, extend generally over the top 3 km, and show considerable along-strike variability.

The waveguides are surrounded by broader damage zones, also limited primarily to the top 3 km, producing seismic anisotropy and scattering

Analyses of repeating earthquakes and spectral ratios show strong co-seismic velocity reductions (~30-50% in the fault zone) followed by logarithmic recovery with time.

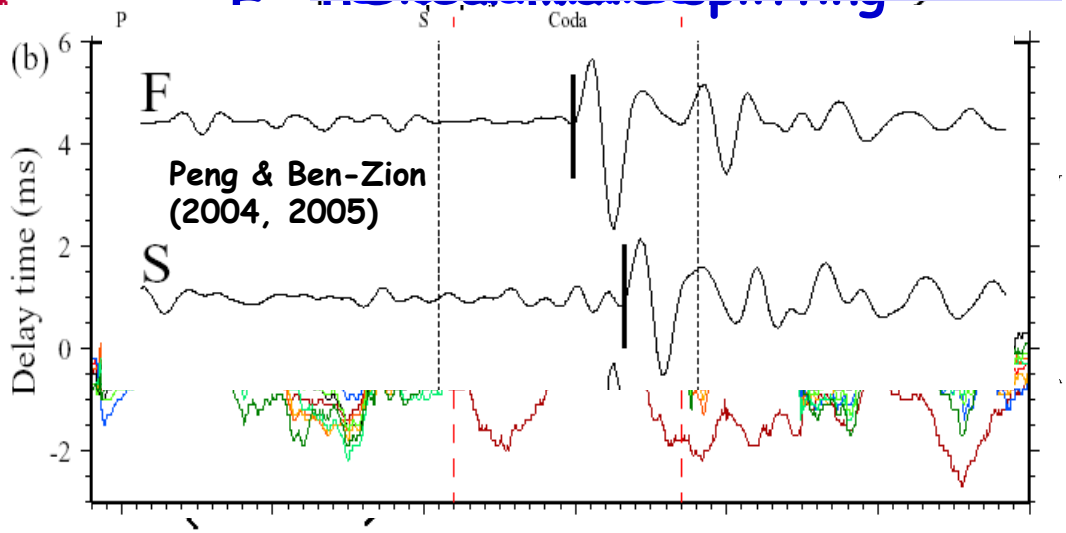

Conclusions

- High resolution imaging of fault zone environments requires using different signals (body waves, head and trapped waves, scattered waves, anisotropy, surface waves, …) and techniques (travel time and waveform tomography, noise correlations, …).
- Earthquake data provide detailed information on the seismogenic sections (depth 3-15 km).
- Ambient noise data provide detailed information on the shallower structure.

- Fault zones have hierarchical flower-type damaged zones and bimaterial interfaces.
- The damage zones have ~100m wide cores with intense damage (e.g. $\Delta\beta$ ~ 30-50%, Q ~ 10-30) that act as seismic trapping structures. They have considerable along-strike variability & discontinuities over length scales of ~5 km and are surrounded by ~3 km zones of lower damage that produce fault-related anisotropy and scattering.
- The bimaterial interfaces extend to the bottom of the seismogenic zone and are continuous over 10s to 100 km.
- The damage zones get re-activated during earthquakes (strong co-seismic velocity reduction of 30-40 % in the top few 100's of m of the crust) followed by log(t) healing.
- The damage zones are often asymmetric w.r.t. the principle slip zone that may reflect preferred propagation direction of earthquake ruptures.

Additional works:

- Correlation of earthquake waveform for high-resolution imaging of the top 500-1000m (Zigone et al.)
- Correlation of ambient noise for constructing trapped noise (with G. Hillers, M. Campillo, P. Roux)
- Analysis of internal fault zone reflections (Yang et al.)
- Additional imaging of the NAF (with Najdahmadi, Bulut, Bohnhoff)
- Attenuation imaging (with Xin Liu)
- Analysis of directional resonance and anisotropy in fault zones (Pischiutta et al.)
- Receiver function for sub-horizontal structures (with Ozakin, Liu, Schulte-Pelkum, Zigone, others)
- Adjoint tomography of body, surface, head and trapped waves (with Amir Allam and Carl Tape)

Thank you